Master's thesis

NTNU
Norwegian University of Science and Technology
Faculty of Natural Sciences
Department of Biology

Karen Irion

Regulation of Fibroblast Growth Factor Receptor (FGFR) Signaling

Master's thesis in Biotechnology
Supervisor: Ellen Margrethe Haugsten
Co-supervisor: Berit Johansen, Rahmi Lale
June 2024

NTNU
Norwegian University of Science and Technology

Oslo University Hospital
Norwegian Radium Hospital

Karen Irion

Regulation of Fibroblast Growth Factor Receptor (FGFR) Signaling

Master's thesis in Biotechnology
Supervisor: Ellen Margrethe Haugsten
Co-supervisor: Berit Johansen, Rahmi Lale
June 2024

Norwegian University of Science and Technology
Faculty of Natural Sciences
Department of Biology

NTNU
Norwegian University of
Science and Technology

ABSTRACT

Fibroblast Growth Factor Receptors (FGFRs) are signaling receptors regulating biological processes such as proliferation and migration. FGFR overactivation is linked to various cancers. The four FGFRs (FGFR1-4) induce the MAPK pathway upon ligand stimulation, leading to the phosphorylation of ERK1/2 and RSK2. Previous research has shown that feedback phosphorylation by RSK2 on FGFR1 and ERK1/2 on FGFR1 and FGFR2, downregulates FGFR signaling. Specifically, RSK2 binds and phosphorylates the C-terminal tail of FGFR1. This phosphorylation is required for proper receptor endocytosis. This study aims to determine if RSK2-mediated endocytosis is a negative feedback mechanism across all FGFRs, and to investigate if FGFR alterations affecting these feedback mechanisms are common in cancer.

Our findings show that RSK2 inhibition decreased the internalization of FGFR2 and FGFR4, similar to FGFR1, while FGFR3 remained unaffected. This suggests that RSK2 is involved in the endocytosis of FGFR2 and FGFR4, possibly through the same feedback mechanism as FGFR1. RSK2 binding to the FGFR1 receptor tail was confirmed upon ligand stimulation, but we could not detect binding between RSK2 and FGFR4. Improved assays or additional experiments will be needed to clarify if RSK2 binds to the other FGFRs. Increased migration was observed in FGFR1-3 expressing cells upon ligand stimulation, while FGFR4 showed increased proliferation. In contrast to our hypothesis, RSK2 inhibition did not enhance migration or proliferation, possibly due to inhibitor toxicity.

We analyzed the prevalence of alterations in FGFRs across tumor samples in the COSMIC database, focusing on those losing the potential negative feedback mechanisms mediated by ERK1/2 and RSK2. This included alterations leading to loss of the C-terminal tail while retaining an intact kinase domain or point mutations directly altering the potential phosphorylation sites. However, few alterations leading to the loss of the potential negative feedback mechanisms in FGFRs were observed.

Our findings suggest that RSK2-mediated feedback is likely occurring for FGFR2 and FGFR4, similar to FGFR1. Further investigations are needed to elucidate how this influences FGFR2 and FGFR4 signaling and their biological responses, and the relevance of these feedback loops in FGFR-driven cancer progression.

SAMMENDRAG

Fibroblast vekstfaktor reseptorer (FGFRer) er signalerings reseptorer som regulerer cellebiologiske prosesser som proliferering og migrering. Overaktivering av FGFRer er knyttet til flere ulike kreftformer. Aktivering av de fire FGFRene (FGFR1-4) ved stimulering med ligand, induserer MAPK-signalveien, noe som fører til fosforylering av ERK1/2 og RSK2. Tidligere forskning har vist at aktiv RSK2 fosforylerer FGFR1 og aktiv ERK1/2 fosforylerer FGFR1 og FGFR2, og dette fører til nedregulereing av FGFR-signalering. RSK2 er vist å fosforylere den C-terminale halen til FGFR1 og at dette er nødvendig for endocytose av reseptoren. I denne oppgaven var målet å avgjøre om RSK2-mediert endocytose fungerer som en negativ feedback mekanisme for alle FGFRene, og å undersøke om FGFR-alterasjoner som påvirker disse feedback-mekanismene forekommer i kreft.

Våre funn viser at RSK2-hemming reduserer internaliseringen av FGFR2 og FGFR4, slik som det er observert for FGFR1, mens FGFR3 er upåvirket. Dette antyder at RSK2 er viktig for endocytose av FGFR2 og FGFR4, muligens via en lignende negativ feedback mekanisme som for FGFR1. Vi detekterte binding av RSK2 til FGF-stimulert FGFR1, men ingen binding ble detektert for FGFR4. Flere forsøk er nødvendig for å bekrefte om RSK2 binder til FGFRene. Ved ligandstimulering ble det observert økt migrering for celler som uttrykker FGFR1-3, mens for FGFR4 ble det observert økt proliferering. Vi så ikke økt migrering eller proliferering når RSK2 var hemmet. Dette er muligens grunnet toksiske effekter av RSK2 hemmingen.

Vi analyserte forekomsten av alterasjoner i FGFRer på tvers av tumorprøver i COSMIC-databasen, med fokus på forandringer som ville føre til tap av de potensielle negative feedback-mekanismene mediert av ERK1/2 og RSK2. Dette inkluderte tap av den C-terminale halen i FGFR uten samtidig å miste kinase domenet, samt punktmutasjoner som direkte forandret de potensielle fosforyleringssetene. Få slike forandringer ble detektert.

Våre funn antyder at RSK2-mediert feedback sannsynligvis regulerer FGFR2 og FGFR4, slik som for FGFR1. Ytterligere undersøkelser er nødvendig for å bekrefte hvordan disse påvirker FGFR signalering og eventuell relevans for FGFR-drevet kreftprogresjon.

PREFACE

This thesis concludes my five-year integrated Master of Science in Biotechnology at the Norwegian University of Science and Technology (NTNU). The work was conducted in Jørgen Wesche's Molecular Biology of Sarcomas group at the Department of Tumor Biology, Institute for Cancer Research at the Norwegian Radium Hospital, from fall 2023 to spring 2024.

I am deeply grateful to my main supervisor, Ellen Margrethe Haugsten, for your consistent guidance, support, and inspiration throughout this journey. Your genuine interest in the research and constant willingness to help made this experience exceptional. I also want to thank Jørgen Wesche for welcoming me into the research group and providing valuable assistance with this thesis. I also appreciate my internal supervisor, Berit Johansen at NTNU, for your follow-up and administrative support, and co-supervisor, Rahmi Lale, for your guidance on bioinformatics questions. Special thanks to the Molecular Biology of Sarcomas group members for their inclusion and for making me feel like a colleague this year. Additionally, thank you to Samfundet for access to the Adobe package and the opportunity to learn how to use it over the years.

Lastly, I am immensely grateful for the love and support from my friends and family. The fun times and good memories with you have made this journey unforgettable.

Trondheim, 07.06.2024
Karen Irion

CONTENTS

LIST OF FIGURES

LIST OF TABLES

ABBREVIATIONS

- **AKT** Protein kinase B
- **ANOVA** Analysis of variance
- **ATP** Adenosine triphosphate
- **BioGrid** Biological General Repository for Interaction Datasets
- **BI** RSK2 inhibitor (BI-D1870)
- **BSA** Bovine serum albumin
- **B-Raf** B-RafV600E
- **CIE** Clathrin independent endocytosis
- **CM** Complete media
- **COSMIC** Catalogue of Somatic Mutations in Cancer
- **Co-IP** Co-immunoprecipitation
- **CRISPR** Clustered regularly interspaced palindromic repeats
- **DAG** Diacylglycerol
- **DAPI** 4',6-diamidino-2-phenylindole
- **DL-FGF1** Dylight550-FGF1
- **DMSO** Dimethyl sulfoxide
- **DMEM** Dulbecco's modified eagle medium
- **DNA** Deoxyribonucleic acid
- **DTT** Dithiothreitol
- **Dusp6** Dual specificity phosphatase 6

- **EDTA** Ethylenediaminetetraacetic acid
- **EEA1** Early endosome antigen 1
- **EGFR** Epidermal growth factor receptor
- **EMT** Epithelial-mesenchymal transition
- **ERK1/2** Extracellular signal-regulated kinases 1 and 2
- **FBS** Fetal bovine serum
- **FDA** Food and Drug Administration
- **FGF** Fibroblast growth factor
- **FGFR** Fibroblast growth factor receptor
- **FGFRL1** Fibroblast growth factor receptor like 1
- **FMI** Foundation Medicine Inc.
- **FRS2** FGFR substrate 2
- **Gab1** Growth factor receptor-bound protein 2-associated binder 1
- **GDP** Guanosine diphosphate
- **GFP** Green fluorescent protein
- **Grb2** Growth factor receptor-bound protein 2
- **Grb14** Growth factor receptor-bound protein 14
- **GTP** Guanosine triphosphate
- **HEPES** 4-(2-hydroxyethyl)-1-piperazineethanesulfonic acid
- **HMF** Hartwig Medical Foundation
- **HRP** Horseradish peroxidase
- **HS** Heparan sulfate
- **HSPG** Heparan sulfate proteoglycan
- **ICGC** International Cancer Genome Consortium
- **iCCA** Intrahepatic cholangiocarcinoma
- **Ig** Immunoglobulin
- **IP** Immunoprecipitation

- **IP3** Inositol trisphosphate
- **IQR** Interquartile range
- **KD** Kinase domain
- **LKB1** Liver kinase B1
- **MAPK** Mitogen-activated protein kinase
- **MEK1/2** Mitogen-activated protein kinase kinase 1 and 2
- **MKP3** MAPK phosphatase 3
- **MVB** Multivesicular body
- **N/A** Not assessed
- **PBS** Phosphate buffered saline
- **PCAWG** Pan-Cancer Analysis of Whole Genomes
- **PCR** Polymerase chain reaction
- **PI3K** Phosphatidylinositol-4,5-bisphosphate 3-kinase
- **PIP** Phosphoinositide
- **PKC** Protein kinase C
- **PLCγ** Phospholipase C-γ
- **P/S** Penicillin-streptomycin
- **PTPRG** Protein tyrosine receptor-type G
- **PVDF** Polyvinylidene difluoride
- **qPCR** Quantitative polymerase chain reaction
- **Raf** Rapidly accelerated fibrosarcoma
- **RCF** Relative centrifugal force
- **RFP** Red fluorescent protein
- **RMS** Rhabdomyosarcoma
- **rpm** Rotations per minute
- **RSK2** Ribosomal S6 kinase 2
- **RTKs** Receptor tyrosine kinases

- **SD** Spinning disk
- **SEF** Similar expression to fibroblast growth factor
- **SFM** Serum free media
- **SHP** Src homology region 2 domain-containing phosphatase
- **siRNA** Small interfering RNA
- **Sos** Son of sevenless
- **SPRED** Sprouty related with Ena/VASP homology 1
- **SPRY** Sprouty proteins
- **SDS-PAGE** Sodium dodecyl sulfate polyacrylamide gel electrophoresis
- **STAT** Signal transducer and activator of transcription
- **TCGA** Cancer Genome Atlas
- **Tf** Transcription factor
- **TMD** Transmembrane domain
- **TKI** Tyrosine kinase inhibitor
- **UniProt** The Universal Protein Resource
- **U0** MEK1/2 inhibitor (U0126)
- **U2OS** Human osteosarcoma cell line
- **U2OS-R1** U2OS cells stably expressing FGFR1
- **U2OS-R2** U2OS cells stably expressing FGFR2
- **U2OS-R3** U2OS cells stably expressing FGFR3
- **U2OS-R4** U2OS cells stably expressing FGFR4

CHAPTER

ONE

INTRODUCTION

Cellular communication plays a crucial role in coordinating activities within multicellular systems [1]. A significant mode of this communication is through ligand-receptor interactions. Ligands are small proteins acting as messengers, which bind to receptors on the surface of recipient cells [2]. These receptors transmit the signal to the nucleus, which subsequently guides the cell to trigger specific responses [3].

Precise communication is essential for regulating various processes in the body, including wound healing and growth. Cell migration, proliferation, and survival are critically governed by signaling pathways. When signaling pathways governing these functions are altered, cells can become invasive and undergo uncontrolled cell division, leading to cancer. These aberrations may involve alterations in ligands (increased availability), changes in receptors (increased activation), or loss of negative regulation [4]. The complexity of cancer development stems from multiple alterations driven by genetic, epigenetic, and environmental factors [5]. Tumor cells can avoid treatments by activating alternative pathways, making cancer progression individualized and dynamic across patients. Effective therapies for advanced cancers often entail combinations of signaling inhibitors and traditional chemotherapeutic agents [4]. Understanding cellular signaling networks and dysfunctions is crucial for unraveling cancer's origins and developing preventive and curative strategies.

1.1 Receptor tyrosine kinases (RTKs)

Receptor tyrosine kinases (RTKs) are a family of transmembrane receptors situated on the cell surface and induce several cellular processes, including growth, proliferation, migration, differentiation, and survival upon stimulation [6].

Humans possess 58 receptor tyrosine kinases (RTKs) [7]. The structure of RTKs includes an extracellular ligand-binding domain, an alpha-helical transmembrane domain, and an intracellular region containing a protein tyrosine kinase domain followed by a carboxy (C)-terminal tail. Upon ligand binding, individual RTK monomers form dimers, which activate the protein

tyrosine kinase domain through the autotransphosphorylation of tyrosine residues. This activation event triggers the recruitment and activation of intracellular signaling proteins [7].

Dysregulation of RTK signaling plays a significant role in various human diseases, particularly cancer. Abnormal activation of RTKs in human cancers typically occurs through four main mechanisms: gain-of-function mutations, genomic amplification, chromosomal rearrangements, and/or autocrine activation. Targeted therapies against RTKs in cancers, employing inhibitors or antibodies, have revolutionized cancer treatment, yet innovative strategies are needed to overcome resistance mechanisms [8].

1.2 Fibroblast growth factor receptors (FGFRs)

The family of fibroblast growth factor receptors (FGFRs), a group of transmembrane cell-surface RTKs, comprises four distinct receptors: FGFR1-4. [9, 10, 11, 12]. In addition, there exists an extra receptor, fibroblast growth factor receptor like 1 (FGFRL1 or FGFR5). However, FGFRL1 lacks the tyrosine kinase domain, rendering it incapable of signaling via autotransphosphorylation [13]. Humans have 22 identified FGF ligands, sharing 35% to 50% sequence homology, with 18 of them, including FGF1 to FGF10 and FGF16 to FGF23, known to activate FGFR signaling pathways [3]. Notably, FGF19 corresponds to FGF15 in mice, and there is no FGF15 in humans, which is why the FGF ligands are numbered up to FGF23 [14]. The FGF/FGFR activation regulates various cellular processes such as growth, migration, survival, and differentiation, as well as plays essential roles in morphogenesis, tissue repair, and regeneration [10, 15, 9]. The remaining FGF ligands are proposed to act intracellularly [3, 16].

While each of the four FGFRs is encoded by distinct genes, they exhibit significant homology, with sequence identity ranging from 56% to 71% [17, 12, 15]. The FGFRs possess a canonical structure typical of RTKs, characterized by three extracellular immunoglobulin (Ig)-like domains (D1,D2 and D3), an acidic box, a transmembrane domain, and an intracellular tyrosine kinase domain followed by a C-terminal tail [12, 9, 18] (Figure 1.2.1) . Alternative splice variants, or isomers, of the FGFRs exist and are activated by distinct subsets of FGF ligands. For example, alternative splicing of the D3 is known for FGFR1-3, and leads to differences in ligand binding. The two isoforms are known as b and c variants due to alternative exon usage [19].

Five FGF (1,4,7,8,9) have paracrine signaling properties and rely on heparan sulfate (HS) proteoglycan (HSPG), or potentially heparin, as a co-receptor to facilitate stable and high-affinity binding with their respective FGFRs. The binding of FGF-HS complexes to their specific FGFRs triggers receptor dimerization, leading to the autotransphosphorylation of the tyrosine kinase domains [3, 20, 21, 12, 22] (Figure 1.2.1). Conversely, endocrine FGFs (such as FGF19, FGF21, and FGF23) have a lower affinity for heparan sulfate, enabling them to act systemically. These endocrine FGFs require Klotho proteins as co-receptors to bind effectively to FGFRs,

which allows them to act in Klotho expressing tissues without being retained in the extracellular matrix [23, 24].

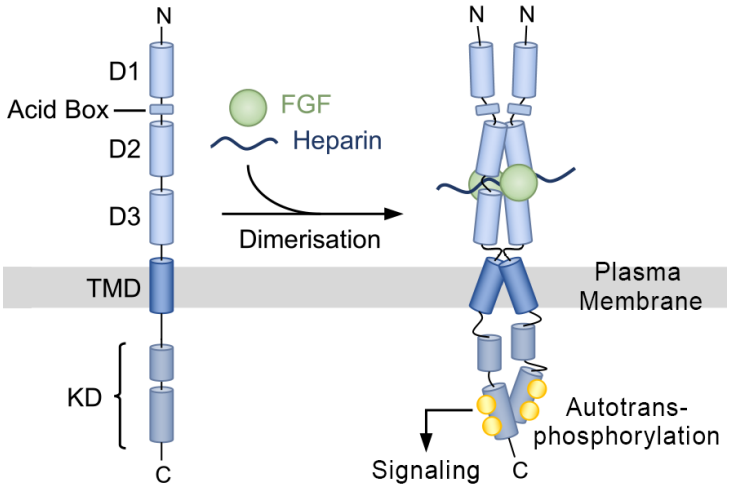

Figure 1.2.1: FGFR structure, dimerization, and activation. FGFRs consist of three extracellular immunoglobulin-like domains (D1, D2, D3), an acidic box, a transmembrane domain (TMD), an intracellular tyrosine kinase domain (KD), and a C-terminal tail. Receptor activation occurs through dimerization induced by FGF ligand binding and interaction with heparin/heparan sulfate cofactors. This activation triggers autotransphosphorylation of the kinase domains, leading to intracellular signaling cascades. Yellow circles indicate autotransphosphorylation. Carboxy (C) and amino (N) termini. The figure is adapted from Farell et al. (2018) [18], an open-access article licensed under a Creative Commons Attribution 4.0 International License (https://creativecommons.org/licenses/by/4.0/). Modifications were made using Adobe Photoshop.

The active tyrosine kinase recruits substrates to activate downstream signaling pathways (Figure 1.2.2), including the phosphatidylinositol-4,5-bisphosphate 3-kinase (PI3K)-protein kinase B (AKT), signal transducer and activator of transcription (STAT), phospholipase Cγ (PLCγ)/protein kinase C (PKC), and mitogen-activated protein kinase (MAPK) pathways, each contributing to various cellular responses such as growth, differentiation, and survival [25, 26]. One main signaling mediator is FGFR substrate 2 (FRS2) that is constitutively bound to the receptor. FRS2 is phosphorylated by the activated FGFRs, leading to the recruitment of proteins such as Growth factor receptor-bound protein 2-associated binder 1 (Gab1), Src homology region 2 domain-containing phosphatase (SHP), and growth factor receptor-bound protein 2 (Grb2). Gab1 is involved in the PI3K-AKT pathway. Grb2 recruits son of sevenless (Sos), leading to the activation of rat sarcoma virus protein (Ras). This cascade proceeds through rapidly accelerated fibrosarcoma (Raf) to mitogen-activated protein kinase kinase 1/2 (MEK1/2), ultimately phosphorylating extracellular signal-regulated kinase 1/2 (ERK1/2). ERK1/2 activates various targets, including ribosomal S6 kinase 2 (RSK2), which phosphorylates liver kinase B1 (LKB1), mediating further cellular responses [25, 27].

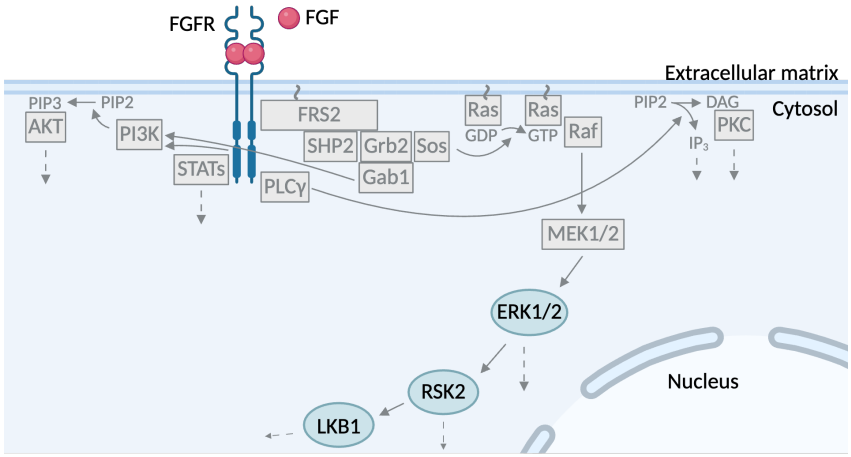

Figure 1.2.2: Overview of main FGFR signaling pathways. FGF stimulates FGFR dimerization and activation. The active tyrosine kinase recruits substrates to activate downstream signaling pathways, including the PI3K-AKT, STAT, PLCγ/PKC, and MAPK pathways. Activation of MAPK pathways leads to phosphorylation of ERK1/2, RSK2, LKB1, and further downstream molecules. (Refer to the abbreviation list for abbreviations). The figure is adapted from Szybowska et al. (2021) [25], an open-access article licensed under a Creative Commons Attribution 4.0 International License (https://creativecommons.org/licenses/by/4.0/). Modifications were made using BioRender.com.

1.3 FGFR alterations in disease

FGFR signaling regulates essential processes throughout human development, from embryonic stages to adulthood. Dysregulated receptor signaling has been demonstrated to contribute to a range of conditions, including skeletal abnormalities and cancer [25]. Inherited FGFR mutations, known to activate the receptor, can lead to skeletal conditions like dwarfism, primarily due to FGFR3 mutations, and craniofacial malformation syndromes, often FGFR1-2 mutations [9].

1.3.1 Implications of FGFRs in Cancer

Cancer begins with genetic changes in individual cells or small cell clusters. Failure of the cell's repair mechanisms results in the accumulation of genetic alterations, eventually leading to cancer and, over time, metastasis. For cells to be cancerous, they undergo distinct behavioral modifications, such as enhancing migration and proliferation capabilities [3].

Alterations in FGF/FGFR signaling observed in cancers are primarily considered gain-of-function mutations [9]. Alterations in FGFR signaling, including point mutations, gene rearrangements or fusions, and genomic amplifications (described in more detail in Figure 1.3.1), are identified in 5–10% of all human cancers [28]. Also, FGF/FGFRs have been found to have pro-angiogenic properties in numerous human tumors, promoting neovascularization and facilitating tumor progression and metastasis [29] (Figure 1.3.1).

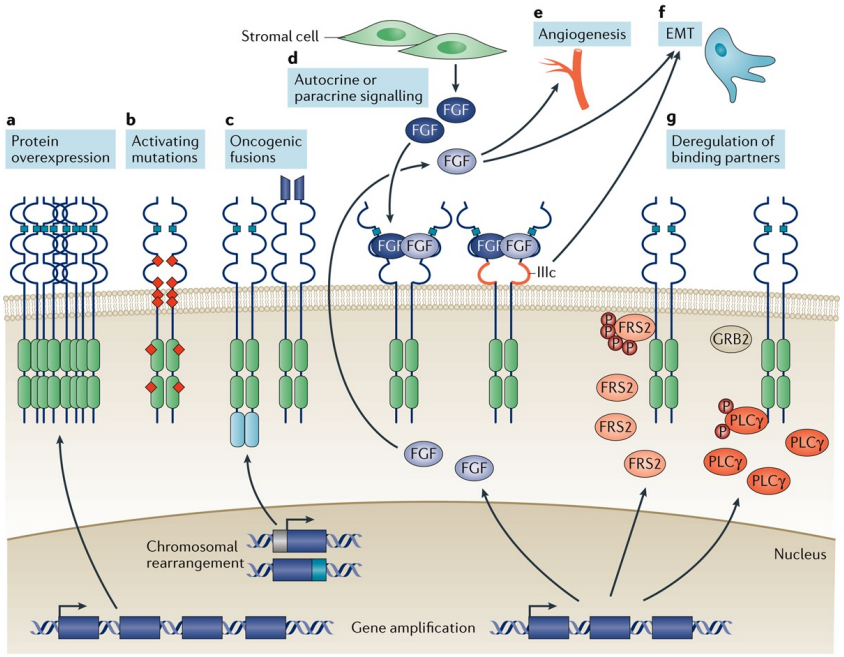

Figure 1.3.1: Pro-tumor alterations targeting FGFR signaling pathways. **a** FGFR gene amplification and enhanced expression may lead to receptor accumulation and, hence, increased signaling. **b** Mutations might increase dimerization in the absence of ligand or lead to constitutive activation of the kinase domain. **c** Fusions, due to chromosomal translocations, of FGFRs with genes encoding proteins at either carboxy (C) or amino (N) termini can increase receptor dimerization (blue fusion). These fusions can also be regulated by promoter regions of other proteins (grey fusion), resulting in hyperactivation without the need of a ligand. **d** FGF ligands being overexpressed, either autocrine (light blue) or paracrine (dark blue). Additionally, the third immunoglobulin (Ig) III loop can be alternatively spliced from the IIIb to the IIIc isoform, altering ligand affinity and leading to signaling. **e** FGFs secreted by the tumor or tumor-associated stromal cells can induce angiogenesis or **f** epithelial-mesenchymal transition (EMT), leading to tumor progression. **g** Deregulation of the FGFR binding partners, such as FRS2 and PLCγ, due to gene amplification or protein overexpression may increase FGFR downstream signaling pathways. The figure is derived from Babina et al. (2017) [30] (License ID: 5800850865717).

Hotspot mutations are common point mutations in the receptors frequently found in the kinase domain (changing the kinase to be constitutively active), close to the transmembrane domain (promoting receptor dimerization leading to activation), and in the extracellular part (promoting ligand binding and activation). For example, a hotspot mutation in FGFR1 is Asparagine to Lysine at position 546 (N546K), associated with glioblastoma and other cancers [31]. See Figure 1.3.2 for common, pathogenic somatic cancer mutations identified in FGFR1-4.

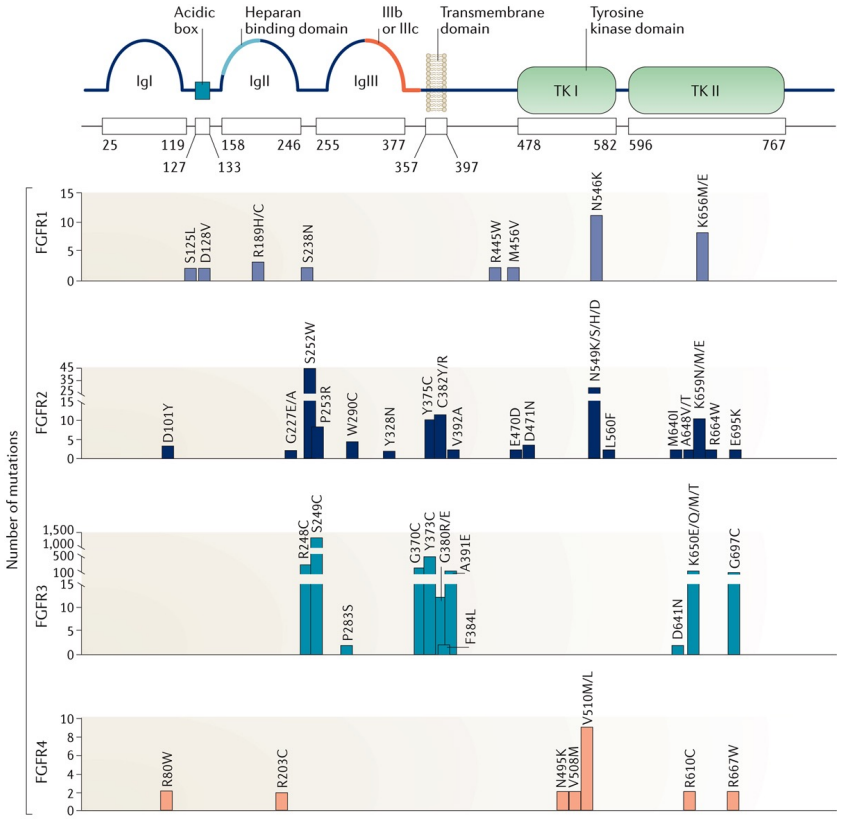

Figure 1.3.2: Somatic mutations in FGFRs. The frequency of FGFR somatic mutations leading to amino acid change reported in cancer patients (based on data extracted from COSMIC database) and considered to be pathogenic (determined by the Functional Analysis through Hidden Markov Models algorithm). Their location on the receptor, with FGFR1 structure as a reference, is shown (on top). Immunoglobulin (Ig). The figure is derived from Babina et al. (2017) [30] (License ID: 5800850865717).

Several cancer types, like certain forms of lung cancer, breast cancer, endometrial cancer, urothelial cancer, and intrahepatic cholangiocarcinoma (iCCA), have a high frequency of FGFR aberrations (10–30%) [28]. See Figure 1.3.3 for an overview of the main cancer forms with high frequency of FGFR alterations. Different alterations in the four FGFRs are associated with various cancers. For example, urothelial cancer was found to be due to 6% FGFR3 fusions, 10-62% FGFR3 mutations, and 7% FGFR1 amplifications [28] (Figure 1.3.3).

While cancer is relatively less prevalent among children and adolescents, sarcomas represent a notable proportion of the malignancies observed in this age group [32]. Sarcomas are a heterogeneous group of rare tumors primarily originating from the embryonic mesoderm with limited therapy options [33, 32]. Soft tissue sarcomas, like rhabdomyosarcoma (RMS), and primary bone tumors, like osteosarcoma, have been identified to have FGF/FGFR alterations [32, 34]. Osteosarcoma, the most frequent bone tumor, mostly affects younger individuals and also has a poor prognosis [34]. RMS is the most prevalent soft tissue sarcoma in children and is known for its aggressive nature and poor prognosis [35, 36]. FGFR4 alterations are associated with RMS, where 7-8 % of these cancers have FGFR4 mutations (Figure 1.3.3).

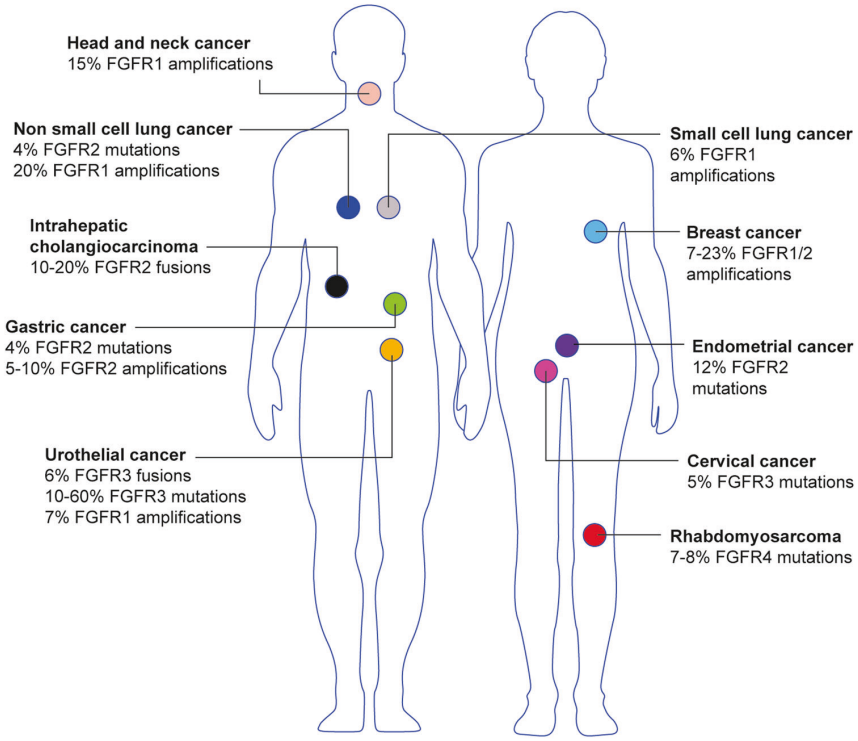

Figure 1.3.3: Overview of FGFR alterations in different cancer types. Cancer associated with FGFR alterations and the frequency of these alterations detected in the various cancers are indicated. The figure is from Krook et al. (2021) [28], an open-access article licensed under a Creative Commons Attribution 4.0 International License (`https://creativecommons.org/licenses/by/4.0/`).

Considering the broad implications of FGF/FGFRs in cancer, there is a growing need for cancer therapy targeting the FGF/FGFR signaling pathway.

1.3.2 FGFR targeted therapy

Multiple therapies targeting FGFRs are under investigation in preclinical and clinical trials, as monotherapy or combination. These therapies comprise a range of strategies, such as selective, non-selective, and covalent small-molecule receptor tyrosine kinase inhibitors (TKIs), along with monoclonal antibodies against the receptors and FGF ligand traps [28]. Non-selective TKIs, multitargeted kinase inhibitors, and selective TKIs, specifically targeting FGFR1-4, reversibly and competitively bind to the adenosine triphosphate (ATP)-binding site of the tyrosine kinase [28, 11]. Covalent inhibitors form irreversible bonds, leading to prolonged inhibition. Monoclonal antibodies selectively disrupt FGFR dimerization or ligand binding. FGF ligand traps are decoy receptors lacking transmembrane and cytoplasmic domains, which capture FGF ligands [28].

A few selective TKIs, such as erdafitinib, a pan-FGFR inhibitor, and pemigatinib, targeting FGFR1/2/3, have received FDA approval [28, 11, 37, 38]. A covalent pan-FGFR inhibitor, futibatinib, has also received Food and Drug Administration (FDA) approval [11, 39]. Erdafitnib is approved for treating urothelial carcinoma in patients with FGFR2/3 alterations [37, 11]. Futibatinib and pemigatinib are approved for patients with FGFR fusions and/or rearrangements

[11, 38, 39]. Common side effects like hyperphosphatemia due to FGFR1 inhibition, as well as the emergence of resistance mutations in FGFR genes might complicate the use of FGFR targeted therapy. [11, 37, 38, 39]. However, futibatinib is less prone to induce resistance development due to its irreversible binding and distinct binding site than the other approved FGFR inhibitors [39]. The next generation of FGFR inhibitors is anticipated to address hyperphosphatemia risk and counteract certain resistance mutations, for instance, the FGFR2 specific antibody bemarituzumab, disrupting FGF-binding [11, 40].

Given the pro-angiogenic properties of FGF/FGFRs, it is believed that there is a necessity for anti-FGF/FGFR drugs to hinder tumor angiogenesis [29]. A clinical response to FGFR inhibitors may also be attributed to their indirect suppression of aberrant angiogenesis in cancer [28]. Understanding FGFR signaling pathways and their regulatory mechanism might guide the development of therapy strategies for patients with FGFR abbreviations.

1.4 Regulation of FGFR signaling

In contrast to FGFR activation and signaling, its regulatory mechanism is less explored. Regulation of FGFR signaling occurs through pathways involving phosphatases, negative regulatory proteins, negative feedback phosphorylation, and endocytosis (Figure 1.4.1). Where endocytosis emerges as the primary FGFR regulatory mechanism by duration and intensity [25].

1.4.1 Regulation of FGFR signaling by phosphatases and negative regulatory proteins

Phosphatases dephosphorylate phosphorylated residues, such as serines/threonines or tyrosines, and thus downregulate signaling (Figure 1.4.1). Hence, phosphatases are suitable for regulating FGFR by dephosphorylating the intracellular part of the receptor, shutting down further downstream signaling [25]. One tyrosine phosphatase, known as protein tyrosine receptor-type G (PTPRG), has been found to dephosphorylate FGFRs within the tyrosine kinase domain [41, 25]. Also, other phosphatases contribute to downregulating FGFR signaling by dephosphorylating downstream signaling molecules. For example, MAPK phosphatase 3 (MKP3) dephosphorylate ERK1/2 [25].

Negative regulatory adaptor proteins, such as Sprouty (SPRY) proteins and Sprouty related with Ena/VASP homology 1 (SPRED) proteins, play pivotal roles in regulating FGFR signaling (Figure 1.4.1). SPRY proteins, SPRY1 and SPRY2, inhibit MAPK signaling by hindering the association of Grb2 with FRS2, thereby preventing downstream signaling [25]. Also, SPRY2 inhibits serine/threonine kinase Raf, which is downstream of Grb2 in the MAPK pathway [42]. Upon ligand binding and excessive RTK signaling, SPRY expression increases as a negative feedback mechanism [43]. SPRED proteins have also been found to suppress Ras signaling. Other molecules like SEF (similar expression to FGF), Grb14, and FGFRL1, the FGF receptor lacking the tyrosine kinase domain, have been suggested to participate in FGFR regulation [25, 13] (Figure 1.4.1).

1.4.2 Regulation of FGFR signaling by negative feedback phosphorylation

Most components in the MAPK signaling cascade are subjected to negative feedback phosphorylation by downstream kinases [44]. For instance, upon ligand stimulation, FGFRs phosphorylate FRS2 on tyrosine residues, activating the MAPK signaling pathway and subsequent ERK1/2 phosphorylation. Active ERK1/2 phosphorylates FRS2 on threonines, reducing FRS2 tyrosine phosphorylation and reducing downstream signaling [25] (Figure 1.4.1).

1.4.2.1 Negative Feedback Mechanism by ERK1/2 in FGFR1 and FGFR2

ERK1/2 has been identified to phosphorylate the C-terminal tail of FGFR1-2 as a negative feedback mechanism (Figure 1.4.1). Specifically, ERK1/2 phosphorylates serine (S)-777 in FGFR1 and the equivalent S780 in FGFR2 [45, 46], where both serines are followed by a proline (P) forming an ERK1/2 phosphorylation site (pS/T-P) [47]. Inhibition of ERK1/2 increased tyrosine phosphorylation and enhanced receptor signaling in FGFR1 and FGFR2 [45, 46]. This indicates that ERK1/2 acts as a negative feedback mechanism within the FGF/FGFR signaling pathway, though the precise mechanisms remain unknown. Moreover, mutations that prevent phosphorylation at the specific serine sites on FGFR1 and FGFR2 result in prolonged receptor activity and increased cellular responses. These findings imply that loss of these phosphorylation sites could have pro-tumorigenic effects [45, 46]. FGFR2 lacking S780 has been detected in human cancers, suggesting the potential importance of negative feedback phosphorylation loops in FGFR signaling to maintain cellular homeostasis [25]. Also, truncating mutations, leading to the loss of exon 18 (the last exon of FGFR2 where S780 is situated), have been identified as a potent driver mutation [48].

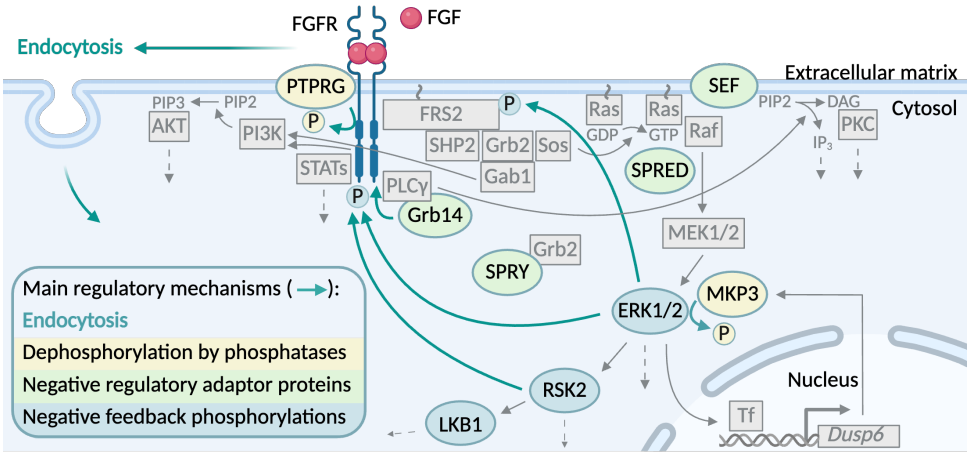

Figure 1.4.1: Regulation of FGFR signaling FGF binds to FGFR and activates downstream signaling pathways, including the PI3K-AKT, STAT, PLCγ)/PKC, and MAPK signaling pathways. Regulation of FGFR signaling occurs through pathways involving phosphatases (yellow), negative regulatory adaptor proteins (green), negative feedback phosphorylation (blue), and endocytosis. Negative regulatory mechanisms are represented by green arrows. RSK2 has been identified to phosphorylate the tail of FGFR1, inducing receptor endocytosis [49]. ERK1/2 has been identified to phosphorylate the tails of FGFR1 and FGFR2 as a negative feedback mechanism [45, 46]. Transcription factor (Tf). (Refer to the abbreviation list for additional abbreviations). The figure is modified from Szybowska et al. (2021) [25], an open-access article licensed under a Creative Commons Attribution 4.0 International License (`https://creativecommons.org/licenses/by/4.0/`). Modifications were made using BioRender.com.

1.4.3 Regulation of FGFR signaling by endocytosis

Endosomes are cellular structures that temporarily transport substances into and out of eukaryotic cells. Small molecules can travel through the plasma membrane through integral membrane proteins, while larger macromolecules are internalized by plasma membrane invagination forming endosomes. The process of internalizing and transporting extracellular material and surface-bound proteins by endosomes is known as endocytosis [50]. Following internalization, macromolecules and surface proteins can undergo various processes: they may be targeted for degradation in lysosomes, recycled back to the plasma membrane, or undergo transcytosis, a vital process for transporting substances to epithelia and blood-brain barrier, in polarized cells [51]. For instance, membrane-bound receptors that undergo endocytosis may either be degraded by lysosomes, reducing receptor activity or recycled back to the membrane to sustain signaling [25, 52].

The main mechanisms for endocytosis are clathrin-mediated and clathrin-independent endocytosis [51]. Clathrin-mediated endocytosis (CME) involves the assembly and maturation of clathrin-coated pits, gathering receptor membrane proteins or macromolecules as the membrane invaginate and pinch off to form clathrin-coated vesicles [53]. CME serves as the primary endocytic pathway for FGFRs. However, the endocytosis of FGFR3 has been observed to engage both CME and clathrin-independent endocytosis (CIE) [25, 54, 55, 56]. Endocytosis plays a regulatory role in the signaling pathways of FGFRs, and the endocytic pathways of FGFRs are dependent on receptor subtype, ligand type, and probably cell type, resulting in diverse

signaling outcomes [25]. Upon activation by FGF1, FGFR1-3 receptors are mainly directed to lysosomes for degradation. Conversely, ligand-bound FGFR4 receptors are primarily recycled, thereby sustaining signaling [57]. The type of ligand can significantly influence the endocytic pathway. For example, when FGF10 binds to FGFR2b, it is primarily recycled while FGF7 to FGFR2b is degraded [25]. Additionally, internalized FGFRs may be translocated to the nucleus, although their function in the nucleus and their impact on signaling remain unclear [25].

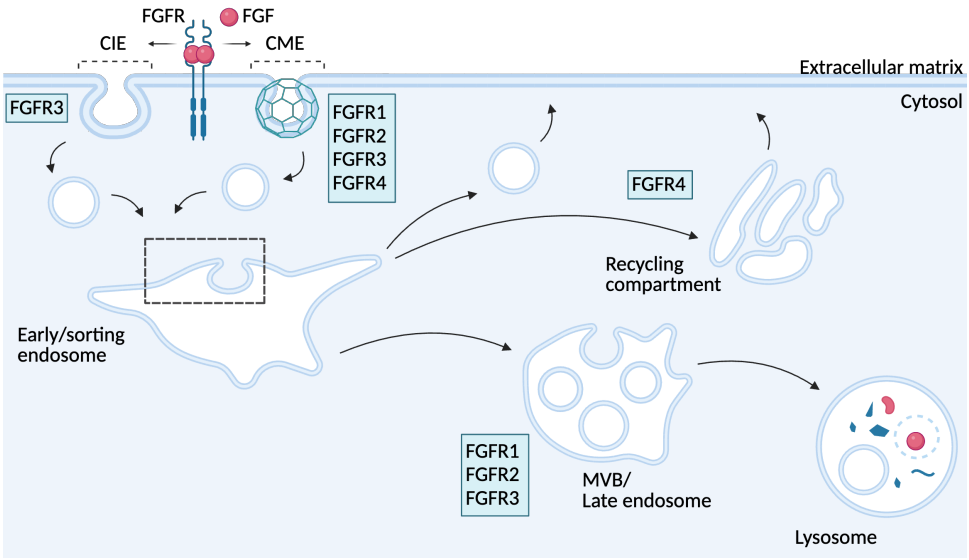

Figure 1.4.2: Endocytic pathways of FGFRs Upon ligand stimulation, FGFRs may be endocytosed by clathrin-mediated endocytosis (CME) or clathrin-independent endocytosis (CIE). FGFR1,2 and 4 are mainly internalized by CME, while FGFR3 can be internalized by CME or CIE mechanisms. First, FGFRs are transported to early/sorting endosomes, where they are either recycled back to the cell surface directly or via the endocytic recycling compartment or sent to be degraded in lysosomes via multivesicular bodies (MVB) and late endosomes. The figure is adapted from Szybowska et al. (2021) [25], an open-access article licensed under a Creative Commons Attribution 4.0 International License (https://creativecommons.org/licenses/by/4.0/). The figure is modified in BioRender.com.

An active receptor kinase is essential for the endocytosis of FGFRs. Inhibition of FGFR1 kinase activity reduced the rate of endocytosis, highlighting the significance of ligand binding, receptor dimerization, and autotransphosphorylation of the kinase domain in facilitating cellular uptake. However, what signals initiate endocytosis of FGFRs are still uncertain [25].

1.4.3.1 RSK2 regulates endocytosis of FGFR1

A previously published study uncovered an interaction between RSK2 and FGFR1. RSK2 is one of four isoforms in the RSK family (RSK1, RSK2, RSK3, and RSK4) [58]. RSK2, positioned downstream of ERK1/2 in the MAPK pathway, is activated by FGFRs. RSK2 is a serine/threonine kinase with several downstream substrates. Interestingly, RSK2 regulates FGFR1 activity upon FGF ligand stimulation. Specifically, activated RSK2 binds and phosphorylates the tail of FGFR1 at serine 789 (S789) [49] (Figure 1.4.1).

The serine/threonine kinase of RSK2 is activated by ERK1/2, leading to autophosphorylation and subsequent phosphorylation of various substrates, including FGFR1 [49, 59]. This phos-

phorylation event, particularly at S789, seems to be important for internalization of FGFR1 and acts as part of a negative feedback mechanism (Figure 1.4.1). As receptors are internalized, fewer FGFR1 receptors remain available on the cell surface for ligand binding and activation [49, 25].

RSK2 recognizes specific consensus sequences for phosphorylation, typically following the pattern R-X-R-X-X-pS/T or R-R-X-pS/T [49, 60]. A similar motif is found in the C-terminal region of FGFR1, specifically at position 784RSSTCS789, with S789 being the residue phosphorylated by RSK2. Mutating S789 impairs RSK2 binding, highlighting the importance of this specific site. Inhibition of RSK2 reduces the amount of phosphorylated FGFR1 [49].

These findings highlight the regulatory role of RSK2 in FGFR1 endocytosis, providing valuable insights into RTK signaling mechanisms [49]. However, it is not yet known whether RSK2 binds to and phosphorylates the other FGFR isoforms (FGFR2, FGFR3, and FGFR4). This thesis will investigate the potential regulatory role of RSK2 in these other FGFRs. Additionally, we will explore whether RSK2 or ERK1/2 negative feedback mechanisms are frequently altered in cancer, potentially leading to increased migration, proliferation, and oncogenic effects.

CHAPTER

TWO

AIM OF STUDY

The main objective of this study is to determine if the RSK2-mediated negative feedback mechanism reported for FGFR1 is also regulating the other FGFRs. Additionally, we aim to investigate whether FGFR alterations impacting the potential negative feedback mechanisms by RSK2 and ERK1/2 for FGFRs are common in cancer.

CHAPTER

THREE

METHODS

3.1 Cell lines and handling procedures

The cell line utilized in this study, U2OS, is a commercially available cell line derived from human osteosarcoma cancer (gift from the Department of Molecular Cell Biology, The Norwegian Radium Hospital). U2OS cells were transfected at the Department of Tumor Biology, Institute of Cancer Research, to stably express desired FGFRs 1-4 individually. Stably transfected cells were selected as clones based on their receptor expression levels. Five variants of the cell lines were employed: wild-type U2OS cell line as a control and four cell lines expressing the four FGFRs individually: U2OS-R1, U2OS-R2, U2OS-R3, and U2OS-R4. Refer to Table 3.1.1 for cell lines, developer names, and references.

Table 3.1.1: Overview of U2OS cells transfected with FGFR1-4 plasmid DNA transfection

Cell lines	Developer	Reference
U2OS-R1	Ellen Margrethe Haugsten	[56]
U2OS-R2	Patrycja Szybowska	[45]
U2OS-R3	Ellen Margrethe Haugsten	[55]
U2OS-R4	Ellen Margrethe Haugsten	[56]

3.2 Cell culture and passaging

The cells were cultured in filter cap cell culture flasks and maintained for proliferation in a humidified carbon dioxide (CO_2) incubator at 37°C. The culture medium used was complete media (CM) prepared with Dulbecco's Modified Eagle Medium (DMEM) (1X) + GlutaMAX (Gibco, Cat. #31966-047) and 10% Fetal Bovine Serum (FBS) (Sigma Life Science, Cat. #F7524). Additionally, 50 U/mL Penicillin-Streptomycin (P/S) (Fisher Scientific, Cat. #11528876) was added to minimize bacterial contamination.

Upon reaching confluence, the cells were passaged individually under sterile conditions to maintain purity and prevent contamination. The passaging process began with removing the old media from the culture flask. Subsequently, the cells were washed with Phosphate Buffered Saline (PBS) 6.7 mM phosphate (Hyclone, Cat. #SH30256.01) to ensure the removal of media and debris. Then, trypsin/ethylenediamine tetraacetic acid (EDTA) 0.05% (Gibco, Cat. #5300-054) was used to detach the adherent cells. This involved incubating the cells with trypsin for approximately 3 minutes until detachment occurred. Once detached, the cells were suspended in fresh CM and transferred to new cell flasks for continued growth.

3.2.1 Cell cryopreservation

Cryopreservation is a technique for preserving biological samples, such as cells. This process is crucial for maintaining the viability and functionality of cells over long periods, allowing for future use in various experimental and clinical applications [61].

In the cryopreservation process, cells are frozen at low temperatures (-196°C) [61]. Cells should grow actively before freezing, and a fresh medium should be provided the day before freezing. Once cells reach confluence, they are detached using trypsin (see section 3.2), washed with PBS, and resuspended in CM. The cells are then centrifuged (1000 rpm equals 235 RCF, 10 minutes), and the supernatant is discarded before resuspending the cell pellet in freeze media, consisting of pre-cooled CM with additional FBS serum to 20% and 5% Dimethyl Sulfoxide (DMSO) anhydrous (Sigma-Aldrich #276855). DMSO acts as a cryoprotectant, preventing ice crystal formation, which can damage cell membranes and intracellular structures [62, 61]. The cells are rapidly transferred to freezing vials, kept on ice, put into a freezing container (Sigma Aldrich, Cat. #CLS432001), and stored in a -80°C freezer for at least 4 hours. This process ensures a temperature/freezing rate drop of -1°C/min. Subsequently, they are transferred to a nitrogen tank (-196°C) for preservation.

Thawing of cryopreserved cells is done rapidly at 37°C, then diluted into a warm growth medium within a cell culture flask. The medium is changed the next day to remove DMSO, which can harm the cells over time. This process improves cell growth and viability after thawing.

3.2.2 Mycoplasma testing

Mycoplasma contamination is a common bacterial infection in cell cultures in many laboratories. This is due to mycoplasma's inherent resistance to standard antibiotics since there is no cell wall to break down [63]. Mycoplasma's small size makes it challenging to detect and allows it to pass through standard filter systems, facilitating its spread. It can proliferate to high concentrations without causing apparent symptoms in cell cultures, complicating its detection and control. Moreover, mycoplasma contamination may lead to false results, compromising the experiments' integrity [63]. Hence, conducting routine mycoplasma testing on cell lines is essential to prevent spread and preserve data integrity.

Cell lines were kept for 3 days for the testing procedure, and cultures had to achieve 90-100% confluency. In this study, two different mycoplasma tests were employed. The first involved using a polymerase chain reaction (PCR)-based kit, Venor GeM Mycoplasma Detection Kit (Minerva Biolabs). Trypsinized cells (100 μL) were transferred to conical microcentrifuge tubes and centrifuged until cell pellets were formed. The supernatant was subsequently removed, and the cell pellets were kept frozen at -20°C until the day of testing. The PCR test was conducted by a technician (Tove Øyjord, Department of Tumor Biology) following the protocol provided by the manufacturer.

The other mycoplasma test employed is a Quantitative PCR (qPCR)-based test, provided as a service by Eurofins Genomics called MycoplasmaCheck Service. Samples were sent to Eurofins Genomics for mycoplasma testing. Before sending the samples, cell culture supernatant from the confluent cell culture (approx. 500 μL), was transferred to a 1.5 mL tube. The supernatant was then boiled at 95°C for 10 minutes. Following this, the sample was briefly centrifuged at approximately 1300 RCF for 5 seconds to pellet cellular debris. Finally, 100-200 μL of supernatant was transferred into a new 1.5 mL tube and sent to Eurofins Genomics.

3.2.3 Cell seeding

Upon cell passaging, cells were seeded onto plates of various sizes tailored to the specific experiment. Seeding densities were adjusted to achieve confluent cells on the day of the experiment for Western blot and immunoprecipitation assays (see section 3.4 and 3.5 for further details) while maintaining subconfluency on the day of the experiment for imaging techniques like confocal microscopy and Incucyte analysis (section 3.6 and 3.7). Cell suspensions were mixed 1:1 with Trypan Blue Stain (0.4%, NanoEntek, Cat. #EBT-001) to ensure accurate seeding and applied to a counting slide (NanoEntek, Cat. #EBT-001). The slide was inserted into the Countess 3 Automated Cell Counter (Invitrogen by Thermo Fisher Scientific). The Countess provides the number of live cells/mL by distinguishing translucent live cells from dark-stained dead cells, enabling precise cell concentration determination for subsequent dilution and seeding.

3.2.4 Cell lysis

In experiments involving immunoprecipitation (section 3.5) and Western blotting (section 3.4), after administering designated treatments to the cells, they were lysed to release proteins for detection via IP or Western blot analysis. For cell lysis, a master mix was prepared using Lysis Buffer (recipe in Table 3.2.1) and Halt Protease and Phosphatase Inhibitor Cocktail (100X) (Thermo Scientific, Cat. #VA296005) in a 100:1 ratio. Cells were washed with cold PBS. Subsequently, 50 μL (for 12-well plates), 0.8 mL for 5 cm plates), or 1.2 mL (for 10 cm plates) of the prepared master mix of cold lysis buffer and Halt protease was added to each plate. The plate was then kept on ice and placed on a shaker for 10 minutes to allow cell lysis. The cells

were then inspected under a microscope to ensure thorough lysis (noting the presence of the cell nucleus at the well bottom while the cell body was no longer visible) before proceeding with subsequent steps outlined in the protocol.

Table 3.2.1: Lysis buffer recipe

Concentration	Component	Supplier	Catalogue no.
0.1 M	Sodium chloride (NaCl)	Subelco	1.06404.1000
10 mM	Di-Natriumhydrogenphosphat-dihydrat (Na_2HPO_4)	Merck	K13159080
1 mM	Ethylenediaminetetraacetic acid (EDTA)	Merck	K13159080
1 %	Triton X-100	VWR Chemicals	28817.295

3.3 Inhibitors

In this thesis, the presence of ERK1/2 and RSK2 negative feedback mechanisms for all FGFRs is being evaluated. Two inhibitors are used: U0126 (Selleck Chemicals, Cat. #S1102), which inhibits MEK1/2 upstream of both ERK1/2 and RSK2, thereby blocking both potential feedback mechanisms; and BI-D1870 (Enzo Life Sciences, Cat. #BML-E1407), which specifically inhibits RSK2 (Figure 3.3.1).

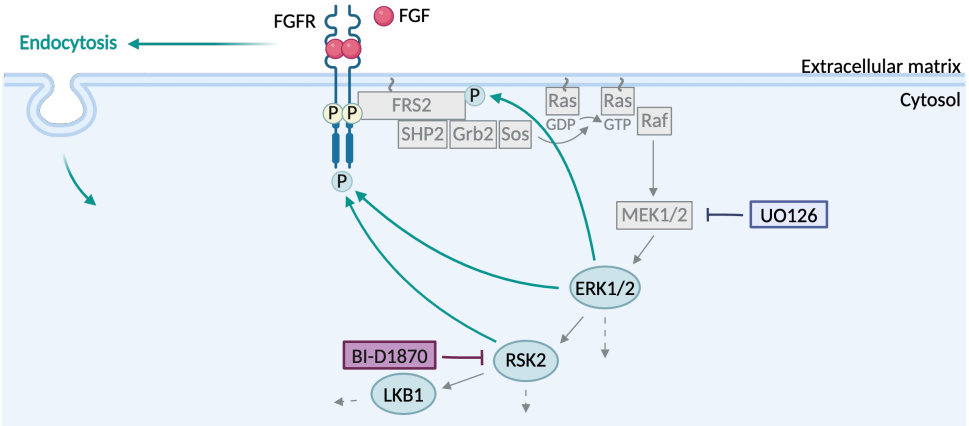

Figure 3.3.1: MEK1/2 and RSK2 inhibitors on FGF/FGFR signaling pathway. The MEK1/2 inhibitor (U0126) leads to inactive ERK1/2 and RSK2. The RSK2 inhibitor (BI-D1870) leads to inactive RSK2, hence no activation of downstream molecules. Activated FGFRs induce MAPK pathway, including activation of MEK1/2, ERK1/2, and RSK2. RSK2 has been identified to phosphorylate the tail of FGFR1, inducing receptor endocytosis [49]. ERK1/2 has been identified to phosphorylate the tails of FGFR1 and FGFR2 as a negative feedback mechanism [45, 46]. (Refer to the abbreviation list for additional abbreviations). The figure is adapted from Szybowska et al. (2021) [25], an open-access article licensed under a Creative Commons Attribution 4.0 International License `https://creativecommons.org/licenses/by/4.0/`. Modifications were made using BioRender.com.

3.4 Western blot

3.4.1 Gel electrophoresis

Sodium dodecyl sulfate Polyacrylamide Gel Electrophoresis (SDS-PAGE) is a technique used to separate proteins based on their molecular size. In this method, proteins are uniformly coated with a negative charge by SDS and placed in a gel matrix with a positive electrode at the bottom. As a result, proteins migrate through the gel, with smaller proteins moving more easily through the gel, leading to their separation by size [64].

Before SDS-PAGE, cells undergo the desired stimulation and are lysed (detailed in section 3.2.4). Then, a master mix of 4X Laemmli Sample Buffer (BioRad, Cat. #1610747) and 10X Sample Reducing Agent (Invitrogen, Cat. #2398613) (10:1) was prepared. Sample Buffer contains SDS, which denatures proteins and imparts a uniform negative charge [64]. Sample Reducing Agent contains dithiothreitol (DTT), which breaks disulfide bonds, enhancing protein separation and better molecular weight estimation in SDS-PAGE [65, 66]. This Sample Buffer Reducing Agent mix was added to the lysate samples (4:1). The samples were boiled (95°C, 5 minutes) and then centrifuged.

This study utilized 10-well, 18-well, and 26-well gels (Table 3.4.1). A 1X solution of 10X Tris/Glycine/SDS (TGS) (BioRad, Cat. #1610772), diluted with distilled water (dH2O), was used.

Table 3.4.1: Overview of gels utilized for SDS-PAGE

Component	Supplier	Catalogue no.
Mini-PROTEAN TGX Gels, 10-well, 50 μL	BioRad	4561094
Criterion TGX Precast Gels, 18-well, 30 μL	BioRad	5671094
Criterion TGX Precast Gels, 26-well, 15 μL	BioRad	5671095

Lysates mixed with sample buffer were loaded to the wells, with the volume adjusted based on the experiment and well comb size. The Precision Plus Protein Dual Color standard (BioRad, Cat. #1610374) was loaded onto the gel adjacent to the samples, with approximately 3 μL on one side and 1.5 μL on the other. This aids in recalling the sample order during analysis. The voltage for gel electrophoresis ranges from 150 to 180 volts, and the duration varies between 40 and 60 minutes, depending on the applied voltage (Figure 3.4.1, step 1).

Next, the separated proteins were transferred from the gel to a polyvinylidene difluoride (PVDF) membrane by semi-dry transfer, assembling a blotting sandwich, and applying an electric current [67] (Figure 3.4.1, step 2). The blotting sandwich consists of an ethanol-soaked PVDF

membrane (BioRad, Cat. #10026934) and transfer stacks (BioRad, Cat. #10026934), both soaked in 5X transfer buffer (BioRad, Cat. #10026938) diluted to 1X with distilled water. Ethanol soaking enhances protein adhesion to PVDF due to its hydrophobic properties and lack of added surfactants [67]. The transfer buffer facilitates the migration of proteins from the gel to the membrane [68].

From top to bottom, the assembly consists of the negatively charged cassette electrode (cathode), transfer stack, gel, blotting membrane, transfer stack, and the positively charged cassette (anode) (Figure 3.4.1, step 2). The transfer stacks are gently pressed with a roller to remove excess liquid and potential air bubbles. The blotting sandwich is then placed in a Trans-Blot Turbo Blotting System (BioRad, Cat. #1704150) for 10 minutes, using the predefined program "Bio-Rad High Molecular Weight (HMW)". Following the transfer, the membrane was soaked in water to rinse off salts and then in ethanol to dry. The membrane was then air-dried for at least 10 minutes. If not used immediately, the membrane was stored in tissue paper at room temperature until ready for immunoblotting.

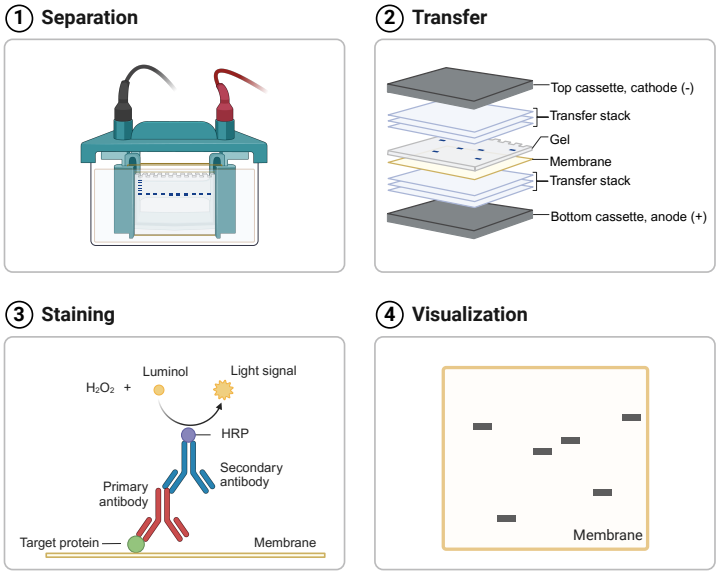

Figure 3.4.1: Methological steps of Western blotting. Step 1. The separation step in SDS-PAGE involves coating proteins with SDS to give them a uniform negative charge. They are then placed in a gel matrix with a positive electrode at the bottom. Applying electric current causes proteins to migrate through the gel. Smaller proteins move more easily, resulting in separation by size. **Step 2.** Protein transfer from the gel to the membrane is achieved using a blotting sandwich, followed by applying an electric current. **Step 3.** Proteins are stained by immunoblotting. A primary antibody binds to the target protein on the membrane, followed by a horseradish peroxidase (HRP)-conjugated secondary antibody. HRP catalyzes the oxidation of luminol in the presence of hydrogen peroxide (H_2O_2), producing a detectable chemiluminescent signal. **Step 4.** Visualization of proteins on the membrane is achieved by detecting the chemiluminescent signal produced during the HRP-catalyzed reaction. The figure was adapted from “Western Blotting Workflow” by BioRender.com (2024). Retrieved from `https://app.biorender.com/biorender-templates`.

3.4.2 Immunoblotting

The antibody incubation process aims to identify specific proteins as bands on the membrane. First, a primary antibody binds to the target protein in the membrane. Next, a secondary antibody, conjugated with horseradish peroxidase (HRP), binds to the primary antibody. HRP catalyzes the oxidation of substrates in the presence of hydrogen peroxide (H_2O_2), producing a detectable signal (see details below) (Figure 3.4.1, step 3) [69, 70].

For the preparation of the antibody dilution buffer and wash buffer, a solution was made by combining 5X Dulbecco's Phosphate Buffered Saline (PBS) (Sigma Aldrich, Cat. #D8537) diluted to 1X with distilled water and stirred with Tween 20 (Sigma-Aldrich, Cat. #P7949) in a ratio of 1000:1 (PBS-Tween). For the antibody dilution buffer, Bovine Serum Albumin (BSA) Fraction V (Sigma-Aldrich, Cat. #10735086001) was diluted in PBS-Tween to 0.05 g/L. BSA blocks non-specific antibody binding to the membrane, and Tween 20 facilitates the washing and blocking process [71, 72].

The primary antibodies were diluted in the antibody dilution buffer (PBS-Tween-BSA) according to stock concentrations. All antibodies used in the project and their dilution factors for Western blotting experiments are provided in Table 3.4.2. Membranes were cut into sections based on protein size, ensuring each section contained the protein of interest. Each section was placed into its respective chamber in a box and briefly immersed in ethanol (Prima, Antibac, Cat. #600068) for 20-30 seconds until no longer water-repellent. They were then washed with PBS-Tween for 5 minutes. The diluted primary antibodies were added to the membrane sections containing the corresponding protein of interest and placed on a shaker for 1 hour to incubate. After incubation, the membranes were washed with PBS-Tween: two quick washes followed by two 5-minute washes.

The secondary antibodies coupled to HRP are essential for detecting primary antibodies bound to target proteins on the membrane [69, 70]. Polyclonal Rabbit anti-Mouse Immunoglobulins/HRP (DakoCytomation, Cat. #P0260) and Polyclonal Goat anti-Rabbit Immunoglobulins/HRP (DakoCytomation, Cat. #P0488) are employed at a 1:5000 dilution with PBS-Tween-BSA solution. The diluted secondary antibodies were applied to the membranes: anti-mouse for membranes incubated with mouse primary antibodies and anti-rabbit for those incubated with rabbit primary antibodies. The membranes were then incubated on a shaker for at least 1 hour. Subsequently, the membranes were washed with PBS-Tween twice rapidly and four times for 5 minutes each.

3.4.3 Signal detection

The signal detection process in Western blotting visualizes specific protein bands on the membrane using chemiluminescence. This light-emitting reaction occurs when HRP interacts with the detection solution, emitting light that correlates with the protein amount, providing semi-

Table 3.4.2: Overview of primary antibodies and dilution factors utilized for Western blot. The "p" preceding the antibody names indicates phosphorylated forms.

Dilution Factor	Component	Supplier	Catalogue No.
1:1000	ERK1/2 (p44/42)	Cell Signaling Technology	9102
1:1000	FGFR1	Cell Signaling Technology	9740
1:1000	FGFR2	Cell Signaling Technology	11835
1:500	FGFR3	Cell Signaling Technology	45745
1:2000	FGFR4	Cell Signaling Technology	8562
1:1000	pERK1/2	Cell Signaling Technology	9106
1:1000	pFGFR	Cell Signaling Technology	3476
1:1000	pFGFR	Abcam	ab173305
1:500	pLKB1	Cell Signaling Technology	3482
1:1000	pPLC-γ	Cell Signaling Technology	14008
1:500	pS789-FGFR1	Gift from Nadratowska-Wesolowska	[49]
1:1000/ 1:500	RSK2	Cell Signaling Technology	5528
1:1000	RSK	BD Biosciences	610225
1:20,000	γ-tubulin	Sigma-Aldrich	T6557

quantitative data. The light signal generated by the oxidation of luminol in the presence of hydrogen peroxide (H_2O_2) offers high sensitivity (Figure 3.4.1, step 3). However, it is only semi-quantitative due to variable reaction conditions and enzyme-substrate interactions affecting the signal intensity and duration [73, 74, 75].

To prepare the signal detection solution, SuperSignal West Dura Stable Peroxide and SuperSignal West Dura Luminol/Enhancer (Thermo Scientific, Cat. #34076) were mixed 1:1. The Stable Peroxide contains H_2O_2, and the Luminol/Enhancer contains the luminol substrate. The peroxide-luminol mix was added to the membranes which were then rapidly placed into the ChemiDoc Imaging System (BioRad, Cat. #12003153) to capture clear images with minimal background noise (Figure 3.4.1, step 4). If the protein bands were weak, the membrane could be washed with PBS-Tween and incubated with a 1:1 mix of SuperSignal Maximum Sensitivity (Thermo Scientific, Cat. #34096). This might intensify the desired protein band but could also increase background noise.

The ChemiDoc imaging settings were adjusted accordingly: the “Chemiluminescent Blot” application was selected with exposure settings ranging from 2 to 480 seconds for a maximum of

96 images. The imaging process was terminated when red dots appeared, indicating signal saturation. Saturation is undesirable because it decreases the quantitative accuracy of the results, as strong signals no longer increase proportionately with protein abundance [75]. All Western blot quantifications in this study were based on signals before saturation. The "Colorimetric Blot" application was chosen for imaging the protein standard with "Rapid Auto-exposure".

The obtained images were analyzed using Image Lab 6.0 and ImageJ. Image Lab superimposed the protein standard image, indicating molecular weights, onto the image with protein bands, aiding in identifying proteins based on their molecular weights. ImageJ was used for band quantification.

Membranes can be stripped to remove previously bound antibodies using Restore Western Blot Stripping Buffer (Thermo Fisher, Cat. #21059). This involves a quick wash in the stripping buffer followed by a 5-minute incubation in the stripping buffer. After stripping, membranes are washed with PBS-Tween: two quick and two 5-minute washes. This prepares the membranes for subsequent antibody applications. Residual antibodies might remain on the membrane even after stripping, potentially affecting results. Using an antibody from a different species after stripping and selecting the next protein with a different molecular weight from the previous one reduces interference. Two gels with the same lysate were often run, one for detection with total protein and the other with the phospho-specific antibody, to avoid stripping and potential cross-reactivity between proteins of the same molecular weight. These steps ensure accurate subsequent detection.

3.5 Immunoprecipitation

Immunoprecipitation (IP) isolates a specific antigen from a complex protein mixture using an antibody and beads, while co-immunoprecipitation (co-IP) extends this method to study protein-protein interactions by co-precipitating proteins bound to the target antigen [76]. This study used co-IP to investigate RSK2 binding to FGFR tails in U2OS cell lines, using protocols with sepharose or magnetic beads, which differed mainly in bead handling procedures.

In each experiment, U2OS wild-type cells, either FGF1-stimulated or not, were included as controls. Additionally, U2OS-R1/R4 cells were either FGF1-stimulated, not stimulated, or FGF1-stimulated with MEK inhibitor added. Cells were seeded on 6 cm (Thermo Scientific, cat. #150326) or 10 cm (Thermo Scientific, cat. #150350) plates 1-2 days prior to ensure confluency on the day of the experiment. Initially, the cells were incubated in Serum-Free Media (SFM) (DMEM + GlutaMAX, Gibco, Cat. #31966-047) for 2 hours to halt signaling. In the last 30 minutes of SFM incubation, the MEK inhibitor was added to one of the plates. Subsequently, heparin sodium salt (Sigma-Aldrich, cat. # H3393) (final conc. 10 U/mL) was added to all samples, and FGF1 ligand (generously provided by Anne Gro Bergesen, produced in the Department of Molecular Cell Biology, Institute of Cancer Research) was

added (final conc. 100 ng/mL) to their designated plates. Following a 10-minute incubation period to facilitate receptor activation, the cells were subsequently lysed (detailed in section 3.2.4).

The beads used were Protein G Sepharose 4 Fast Flow resin (Cytiva, Cat. #17061801) and Dynabeads Protein G (Life Technologies, Cat. #10004D). A master mix with 20 μL of Sepharose beads (20% solution) or 25 μL of Magnetic beads (30 mg/mL) per sample was prepared. The beads were transferred to Eppendorf tubes using a pipette with a cut tip to avoid loss of beads.

The beads underwent three washes with a mix of PBS:Lysis buffer (5:1) to ensure thorough cleaning. Each washing included adding the PBS:Lysis buffer mix, shaking, and then the tubes were either placed in a magnetic rack (Invitrogen, Cat. #12321D) for magnetic beads or centrifuged briefly (approximately 30 seconds at 100 RCF) for sepharose beads, to separate the beads from the supernatant. The supernatant was removed carefully, and PBS:Lysis buffer was added to reach a total volume of approximately 1 mL. Next, the beads were loaded with 5 μL of primary antibodies: FGFR1 (Cell Signaling, Cat. #9740) or FGFR4 (Cell Signaling, Cat. #8562). The beads and antibodies were rotated at 4°C for at least 1 hour. Then, the beads were washed three times with a PBS:Lysis buffer mix, as described above, and divided into 5 Eppendorf tubes with an equal amount in each.

Following the 10-minute cell lysis, the lysates were transferred into five Eppendorf tubes, and then equal amounts of each sample/lysate were transferred to Eppendorf tubes containing the beads. Most of the lysate was used for IP. A small percentage (1-3%) of the lysate was added to separate tubes as input controls, which helped assess the IP efficiency and loading consistency by comparing receptor levels in the input and immunoprecipitated samples. The lysates were kept on ice while the lysate-antibody bead mixture was rotated for 2 hours at 4°C (Figure 3.5.1, step 1).

Following rotation, the beads were collected using a magnetic rack or by centrifugation (described above), and the supernatant was discarded. The beads underwent four washes with PBS:Lysis buffer (5:1) (Figure 3.5.1, step 2). 4X Laemmli Sample Buffer (BioRad, Cat. #1610747) was supplemented with NuPAGE™ Sample Reducing Agent, 10X (1:10). The 4X Sample Buffer was diluted to 2X with PBS. The supernatant was removed, and beads were resuspended in 2X buffer, which diluted to approximately 1X. The lysates were resuspended in 4X Sample Buffer, diluted 1:4 to achieve 1X. Then, the beads were boiled at 100°C for 10 minutes to dissociate the immunocomplexes, and the lysates were boiled at 95°C for 5 minutes. After boiling, the beads were spun down (for sepharose beads) or collected on a magnetic rack (for magnetic beads). The supernatant was collected and transferred to new Eppendorf tubes (Figure 3.5.1, step 3). The samples were either stored at -20°C until analysis or analyzed directly by Western blotting (Figure 3.5.1, step 4).

In one of the three IP experiments presented in the thesis (which used sepharose beads with

U2OS-R4 cells), Antoni Wiedlocha from the Department of Molecular Cell Biology at the Institute of Cancer Research executed the process from after-cell lysis to parts of the Western blotting.

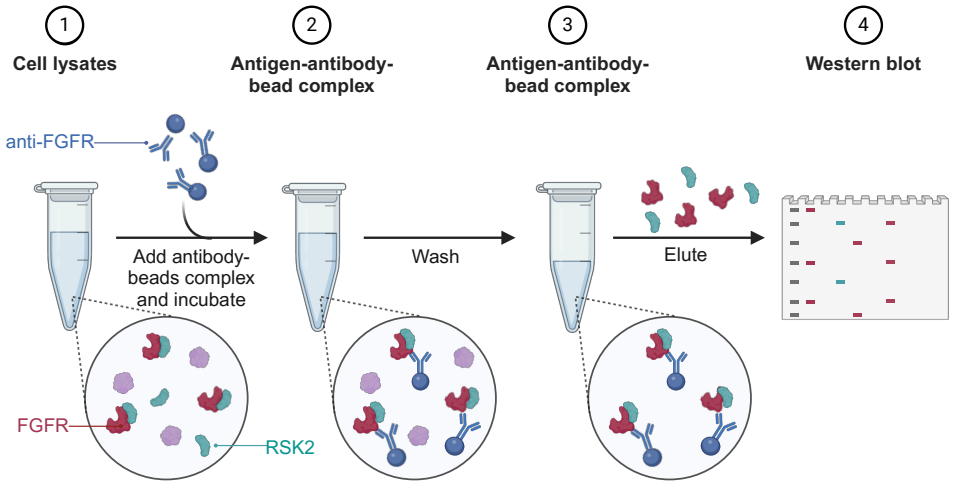

Figure 3.5.1: Methological steps of co-IP. Step 1. Cell lysate is incubated with anti-FGFR Sepharose/-magnetic beads. The FGFR primary antibodies bind to FGFR in the lysate, where RSK2 may be bound. **Step 2.** The antigen-antibody-bead complexes are washed to remove excess proteins not bound to the beads. **Step 3.** The proteins are eluted from the beads. **Step 4.** The eluted proteins are separated and visualized by Western blotting. The figure was adapted from "Immunoprecipitation Protocol", by BioRender.com (2024). Retrieved from `https://app.biorender.com/biorender-templates`.

3.6 Confocal microscopy

Confocal microscopy is a technique that uses point illumination and a pinhole to block out-of-focus light, producing high-resolution images and enabling optical sectioning for 3D reconstruction. A spinning disk confocal microscope uses a disk with multiple pinholes to scan the sample quickly, allowing for high-speed imaging while the pinholes improve image resolution. This method is particularly effective for imaging thick tissues [77].

The main protocol for the confocal microscopy experiment will here be explained in detail. However, it is important to note that there are two independent experiments that differ from this main protocol. The first experiment involves a quality assessment of the washing step using high salt low pH (HSLP) conditions. This will be further described later in this section 3.6.1 and in the results section 4.3.1. The second experiment is a quality check of the protocol itself. This experiment follows the same protocol as described below, but U2OS-R1 cells were used in conjunction only with the MEK inhibitor, detailed description in result section 4.3.2.

U2OS cells and U2OS cells stably expressing FGFRs were seeded in 12-well plates to ensure subconfluency on the experiment day. Each well contained two coverslips (High Precision Microscope Cover Glasses 10 mm, Marienfeld, Cat. #0117500). Three treatments were applied per cell line: no inhibitors, MEK inhibitor, RSK2 inhibitor, and all were stimulated with DL-

FGF1 (dylight550-FGF1, provided by Linlin Song, Department of Tumor Biology) and heparin sodium salt (Sigma-Aldrich, Cat. #H3393) (Figure 3.6.1). The experiments were conducted three biologically independent times for U2OS-R2, R3, and R4, and once for R1. In addition, U2OS wild-type cells were included as a negative control, treated similarly with DL-FGF1 and heparin, and incubated with the respective FGFR1/2/3/4 antibody followed by a labeled secondary antibody for receptor staining. The receptor staining process is described in detail later in this section. Note that U2OS wild-type cells were only included in the first experiment for each receptor.

The designated cells were treated with master mixes of CM containing inhibitors U0126 (final conc. 20 μM) and BI-D1870 (final conc. 10 μM) for 30 minutes. A master mix containing heparin (final conc. 50 U/ml) and DL-FGF1 (final conc. 100 ng/ml) in CM was prepared. For the samples treated with inhibitors, this master mix was supplemented with U0126 (final conc. 20 μM) or BI-D1870 (final conc. 10 μM). After the initial 30-minute inhibitor treatment, media was removed and all cells, including those in wells without inhibitors, were treated with the heparin-FGF1 master mix plus/minus inhibitors (final conc. 50 U/ml heparin, 100 ng/ml DL-FGF) for 20 minutes at 37 °C. This resulted in a total treatment time with inhibitors for 50 minutes (Figure 3.6.1).

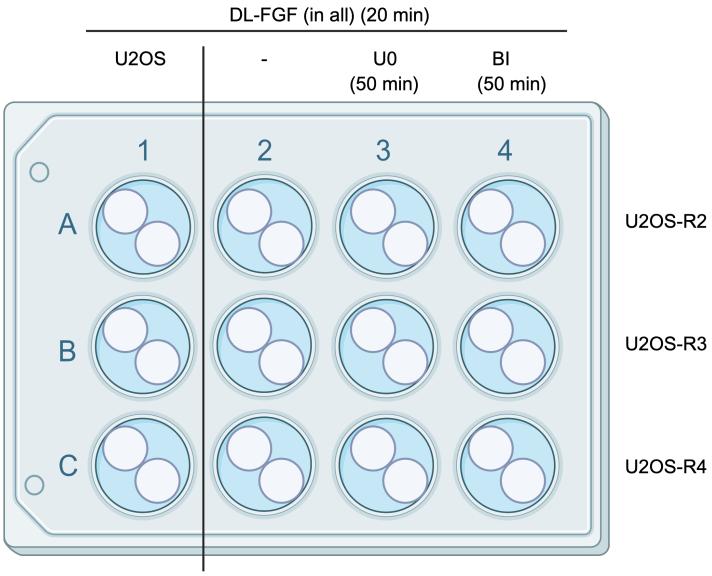

Figure 3.6.1: Example of an experimental setup for confocal microscopy. Cells were seeded in a 12-well plate with two coverslips placed in each well and treated as indicated. Created with Biorender.com.

HSLP can wash away FGF ligands bound to FGFRs on the cell surface [78]. After 20 minutes of DL-FGF1 stimulation, cells were washed twice with ice-cold HSLP buffer (Table 3.6.1) and once with cold PBS while kept on ice (Figure 3.6.2). Cells were fixed with formalin solution (10% Neutral Buffered (4% formaldehyde), Sigma-Aldrich, Cat. #HT5012-60ML) on ice under a safety hood for 15 minutes. Formalin solution acts by cross-linking proteins, effectively preserving cellular structures and preventing degradation [79]. Next, the cells were washed three times with PBS.

Table 3.6.1: HSLP buffer recipe. pH adjusted to 4 by hydrochloric acid (HCl)

Concentration	Component	Supplier	Catalogue no.
2 M	Sodium chloride (NaCl)	Subelco	1.06404.1000
20 mM	Sodium acetate (Na-acetate)	Sigma-Aldrich	S2889-250G

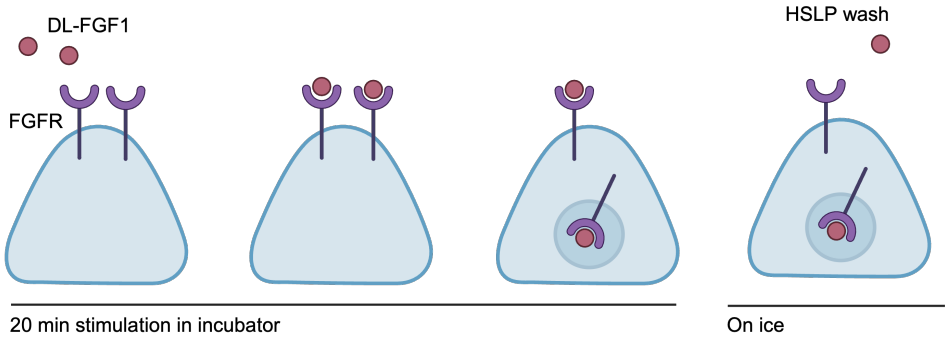

Figure 3.6.2: DL-FGF1-stimulation and HSLP washing mechanism. U2OS cells stably expressing FGFR1-4 were stimulated with DL-FGF1 for 20 minutes before being washed with HSLP to remove ligands remaining on the cell surface. Created with Biorender.com.

Antibody staining was performed to visualize the levels of FGFR1-4 in the cells. Even though the cell lines were made by selecting stably transfected clones based on receptor expression levels, cells can be heterogeneous, showing varying FGFR levels, which may influence DL-FGF1 measurements. First, the cells were permeabilized using Triton X-100 (VWR Chemicals, Cat. #28817.295) diluted in PBS (1:100) for 5 minutes at room temperature. Each cell line, including the U2OS control, was then incubated with its respective antibody and diluted in PBS as specified, see Table 3.6.2. 20 μL of the antibody-PBS solution was placed on parafilm on a damp paper. Coverslips were positioned cell-side down on the droplets and incubated for at least 20 minutes in the dark at room temperature (Figure 3.6.3). The dark environment is to prevent photobleaching of DL-FGF1. Coverslips were handled by the edges to avoid disrupting the cells.

Table 3.6.2: Overview of primary antibodies and dilution factors utilized for confocal microscopy staining. All antibodies are produced in rabbit.

Dilution Factor	Component	Supplier	Catalogue No.
1:200	FGFR1	Cell Signaling	9740
1:200	FGFR2	Cell Signaling	11835
1:100	FGFR3 (C51F2)	Cell Signaling	45745
1:200	FGFR4	Cell Signaling	8562

Each coverslip was carefully placed back into the wells of the cell culture plate with the cells facing up and washed twice with PBS. A secondary antibody, Alexa Fluor 488 anti-Rabbit antibody (Jackson, Cat. #711-545-152), diluted 1:200 in PBS, was then applied following the same protocol as the primary antibodies, with 20 μL droplets of the solution placed on parafilm. Coverslips were incubated on the droplets in the dark for at least 20 minutes (Figure 3.6.3). After incubation, coverslips were placed back into the wells and washed three times with PBS.

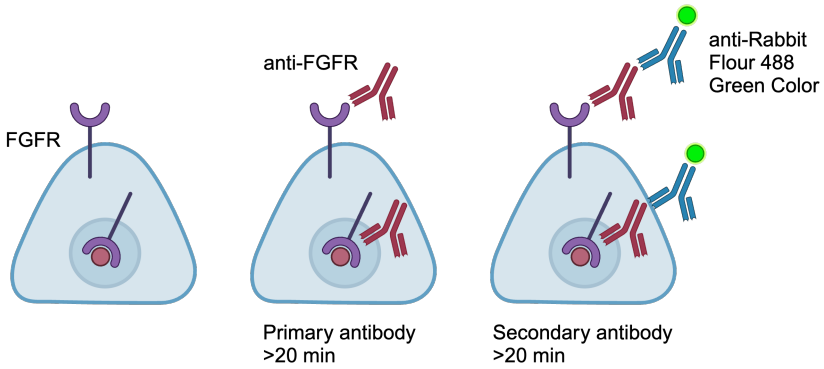

Figure 3.6.3: Mechanism of immunostaining of FGFRs. U2OS cells stably expressing FGFR1-4 were incubated with primary antibodies (anti-FGFR1/2/3/4) for 20 minutes, followed by a labeled secondary antibody (anti-Rabbit Fluor 488, green) for another 20 minutes. Created with Biorender.com.

Nuclear staining was conducted using Hoechst 33342, dihydrochloride, trihydrate (Invitrogen, Cat. #H2570). The cells were incubated with Hoechst diluted 1:10000 in PBS. 1 mL of the Hoechst solution was added to each well containing the coverslips, and the cells were incubated for 5 minutes at room temperature. To mount the coverslips, Prolong Gold antifade reagent (Life Technologies, Cat. # P36935) or Prolong Diamond antifade Mounting (Invitrogen, Cat. # P36935) was used. The Prolong reagent was carefully transferred to a new Eppendorf tube to avoid bubble formation. Droplets of 5 μL Prolong were dispensed onto object glass, one object glass at a time, to prevent premature hardening. Coverslips were then immersed in distilled water and dabbed on paper to remove excess liquid. Subsequently, each coverslip was positioned with the cells facing down on the Prolong droplet. The samples were then incubated at 37°C for approximately 30 minutes and stored in the fridge until the day of imaging.

3.6.1 HSLP quality assessment experiment

This experiment aimed to assess the effectiveness of HSLP buffer in washing away FGF ligands bound to FGFRs on the cell surface [78]. U2OS-R1, U2OS-R2, U2OS-R3, and U2OS-R4 cells were used, with two wells per cell line. Cells were incubated with two coverslips in each well of a 12-well plate with DL-FGF1 (100 ng/mL) and heparin (50 U/mL) in cold HEPES medium (a generous gift from Anne Engen, Department of Molecular Cell Biology, Institute of Cancer Research) on ice for 1 hour. HEPES was chosen for its ability to maintain stable pH conditions [80]. Following incubation, half of the cells were washed with HSLP buffer (two washes with cold HSLP and one with cold PBS), as described above, and the other half was washed three times with cold PBS. No treatments with inhibitors or antibody steps were included. The cells

were then fixed with formalin, stained with Hoechst, and mounted as described above.

3.6.2 Imaging by confocal microscopy

Nikon spinning disc confocal microscopy was used to image and quantify DL-FGF1. Two confocal microscopes with similar properties were used. Most of the experiments were performed using a Nikon ECLIPSE Ti2-E inverted microscope (Nikon Corp) equipped with a CSU-W1 dual spinning disc (50 μm pinhole) (and a 50 μm SoRa disk) confocal unit (Yokogawa Electric Corp), a two Prime BSI sCMOS cameras (Teledyne Photometrics), a laser unit with 405/488/561/638 nm lasers (120/100/100/100 mW), a multichannel LED light source (Lumencor SprectraX Chroma). The other confocal microscopy was the Nikon ECLIPSE Ti2-E inverted microscope (Nikon Corp) equipped with a CrestOptics X-Light V3 Spinning Disk confocal (50 μm pinhole) (50:250 μm) (two) Photometrics Kinetix camera, and a Lumencor Celesta laser unit with seven lasers (405/446/477/520/546/638/749 nm). The imaging was conducted using a 100X (Nikon CFI Plan Apo λ D 100X Oil NA 1.45 or Nikon CFI Plan Apo λ 100x Oil NA 1.45) objective. This objective facilitated the visualization of multiple cells within each image while ensuring high resolution for accurate quantification of DL-FGF1 uptake. Immersion Oil Type F for Microscopy (Nikon, Cat. #MXA22168) was applied to the objective before lowering the objective glass with the coverslip towards the objective.

The imaging process was performed using the NIS-Elements AR software. Lasers were selected to match the excitation maxima of the fluorophores: a 405 nm laser spinning disk 4',6-diamidino-2-phenylindole (SD DAPI) for Hoechst staining (excitation 360 nm [81]), a 488 nm laser SD green fluorescent protein (SD GFP) for Alexa 488 antibody staining (excitation 488 nm), and a 546(Crest)/561 (SoRa) nm laser SD red fluorescent protein (SD RFP) for DL-FGF1 (excitation 550 nm). In fluorescence microscopy, the fluorophore absorbs the excitation wavelength, causing it to move to an excited state. Upon returning to the ground state, the fluorophore emits light at a longer wavelength due to energy loss as heat. Single-band bandpass emission filters ensure that emitted light can be detected without interference from the excitation light and light from the other fluorophores, allowing for precise imaging of cellular components [82, 83].

First, the cells were located using the oculars by adjusting the Z-position, typically a Z-position around 5500. Once located, adjustments were made to the "Cam1Spinning Disk" to optimize image quality. A 12-bit sensitivity setting was chosen to improve the detection range, allowing for better resolution and more accurate capture of weak signals. This involved fine-tuning imaging parameters such as laser intensity and exposure time for each fluorescence channel across all biological replicates. The goal was to set parameters ensuring the emission intensity from the sample was within the dynamic range, avoiding saturation and data loss. Laser intensity typically ranged between 50% and 100% for all three lasers, with exposure times generally between 50-100 milliseconds (ms). For strong signals, exposure times occasionally dropped to

30 ms, while for weak signals, they peaked at 300 ms for Alexa488 and 800 ms for DL-FGF1. Weak fluorescent signals were common in U2OS-R3 cells, necessitating higher laser output within the specified range. Imaging parameters remained consistent for each receptor type across all treatments within each biologically independent experiment to ensure comparability.

Z-stack settings were standardized with a step size of 0.2 μm, encompassing 20 steps from -0.8 μm below to +2.3 μm above the focal plane, which was positioned just above the basal surface of the cells. The "Z-device Triggered Piezo" was activated to maintain precise Z positions and centering. During imaging, lasers were used sequentially, starting with the SD RFP laser (546/561 nm), followed by the SD GFP laser (488 nm), and concluding with the SD DAPI laser (405 nm). This sequence minimized unnecessary exposure and potential bleaching, preserving sample integrity. For each coverslip (two coverslips per treatment), generally 10 images per coverslip (20 images per treatment) were captured. For the U2OS control, only 3 images were taken for visualization, as it was assumed that minimal to no receptors would be present, and the analysis was intended to be qualitative rather than quantitative. Images were captured sequentially from one end of the coverslip to the other to ensure comprehensive coverage and avoid duplicate imaging of the same area. SD GFP was used to select areas for imaging due to its minimal bleaching effect compared to SD DAPI, which ensured an unbiased selection without knowledge of the fluorescent signal of SD RFP (DL-FGF1). Areas with Alexa488 fluorescence, indicating the presence of FGFR-expressing cells, were chosen for imaging across all treatments and cell lines. After capturing the images, the health of the cell nuclei was evaluated. Images were excluded if the nuclei appeared abnormal (e.g., not round and healthy) or artificially strong red signals were detected without corresponding receptor staining. In such cases, alternative areas were imaged.

3.6.3 DL-FGF1 quantification

Images were analyzed and quantified using NIS-Elements AR Analysis. A customized quantification pipeline was established to include the fluorescent signal from channels corresponding to SD GFP (receptor staining) and SD RFP (DL-FGF1 staining) lasers. Maximum Projection was applied to the GFP channel for visualization, while Integrate Projection was used for the RFP channel to quantify internalized DL-FGF1 levels accurately. Maximum Projection collects the brightest pixels from the image stack into a single image, while Integrate Projection sums the intensity of all pixels, providing a more accurate total fluorescence signal [84, 85].

Thresholding was performed on the Maximum Projection of GFP/receptor staining to define cell areas, with threshold values adjusted individually for each biologically independent experiment but kept constant between samples in the same experiment for each receptor (range: 118 to 140). RFP/DL-FGF1 quantification was limited to the cell regions defined by the GFP/receptor staining. For RFP/DL-FGF1 quantification, an integrated projection was followed by background subtraction (constant: 2000) and thresholding to define RFP areas (range: 118

to 2000, typically 300-800). The background subtraction value of 2000 was determined by measuring the approximate background intensity across several images, calculating an average of 100 per image, and multiplying by the number of stacks (20 stacks × 100 = 2000). This ensured that only the red signal of interest (intracellular DL-FGF1) was quantified, effectively excluding background noise. The threshold values were adjusted individually for each biologically independent experiment but kept constant between samples in the same experiment for each receptor. A verification step eliminated non-receptor-bound RFP signals, to ensure only RFP signals within GFP areas were analyzed. DL-FGF1 internalization was quantified by dividing the sum intensity of red pixels within the green-marked areas by the green surface area, yielding values per image. The pipeline is presented in the Appendix Figure A.1.

3.7 Live-cell imaging

Live-cell imaging is a technique that allows the observation of live cells over time using time-lapse microscopy. We have used Incucyte S3 microscopy (Sartorius) with phase contrast imaging. It enables the study of dynamic processes such as cell migration and proliferation in real-time without needing staining, thus preserving the cells' natural state [86]. Cell migration and proliferation were measured using live-cell imaging with the Incucyte S3 (Sartorius) and an automatic tracking program, Celltraxx. The cells were sparsely seeded on an Incucyte Imagelock 96-well Plate (Sartorius, Cat.# BA-04855) the day before stimulation and imaging.

Four cell lines, U2OS-R1, U2OS-R2, U2OS-R3, and U2OS-R4, were seeded and subjected to four different treatments: control, FGF1-stimulation (final concentration 100 ng/mL), RSK2 inhibitor (BI-D1870, final concentration 10 μM), and a combination of FGF1 and RSK2 inhibitor. For all treatments, we used serum-reduced media (1% serum) with heparin diluted to 10 U/mL to minimize signaling pathway activation while maintaining cell viability. DMSO was added at 1:1000 to the control and FGF1-treated samples to match the DMSO concentration in treatments containing inhibitors, ensuring any observed effects on proliferation were due to the specific treatments rather than DMSO toxicity. The 96-well plates were then placed in the Incucyte S3 machine, and imaging was initiated on a 10-minute schedule for 19 hours and thereafter every third hour for 69 hours. Three technical replicates were included for each condition, meaning 3 wells per treatment.

CellTraxx is an automated tool for label-free cell tracking in phase contrast images. It measures migration and proliferation, analyzing hundreds of cells per image without user interference. It identifies cell nuclei and tracks their movement from one image to the next [87]. CellTraxx can be utilized as a macro in ImageJ/Fiji to provide a user-friendly interface. The macro and the "CellTraxx User Manual," which includes detailed settings descriptions, are available at `https://github.com/borge-holme/celltraxx_download`. This study conducted single-cell random migration and proliferation experiments using CellTraxx to analyze images captured by the Incucyte S3 machine. This analysis assessed how ligand stimulation and RSK2 inhibition

affected U2OS cell behavior over time. The settings used for the analyses are listed in Appendix Table A.1.

3.8 Databases, software, and analysis

3.8.1 Databases

The Universal Protein Resource (UniProt, uniprot.org) is an open-access repository for protein sequences and functional annotations [88]. UniProt was used to identify canonical and isoform sequences of FGFR1-4.

Biological General Repository for Interaction Datasets (BioGRID, thebiogrid.org) is an open-access database resource that aggregates information on protein, genetic, and chemical interactions categorized by screening methods [89]. BioGRID was used to find and count the number of experimental studies reporting interactions between FGFR1-4 and RSK1-4 in humans.

PhosphoSitePlus (phosphosite.org) is a comprehensive resource providing experimental data on post-translational modifications [90]. PhosphoSitePlus was used to identify phosphorylation events reported in the receptor tails of FGFRs.

The Catalogue of Somatic Mutations in Cancer (COSMIC) database, sourced from various large-scale sequencing projects such as Cancer Genome Atlas (TCGA) and the International Cancer Genome Consortium (ICGC)/TCGA Pan-Cancer Analysis of Whole Genomes project (PCAWG), offers a comprehensive collection of somatic mutations found in cancer. These projects have collectively analyzed thousands of primary cancer samples across multiple cancer types to identify common mutation patterns [91, 92]. Published tumor sample sequencing data from the COSMIC database was used to identify and count mutations affecting known or potential ERK1/2 and RSK2 feedback mechanisms in FGFRs. CSV files were downloaded and analyzed using a Python script (Appendix B).

3.8.2 Software and versions

Software and versions used in this thesis are as follows: The thesis was written in Overleaf Latex (2024), and citations were managed using Zotero (Version 6.0.37). Other programs used, as mentioned in the text, include Jalview (Version 2.11.3.3) with Clustal multiple alignment function, GraphPad Prism (Version 10.2.3), Image Lab 6.0, Visual Studio Code Python (Version 3.10.2) with the Pandas extension, Microsoft Excel (Version 16.85), Fiji ImageJ (Version 2.14.0), NIS-Elements AR (Version 5.30.04), Biorender (2024), Github (2024), CellTraxx (Version 4.6), Adobe Illustrator (2022), Adobe InDesign (2022), and Adobe Photoshop (2022).

3.8.3 Statistical analysis

In some cases (as indicated), outliers were removed from the dataset. The Interquartile Range (IQR) method identifies outliers by measuring the spread of the middle 50% of data. IQR is found by subtracting the first quartile (Q1) from the third quartile (Q3). Outliers are defines as data points below Q1 - 1.5IQR or above Q3 + 1.5IQR [93].

One-Way Analysis of Variance (ANOVA) and the Tukey-Kramer test were used to compare the control group with both treatment groups and the treatments with each other. One-way ANOVA detects significant differences among three or more group means, suitable for our experiment [94, 95, 96]. If differences are found, the Tukey-Kramer test identifies which pairs of groups differ (p-value < 0.05) [94]. Due to variations in sample numbers caused by data loss (e.g., loss of one of the two coverslips as technical replicas in a confocal microscopy experiment) or the IQR method, the Tukey-Kramer test was ideal for handling unequal sample sizes [94, 95, 96].

CHAPTER

FOUR

RESULTS

To ensure the integrity of the results, all cell lines were tested for mycoplasma contamination twice: once at the beginning of their use and again towards the end. All tests were negative.

4.1 Data mining indicates a possible RSK2 mediated feedback loop for FGFRs

4.1.1 The serine phosphorylation sites by RSK2 and ERK1/2 are conserved in FGFRs

In our study, we used U2OS cells stably expressing FGFR1-4. Examining the sequences employed in the deoxyribonucleic acid (DNA) plasmid construct to create these U2OS cells, all FGFR variants are canonical except for FGFR1, which is deficient in two amino acids (Figure 4.1.1a). The Universal Protein Resource (UniProt) defines the canonical sequences by these protein IDs: P11362-1, P21802-1, P22607-1, and P22455-1. To investigate potential feedback mechanisms in FGFR2-4 similar to those in FGFR1, we aligned the canonical sequences of FGFR1-4. The alignment revealed that all four receptors have conserved serine residues at positions corresponding to the phosphorylation sites by ERK1/2 and RSK2 in FGFR1 (Figure 4.1.1b). Specifically, the YSP sequence adjacent to serine 777 (an ERK1/2 site) in FGFR1 is conserved across all receptors, which is notable because SP is a known ERK1/2 phosphorylation motif [97]. For the RSK2 site at serine 789 in FGFR1, the neighboring cysteine is conserved in FGFR2 and FGFR4 but is replaced by serine in FGFR3 (Figure 4.1.1b). This substitution in FGFR3 could indicate functional differences in phosphorylation. Experimental validation is needed to confirm whether or not the conserved sequences result in similar negative feedback loops for all FGFRs.

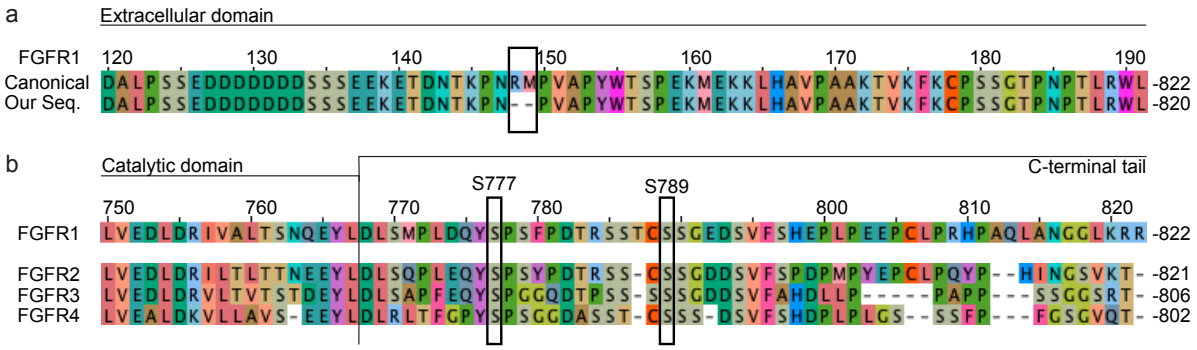

Figure 4.1.1: The serines phosphorylated by ERK1/2 and RSK2 in FGFR1 are conserved across all FGFRs, with similar flanking sequences, though FGFR3 shows the most variation. a) Alignment of the canonical FGFR1 sequence (P11362-1) with the sequence used in U2OS-R1 cells, highlighting the two amino acid differences. Only a small part of the extracellular domain is shown. b) Alignment of the canonical sequences for FGFR1-4 (P11362-1, P21802-1, P22607-1, P22455-1) from UniProt, showing conserved serines phosphorylated by ERK1/2 (S777) and RSK2 (S789). Only the C-terminal tail of the receptors are shown. The alignment was performed using Jalview with Clustal multiple alignment and visualized in Adobe InDesign. Domain definitions are based on Katoh et al. (2024) and Moes-Sosnowska et al. (2022) [11, 98].

4.1.2 RSK2 potentially binds to all FGFRs

We hypothesized that RSK2 needs to bind to FGFRs to phosphorylate them. We examined publicly available datasets on reported possible interaction partners to explore potential interactions between RSK2 and FGFRs in humans. We included the whole RSK family, which includes four isoforms: RSK1, RSK2, RSK3, and RSK4. Each isoform has two functional kinase domains separated by a linker region [58]. Due to this structural similarity, RSK2-mediated endocytosis and phosphorylation mechanisms could also apply to other RSKs. We utilized the BioGRID database, containing high-throughput and low-throughput screening data. High-throughput screenings involve large-scale experiments, whereas low-throughput screenings use specific, reliable methods like immunoprecipitation (IP) and Western blots.

All FGFRs were found to have binding interactions with RSK2, but only FGFR1 interaction with RSK2 was confirmed by several low-throughput experiments (Table 4.1.1). Note that one of the studies involving FGFR1 and RSK2 in BioGRID, classified as low-throughput, did not include data on RSK2 and was excluded from the table [99]. Interestingly, a low-throughput report indicated an interaction between FGFR3 and RSK2. In this report, it was shown that recombinant RSK2 is phosphorylated by a recombinant FGFR3 kinase domain [100]. The relevance of this study for a possible RSK2-mediated binding and phosphorylation of the C-terminal tail of the receptor is somewhat vague. Therefore, the study is labeled with an asterisk in the table. Additionally, several low-throughput screenings showed that RSK1 might bind to FGFR1. However, the reports included evidence for binding to the tyrosine kinase region of FGFR1 [101, 100].

The other interactions were either identified through high-throughput screenings or were not

assessed/reported (N/A). Taken together, interactions between RSK2 (as well as other RSK family members) and FGFRs have been reported and are likely to occur.

Table 4.1.1: Potential interaction between FGFRs and RSK family members reported in BioGRID. The table summarizes interactions between RSK1-4 and various FGFRs (FGFR1, FGFR2, FGFR3, FGFR4) based on data from the BioGRID database. RSKs are listed with their gene names in parentheses. Interactions are derived from large-scale (high-throughput) and targeted (low-throughput) experiments, encompassing different binding experiments. The number of reported experiments is indicated in parentheses. Low-throughput studies were specifically examined to determine if the experiment involved RSK binding the tail of the FGFR. If the interaction is not due to RSK binding to the tail of the FGFR, it is indicated with "*". "N/A" means not assessed. Made in Excel.

	RSK1 (RPS6KA1)	RSK2 (RPS6KA3)	RSK3 (RPS6KA2)	RSK4 (RPS6KA6)
FGFR1	Low(3)*/High(2)	Low(4)/High(4)	High(1)	N/A
FGFR2	High(2)	High(6)	High(3)	N/A
FGFR3	N/A	Low(1)*	N/A	N/A
FGFR4	High(1)	High(1)	N/A	High(1)

4.1.3 Reported phosphorylation events in the C-terminal tail of FGFRs

We have examined the alignments of receptor sequences, revealing conservation around the possible phosphorylation sites targeted by RSK2 and ERK1/2 in all FGFRs. Moreover, RSK2 potentially binds to FGFRs. Next, we investigated whether any phosphorylation events had been reported at these sites in the four FGFRs. We reviewed the phosphorylations reported on FGFR tails using the PhosphoSitePlus database, which provides experimental data on post-translational modifications. This analysis could help us understand the potential presence of an RSK2-mediated negative feedback loop in FGFRs other than FGFR1.

Phosphorylation events in the C-terminal tail of canonical receptor sequences, with a particular focus on S777 and S789 in FGFR1 and their counterparts in other receptors, were examined. We visualized the frequency of low and high-throughput references for each receptor (Figure 4.1.2). High-throughput references include data from mass spectrometry, while low-throughput references involve specific experiments such as immunoprecipitation and Western blots.

As expected, FGFR1 showed several low-throughput references for the known ERK1/2 phosphorylation at S777 and RSK2 phosphorylation at S789 [46, 49]. Similarly, the phosphorylation of S780 in FGFR2, corresponding to ERK1/2 phosphorylation at S777 in FGFR1, was also reported [45]. Interestingly, S791 in FGFR2, corresponding to the RSK2 phosphorylated serine in FGFR1, was found phosphorylated in a high-throughput study. Notably, no phosphorylations were reported for FGFR3 and FGFR4 at these positions (Figure 4.1.2).

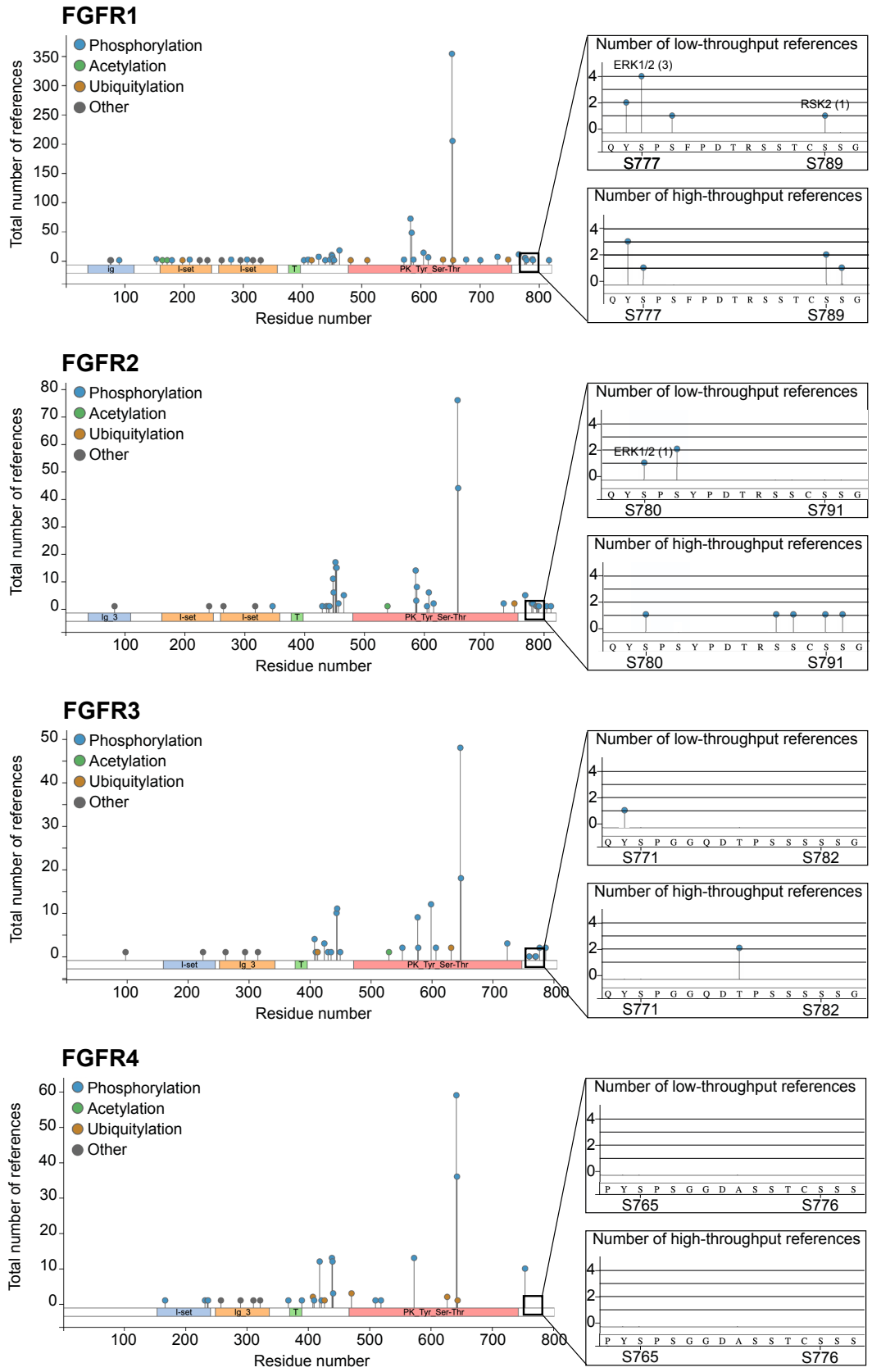

Figure 4.1.2: Phosphorylation events on possible ERK1/2 and RSK2 sites reported for FGFR1 and FGFR2. Reported phosphorylation (blue), acetylation (green), and ubiquitylation (red) sites of FGFR1-4 are shown. The receptor tail, including serine (S)777 and S789 in FGFR1 and corresponding serines in the other FGFRs, are shown to the right with reported phosphorylated sites. Low-throughput references involve specific experiments such as immunoprecipitation and Western blots. High-throughput references include data from screening, such as mass spectrometry. Data and plots are sourced from the PhosphositePlus database and visualized in Adobe Indesign.

4.2 Assessment of cell signaling upon inhibition of MEK1/2 and RSK2

We have observed conservation around the possible RSK2 and ERK1/2 phosphorylation sites in all FGFRs. Possible interactions between FGFRs and RSK2, have been reported. Moreover, a possible phosphorylation event at the predicted RSK2 site in FGFR2 was reported in addition to the previously well-documented phosphorylation events by ERK1/2 and RSK2 on the C-terminal tail of FGFR1, and by ERK1/2 on FGFR2. It is possible that the negative feedback loop mediated by RSK2 phosphorylation for FGFR1 also applies to the other FGFRs. Since prevention of RSK2 phosphorylation led to reduced FGFR endocytosis, our next step is to investigate changes in endocytosis and internalization for FGFR2, 3, and 4 upon RSK2 inhibition. For this we will use U2OS cells stably expressing FGFR1-4 (U2OS-R1, -R2, -R3, and -R4). Before these main experiments, it's essential to validate FGFR expression, ligand-induced receptor phosphorylation, MAPK pathway activation, and the functionality of MEK1/2 (U0126) and RSK (BI-D1870) in these cell lines. This validation was performed using Western blotting. All cells were serum starved to turn off possible signaling before the cells were either left untreated or treated with FGF1 in the presence or absence of MEK1/2 or RSK2 inhibitors. Inhibitors were added 30 minutes before FGF1-stimulation to ensure proper inhibition, and cells were stimulated for 10 minutes with FGF1. FGFR levels and their activation, as well as the efficiency of the MEK1/2 and RSK2 inhibitors, were analyzed by Western blotting.

4.2.1 U2OS cell lines express FGFRs, activate MAPK pathway upon ligand stimulation, and respond to MEK1/2 and RSK2 inhibitors

First, we tested U2OS wild type and U2OS stably expressing FGFR1 for FGFR1 expression and reaction to ligand stimulation and inhibitors. In later experiments, U2OS-R1 cells will be used as a positive control and U2OS cells as a negative control. Since U2OS wild type has some endogenous FGFR expression, it is important to determine if FGF ligand stimulation induces detectable signaling (i.e., phosphorylated (p)-FGFR and downstream molecules) in U2OS as well. Detection of pFGFR revealed phosphorylation exclusively in U2OS-R1, affirming FGFR1 activation (Figure 4.2.1). Additionally, FGFR activation was assessed by examining downstream signaling phosphorylation. PLC-γ binds 1:1 to FGFRs upon FGFR stimulation [102]; hence, phosphorylated PLC-γ (pPLC-γ) serves as a reliable marker reflecting FGFR activation. The phosphorylation of PLC-γ confirmed ligand-induced receptor phosphorylation in U2OS-R1, which is evident by stronger bands in FGF1-stimulated samples compared to unstimulated U2OS-R1 cells (Figure 4.2.1). Conversely, minimal to no bands were observed in the U2OS cell line, validating pPLC-γ as an effective measure for testing FGFR activation.

The MAPK pathway amplifies the signal in a kinase cascade [103]. Thus, compared to pPLC-γ, which binds 1:1, any small signaling event will be amplified. This might explain the presence of phosphorylated ERK1/2 (pERK1/2) and phosphorylated LKB1 (pLKB1), downstream molecules in the MAPK pathway, in both U2OS and U2OS-R1 cells (Figure 4.2.1). The functionality of the MEK1/2 inhibitor (U0126, U0) was evident as the downstream pERK1/2 band

disappeared upon inhibitor addition. Similarly, the RSK2 inhibitor (BI-D1870, BI) reduced the band corresponding to pLKB1 to background levels (no stimulation). As anticipated, LKB1 phosphorylation was also reduced to background levels upon the addition of U0 (Figure 4.2.1), given that LKB1 lies downstream of MEK1/2 and RSK2. This confirms the efficiency of the inhibitors. γ-tubulin served as a loading control. In summary, U2OS-R1 cells are activated by FGF1-stimulation. The U2OS cell line exhibited weak FGFR expression, as evidenced by the absence of pFGFR/FGFR1 but induction of FGF1-stimulated activation of MAPK signaling. More importantly, the inhibitors were functional at the concentrations tested.

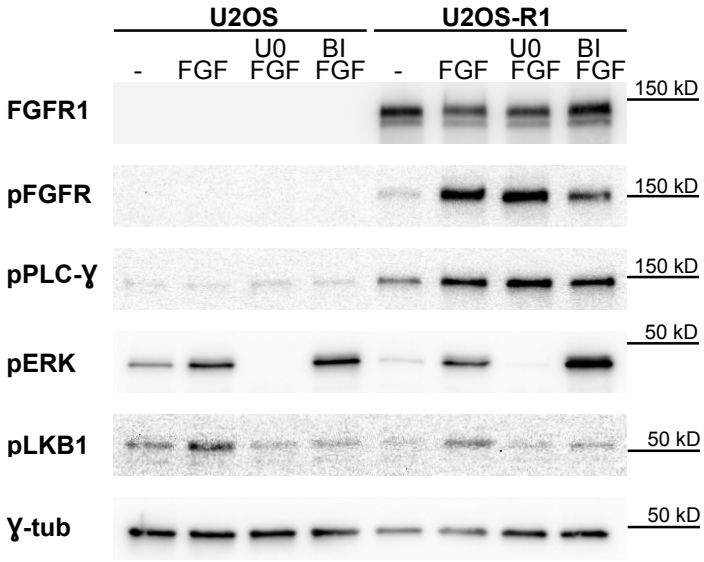

Figure 4.2.1: FGF1-induced MAPK signaling in U2OS-R1 are efficiently reduced by MEK1/2 and RSK2 inhibitors. U2OS and U2OS-R1 cells were serum-starved for 1 hour in SFM, with MEK1/2 inhibitor U0126 (U0, 20 μM) and RSK inhibitor BI-D1870 (BI, 10 μM) added during the final 30 minutes. Cells were stimulated with FGF1 (100 ng/mL) for 10 minutes, lysed, and analyzed by SDS-PAGE/Western blot using the listed antibodies. Phosphorylated forms are indicated with a p in front of the antibody name. Images were contrast-adjusted in Fiji ImageJ and visualized in Adobe InDesign.

Having evaluated U2OS and U2OS-R1 under ligand stimulation and inhibitor treatment, we wanted to conduct the same analysis for FGFR2-4. Cells were treated similarly as described above. Briefly, all cells were serum starved and either left untreated or treated with FGF1 in the presence or absence of MEK1/2 or RSK2 inhibitors and analyzed by Western blotting. The Western blot membranes were incubated with suitable antibodies for each cell line, FGFR1-4 and pFGFR (recognizing all FGFRs). Results indicated expression of the designated FGFR in the cell lines (Figure 4.2.2). Note that the levels of receptors are not directly comparable since the antibodies might bind with different affinity, the exposure time varies from cell line to cell line, and each image has been contrast-adjusted to optimize visualization. However, the difference between the treatments within each cell line is comparable and was therefore quantified for easy visualization.

For pFGFR, allowing direct detection of the phosphorylation status of the individual receptors, bands were only increased with FGF1 in the case of FGFR1 and FGFR2. Therefore, identifying the correct band for pFGFR in FGFR3 and FGFR4 samples was challenging; see marked stars

in the top right corner in Figure 4.2.2. This could have been caused by low receptor levels or the possibility that pFGFR does not recognize FGFR3 and 4 very well. As stated previously and seen in Figure 4.2.1, PLC-γ can reflect FGFR activation. Phosphorylation of PLC-γ confirmed ligand-induced receptor phosphorylation for all cell lines, although weaker in FGFR3 and FGFR4 sample (Figure 4.2.2).

Evaluation of MEK1/2 inhibitor (U0) functionality showed the absence of downstream phosphorylated ERK1/2 in treated samples, confirming inhibitor efficacy. Evaluation of RSK inhibitor (BI) functionality demonstrated decreased phosphorylation of the downstream substrate LKB1 in inhibitor-treated samples compared to FGF1-stimulated, indicating functional inhibition of RSK2 (Figure 4.2.2). γ-tubulin served as a reference protein for normalization in quantification analysis.

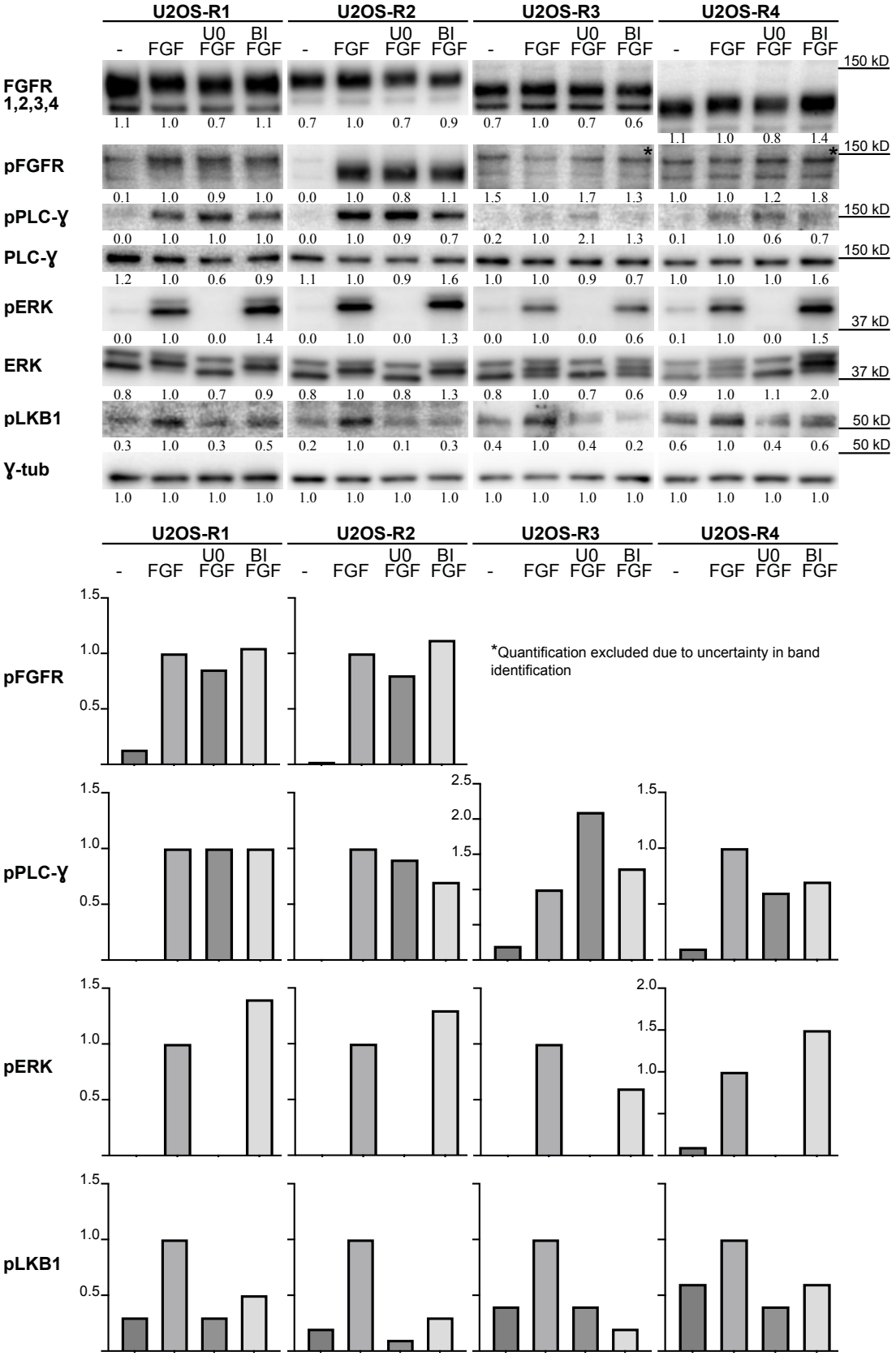

Figure 4.2.2: FGF1-induced MAPK signaling are efficiently reduced by MEK1/2 and RSK2 inhibitors for all FGFRs. U2OS and FGFR1-4 expressing U2OS cells were serum-starved for 1 hour in SFM, with MEK1/2 inhibitor U0126 (U0, 20 μM) and RSK inhibitor BI-D1870 (BI, 10 μM) added during the final 30 minutes. Cells were stimulated with FGF1 (100 ng/mL) for 10 minutes, lysed, and analyzed by SDS-PAGE/Western blot using the listed antibodies. Phosphorylated forms are indicated with a p in front of the antibody name. Images were contrast-adjusted in Fiji ImageJ and visualized in Adobe InDesign.

4.3 RSK2 inhibition reduces FGFR2 and FGFR4 but not FGFR3 internalization

4.3.1 HSLP removes bound ligands from cell surface receptors

After confirming that the inhibitors are efficient in all four FGFR cell lines, we wanted to examine the internalization of FGFRs upon inhibition of RSK2 using both U0126 and BI-D1870. For this purpose, we wanted to use confocal microscopy and quantify the uptake of FGF1 labeled with a fluorophore DL-FGF1 in FGFR-expressing U2OS cells. To ensure that the DL-FGF1 signal observed in the microscope solely represents the portion of FGF1 that has been internalized along with its receptor and is not present on the cell surface or extracellularly, we used a high salt low pH buffer (HSLP). HSLP buffer can wash away FGF ligands bound to FGFRs on the cell surface [78]. Thus, confirming that HSLP effectively removes ligands bound to all four FGFRs on the cell surface was essential.

To achieve this, all four FGFR-expressing cells were incubated with DL-FGF1 on ice to allow binding to the cell surface while preventing internalization. Subsequently, the cells underwent two treatments: washing with HSLP followed by a single wash with PBS, designated for the endocytosis experiment, or washing with only PBS. The latter served as a control, where, theoretically, the ligand should remain bound to the receptor on the cell surface while the ligand should be lost with the HSLP wash. The cells were then imaged by confocal microscopy. Stacks of 20 images and Maximum Projection for visualization purposes were used (Figure 4.3.1). Results indicated that cells washed with PBS retained the ligand in patterns resembling cell surfaces. In contrast, cells washed with HSLP showed minimal to no DL-FGF1, suggesting efficient removal of surface-bound ligands. These findings indicate that HSLP efficiently removes ligands bound to cell-surface receptors across all four FGFR-expressing cell lines.

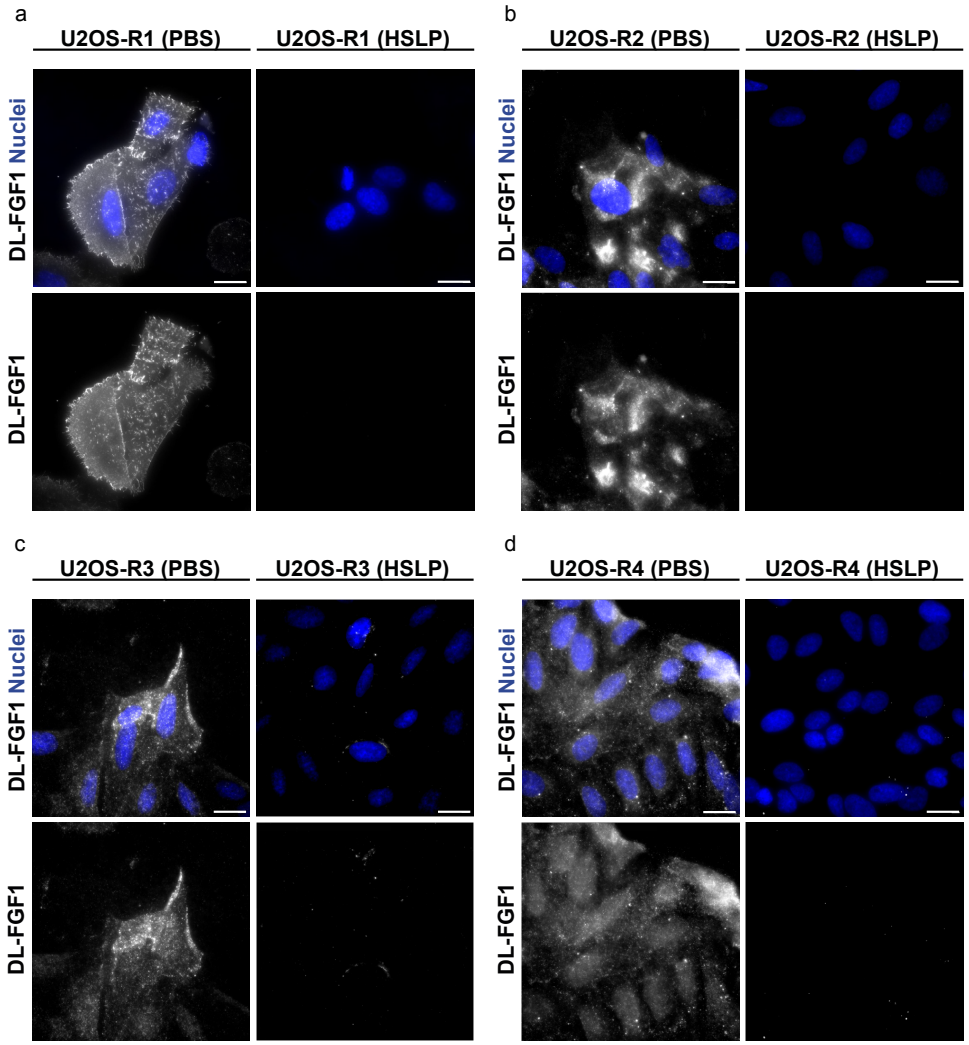

Figure 4.3.1: HSLP effectively removes surface-bound DL-FGF1 from U2OS cells expressing FGFR1-4 (a-d). U2OS cells expressing individual FGFRs were grown on coverslips and incubated with DL-FGF1 (final conc. 100 ng/mL) and heparin (50 U/mL) in cold HEPES medium on ice for 1 hour. Subsequently, cells were washed twice with HSLP and once with PBS or thrice with PBS. Confocal microscopy imaging was conducted to visualize DL-FGF1 (in grayscale) and nuclei (in blue). Maximum Projection was applied to Z-stacks of 20 sections covering the entire cells. The images were taken with identical settings, and consistent contrast settings were maintained during image processing. Images were contrast-adjusted in Fiji ImageJ and visualized in Adobe InDesign. Scale bar, 20 μm.

4.3.2 Confirming regulation of FGFR1 by RSK2 phosphorylation by confocal microscopy

Previous research has demonstrated that RSK2 phosphorylates FGFR1 on serine 789. Inhibition of RSK2 activity has been shown to reduce FGFR1 endocytosis, leading to prolonged signaling activity [49]. This study used confocal microscopy to visualize FGF1 internalization using fluorophore-labeled FGF1. Results revealed a significant reduction in internalized FGF1 in FGFR1-expressing cells pretreated with RSK2 (BI-D1870) or MEK1/2 (U0126) inhibitors, highlighting the regulatory role of RSK2 in FGFR1 endocytosis.

The primary objective of this study is to assess whether RSK2 exhibits similar effects on the other three FGFRs: FGFR2, FGFR3, and FGFR4. First, the effectiveness of the experimental set-up was evaluated by aiming to replicate the results obtained in the above-mentioned

study for FGFR1. An experiment similar to the one in the FGFR1 study was performed to achieve this. U2OS-R1 and U2OS cells underwent stimulation with DL-FGF1. In addition, U2OS-R1 cells were also treated with MEK1/2 inhibitor (U0). Following stimulation, the cells underwent HSLP wash to remove surface-bound DL-FGF1 before fixation. FGFR1 was then stained using an FGFR1 antibody, while nuclei were stained with Hoechst dye. The cells were then examined by confocal microscopy. Note that all images were taken with the same settings and that the same image adjustments were performed on all images, allowing direct comparison.

Internalized DL-FGF1 was detected in U2OS-R1 cells but not in U2OS cells (Figure 4.3.2a). This indicates that the DL-FGF1 detected was specifically internalized by FGFR1. The FGFR staining was also only visible in the FGFR1-expressing cells, indicating that the cells express FGFR1 and that the detected signal is specific. Furthermore, the results demonstrate a reduction in internalized DL-FGF1 when cells were treated with the MEK1/2 inhibitor compared to control cells, which were U2OS-R1 cells stimulated with the ligand alone. This contrast is evident in the grayscale images representing internalized FGF1 in Figure 4.3.2a, lower panel, where control cells exhibit higher levels compared to those treated with the MEK1/2 inhibitor. Quantification analysis confirmed a noticeable decrease in internalized FGF1 (Figure 4.3.2b).

These findings established that this protocol can be used to investigate RSK2 mediated endocytosis in FGFR2, FGFR3, and FGFR4-expressing cells. This will provide valuable insights into the regulatory mechanisms of FGFR signaling pathways.

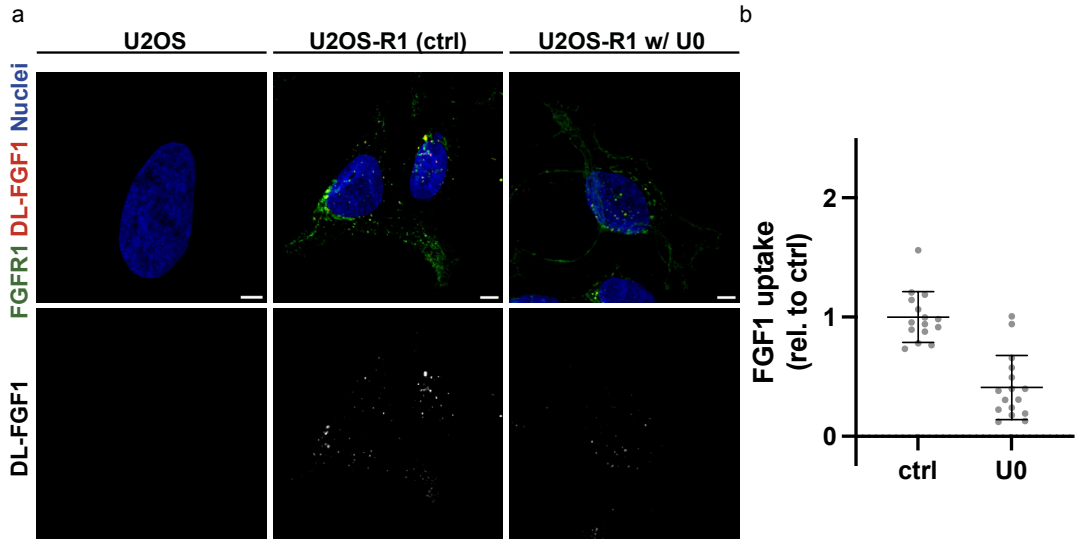

Figure 4.3.2: MEK1/2 inhibition leads to decreased FGFR1 internalization. U2OS and U2OS-R1 cells were subjected to MEK1/2 inhibitor treatment (U0126, U0) (final conc. 20 μM), for 50 minutes, followed by stimulation with heparin (50 U/mL) and DL-FGF1 (final conc. 100 ng/mL) for the last 20 minutes. After washing with HSLP buffer and fixation, the cells were stained with FGFR1 antibody to detect FGFR1, and nuclei were stained with Hoechst dye. Confocal microscopy images were captured as Z stacks of 20 images. The images were taken with identical settings and consistent contrast settings were maintained during image processing **a)** Maximum projections for all color channels with identical contrast settings are shown. The upper row shows FGFR1 (green), nuclei (blue), and DL-FGF1 (red); the lower row shows DL-FGF1 only (grey). Representative images are shown. Scale bar, 5 μm. **b)** The images were quantified using NIS elements. For quantification, 8 images from 2 coverslips per treatment were obtained. FGFR1 staining defined the cell area and the DL-FGF1 intensity within this area was measured by integrate projection, subtracting, and removing background noise. The total DL-FGF1 intensity in each image was divided by the total cell area and normalized to the mean of the control (U2OS-R1 stimulated with DL-FGF1). Each data point represents the normalized ratio from one image, with mean and standard deviation indicated. n=1. Outliers were removed by the IQR method. Images were contrast-adjusted in Fiji ImageJ and visualized in Adobe InDesign.

4.3.3 Reduced internalization of DL-FGF1 in FGFR2 and FGFR4 cells upon RSK2 inhibition, while FGFR3 endocytosis seems unaffected

Having validated previous research indicating reduced internalization of FGFR1 upon RSK2 inhibition, we utilize our protocol to determine whether RSK2 mediated endocytic downregulation also occurs with FGFR2, FGFR3, and FGFR4. With MEK1/2 and RSK2 inhibitors validated in all FGFR-expressing U2OS cells (Figure 4.2.2), alongside effective HSLP washing (Figure 4.3.1) and assay functionality for quantifying FGFR internalization in U2OS-R1 (Figure 4.3.2), we believe we can detect potential RSK2 involvement in FGFR2, 3, and 4 endocytosis with this assay.

Therefore, we conducted a similar assay with the other U2OS-FGFR cells (as in section 4.3.2). RSK2-specific inhibitors (BI) were used alongside the MEK1/2 inhibitor (U0). As MEK1/2 inhibition leads to the inhibition of many downstream targets besides RSK2, direct inhibition of RSK2 is important for the interpretation of the results. Moreover, similarities or differences in the effects of the two inhibitors on FGF internalization could suggest the involvement of

ERK1/2 or other factors in the process.

Wild-type U2OS cells, not overexpressing any FGFR, were included and subjected to the same treatments as the U2OS cells expressing the different FGFRs. U2OS were only included in the first biological experiment for all FGFRs (FGFR2-4). This was implemented to ensure that the receptor staining and the DL-FGF1 uptake were specific.

The endocytic uptake of DL-FGF1 was evaluated in all cell lines. The experiment was conducted in three biologically independent experiments. Cells were sourced from different culture flasks for each replicate, followed by a new round of seeding, stimulation, and confocal imaging. This approach was taken to ensure the reliability and reproducibility of the results. Moreover, the microscopy settings were kept the same for all conditions in each experiment for each receptor type. To avoid bias, areas to image on the coverslips were selected randomly but with the criteria that a visible descent amount of receptor staining was present.

In the case of FGFR2, treating cells with either the MEK1/2 inhibitor (U0) or the RSK2 inhibitor (BI) led to a decrease in internalized DL-FGF1 levels compared to U2OS-R2 cells stimulated solely with the ligand (Figure 4.3.3a-b). This is evident in the grayscale images showing more internalized DL-FGF1 in U2OS-R2 cells over time than in U2OS-R2 cells treated with either of the inhibitors. U2OS cells showed little to no FGFR2 staining, indicating specific FGFR2 staining in U2OS-R2. Moreover, no FGF1 was detected in the U2OS cells, confirming the specificity for FGFR2 in U2OS-R2 cells (Figure 4.3.3a). Quantification of the internalized DL-FGF1 (relative to FGFR2 receptor area per image) across the three U2OS-R2 treatments showed that both inhibitors significantly reduced FGF1 uptake. Specifically, the MEK1/2 inhibitor reduced FGF1 uptake to about 10%, and the RSK2 inhibitor reduced it to around 20%, compared to the U2OS-R2 control (Figure 4.3.3b). Although there was a small difference in FGF internalization between U0 and BI, it was not insignificant, suggesting that no downstream substrate to MEK1/2 other than RSK2 induces endocytosis for FGFR2. Significant decrease in FGFR2 internalization with RSK2 inhibition demonstrates that FGFR2 endocytosis depends on RSK2 activity, similarly to FGFR1.

In the case of FGFR3, the results indicate no change in internalized FGFR3 levels when cells were treated with either the MEK1/2 inhibitor (U0) or the RSK2 inhibitor (BI) compared to U2OS-R3 cells stimulated solely with the ligand (Figure 4.3.3c-d). This suggests that functional RSK2 may not be necessary for FGFR3 internalization. Some FGFR3 antibody staining was observed in the U2OS cell line, indicating background, but no DL-FGF1 signal was detected. The uptake of DL-FGF1 in U2OS-R3 cells was generally poor, likely due to low FGFR3 levels in these cells. However, despite the low uptake, the grayscale DL-FGF1 visualization in Figure 4.3.3c reveals that some FGF1 ligands were internalized across all treatments. Although the internalization rate is generally low, it exceeds that of the U2OS control, suggesting that the detected signal is specific for FGFR3. Quantification revealed that neither the MEK1/2

nor the RSK2 inhibitor significantly altered FGF1 uptake in U2OS-R3 cells (Figure 4.3.3d). It appears that FGFR3 endocytosis is not dependent on active RSK2, unlike FGFR1 and FGFR2.

Similar to U2OS-R2 cells, FGFR4-expressing cells showed a significant decrease in internalized DL-FGF1 levels when treated with either the MEK1/2 inhibitor (U0) or the RSK2 inhibitor (BI) compared to the U2OS-R4 control (Figure 4.3.3e-f). Both inhibitors significantly reduced FGF1 uptake, with the MEK1/2 inhibitor reducing uptake to approximately 30% and the RSK2 inhibitor to around 35% of control levels (Figure 4.3.3f). This significant decrease in FGFR4 internalization with RSK2 inhibition by both inhibitors indicates that FGFR4 endocytosis depends on RSK2 activity, similarly to FGFR1 and FGFR2.

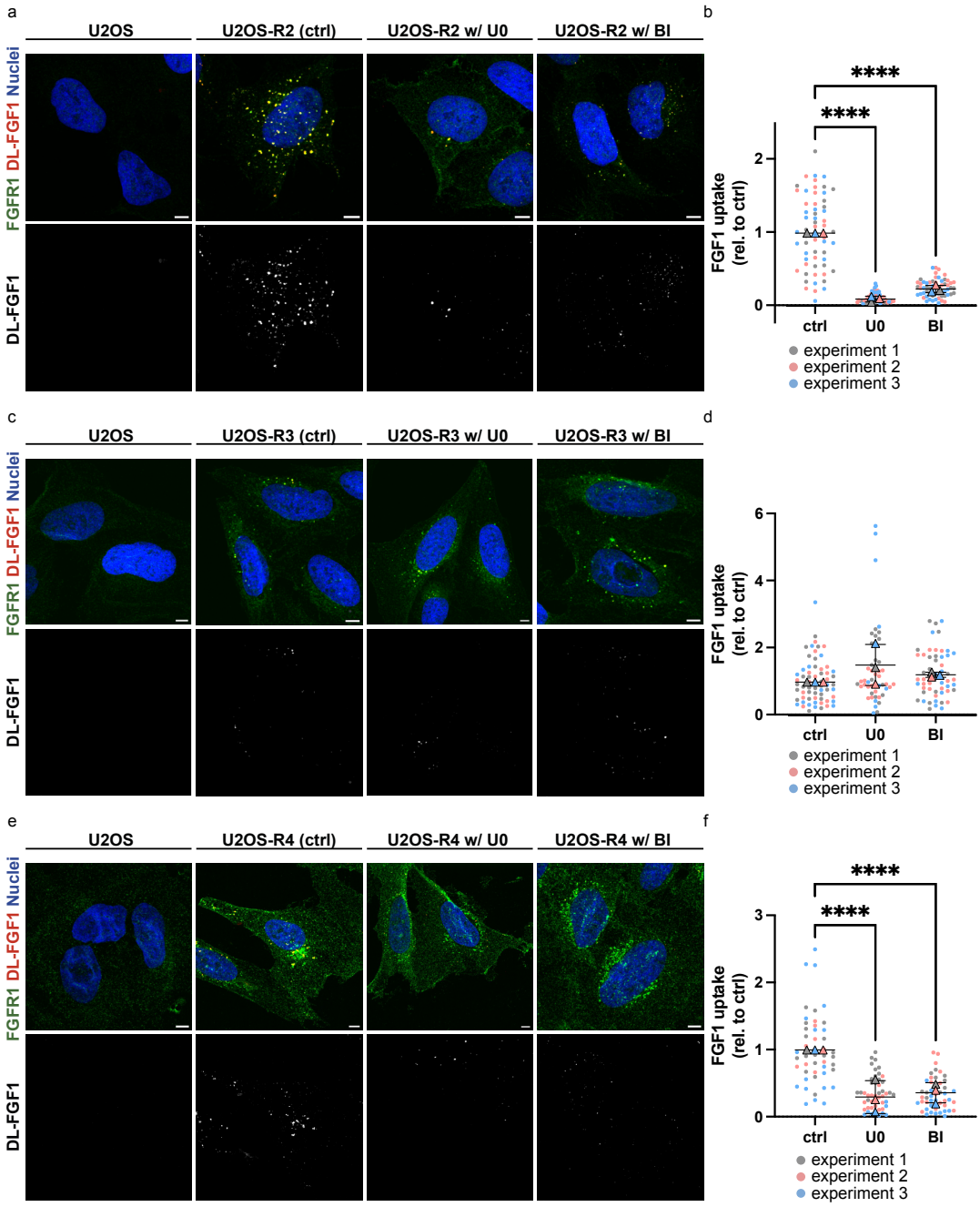

Figure 4.3.3: MEK1/2 and RSK2 inhibition on FGF1-induced FGFR2 (a-b) and FGFR4 (e-f) results in decreased receptor internalization, whereas FGFR3 (c-d) remains unaffected. Cells were treated with MEK1/2 inhibitor (U0126, U0) (20 μM) or RSK2 inhibitor (BI-D1870, BI) (10 μM) for 50 minutes, followed by stimulation with heparin (50 U/mL) and DL-FGF1 (100 ng/mL) for 20 minutes. After HSLP washing and fixation, cells were stained with FGFR2, FGFR3, or FGFR4 antibodies, and nuclei were stained with Hoechst dye. Confocal microscopy images were captured as Z stacks of 20 images. **a,c,e)** Maximum projection images for all color channels with identical contrast settings are shown. The upper row shows FGFR1 (green), nuclei (blue), and DL-FGF1 (red); the lower row shows DL-FGF1 only (grey). **b,d,f)** For quantification, 10 images per 2 coverslips per treatment were obtained for U2OS-FGFR treatments and quantified using NIS-elements. FGFR staining defined the cell area, and the DL-FGF1 intensity within this area was measured by integrate projection, subtracting, and removing background noise. The total DL-FGF1 intensity in each image was divided by the total cell area and normalized to the mean of the control (U2OS-R2,3,4 stimulated with DL-FGF1). Each data point represents the normalized ratio from one experiment, with mean and standard deviation indicated. Outliers were removed by the IQR method. n=3. Raw data were analyzed using one-way ANOVA with Tukey's multiple comparisons test. * = $p < 0.05$, **** = $p < 0.0001$. Images were contrast-adjusted in Fiji ImageJ and visualized in Adobe InDesign.

4.4 Binding of RSK2 to FGFRs by immunoprecipitation was detected with U2OS-R1 but not U2OS-R4

Next, we aim to investigate whether RSK2 binds to FGFR2-4 in cell lines expressing the different FGFRs. Previous studies have shown that RSK2 binds to the receptor tail of FGFR1 through high and low-throughput screening methods (Table 4.1.1). RSK2 was identified through immunoprecipitation to bind to FGF1-stimulated FGFR1, but this was not evident in the absence of FGF1-stimulation [49]. This suggests that upon FGF ligand stimulation, RSK2 binds to the receptor tail following activation through the MAPK pathway. We aimed to investigate whether this was the case for the other FGFRs. Co-IP assays were conducted using U2OS-R1 cells with sepharose beads and U2OS-R4 cells with sepharose and magnetic beads. Treatments included non-stimulated and FGF1-stimulated conditions with and without additional treatment of the MEK1/2 inhibitor (U0126, final concentration 20 μM) for FGFR-expressing U2OS cells.

4.4.1 Binding of RSK2 to FGFR1 detected upon ligand stimulation

We first aimed to replicate previous findings on RSK2 binding to the FGFR1 receptor tail, as in Nadratowska-Wesolowska et al. (2014) reported [49]. Western blots of the immunoprecipitated material showed strong bands for FGFR1 in U2OS-R1 cells, confirming successful capture, while no bands were detected in U2OS cells (Figure 4.4.1, right panels). For RSK2, faint bands were observed in the IP for U2OS-R1 cells, slightly stronger in the two ligand-stimulated samples compared to the unstimulated sample. The RSK2 bands were much more prominent in the lysate (3% of input) than in the IP (Figure 4.4.1). The RSK2 antibody recognized two bands: the upper band, representing RSK2, and the lower band as background. This was confirmed by an experiment conducted by Ellen Margrethe Haugsten from the Department of Tumor Biology, where targeting RSK2 with small interfering (siRNA) eliminated the upper band, identifying it as RSK2, while the lower band remained as background noise (Appendix Figure D.1). siRNA works by targeting specific mRNA molecules for degradation, thereby preventing the production of specific proteins [104].

Unexpectedly, RSK2 was detected in MEK1/2 inhibited samples, contrary to the hypothesis that non-phosphorylated RSK2 would not bind to the FGFR1 tail and thus not be co-immunoprecipitated. The original study did not detect RSK2 bands in MEK1/2 inhibited samples [49]. To confirm MEK1/2 inhibitor functionality, we checked ERK1/2 phosphorylation (pERK1/2) and found no phosphorylation when MEK1/2 was inhibited, indicating effective inhibition of both MEK1/2 and RSK2 (Figure 4.4.1).

Next, we investigated if serine 789 in FGFR1, the phosphorylation site for RSK2, showed phosphorylation in response to FGF1-stimulation using a specific antibody for phosphorylated serine 789 (pS789) [49]. A stronger band at the expected molecular weight in FGF1-stimulated

samples suggested phosphorylation, although weak bands were observed in all samples. This suggests detectable binding between FGFR1 and RSK2 and possible phosphorylation of FGFR1 at S789 in this assay.

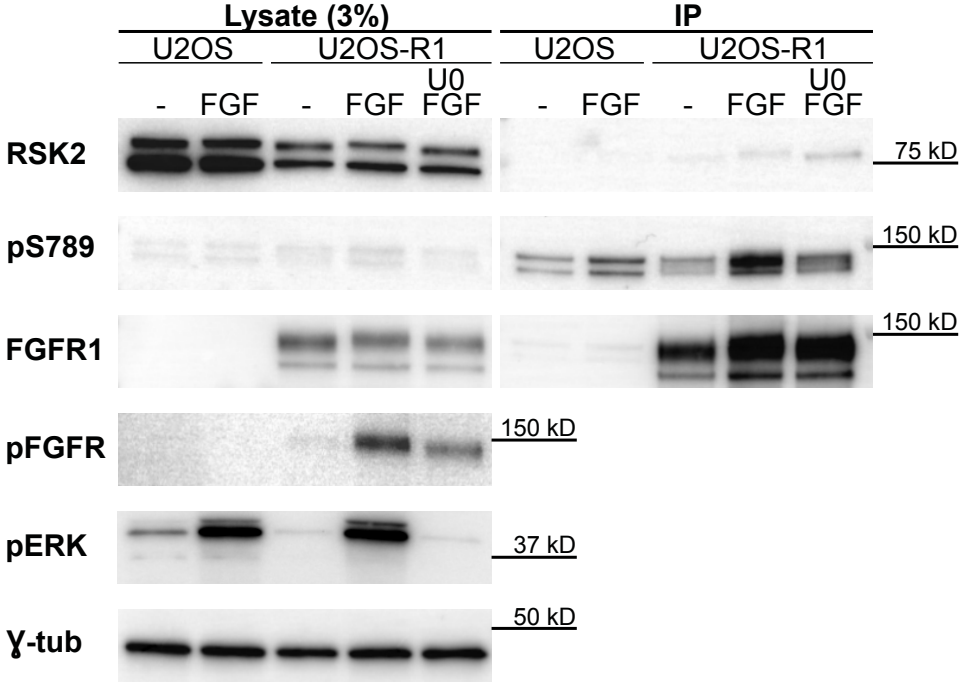

Figure 4.4.1: Immunoprecipitation of FGFR1 and co-immunoprecipitation of RSK2 in U2OS-R1 cells, including conditions with RSK2 inhibition. Cells were serum-starved for 2 hours, with the addition of the MEK1/2 inhibitor (U0126, final conc. 20 μM) during the last 30 minutes, followed by stimulation with FGF1 (final conc. 100 ng/ml) and heparin (50 U/ml) for 10 minutes. U2OS cells with and without FGF1-stimulation were included as controls. Subsequently, the cells were lysed, and the lysates were incubated with sepharose beads coupled to the FGFR1 antibody. The lysates (3% of IP) and immunoprecipitates were subjected to Western blotting using designated antibodies. γ-tubulin (γ-tub) is the loading control. The "p" preceding the antibody names indicates phosphorylated forms. Images were contrast-adjusted in Fiji ImageJ and visualized in Adobe InDesign.

4.4.2 Binding of RSK2 to FGFR4 was not detected

Since we could detect binding between FGFR1 and RSK2, we wanted to continue testing if RSK2 binds to the other FGFRs. We increased the number of cells used for the first attempt compared to the previous experiment (cell confluency on 6 cm plates to 10 cm plates). We also included the addition of the RSK2 inhibitor (BI-D1870, final conc. 10 μM). Strong bands for immunoprecipitated FGFR4 were detected in U2OS-R4 cells, confirming successful capture, while no bands were detected in U2OS cells as expected (Figure 4.4.2a, right panels). However, RSK2 was not detected in the IP. It also appears absent in the lysate, as the upper band is missing, leaving only the strong background band. The upper band corresponds to the molecular weight of the band that disappears with RSK2 knockdown (Appendix Figure D.1). Additionally, RSK2 should be around 90 kDa [105] (Figure 4.4.2a, left panels).

Since RSK2 binding to FGFR4 was not detected, we aimed to improve the experiment by using magnetic beads instead of sepharose beads. In this case, immunoprecipitated FGFR4 was also

successfully detected in U2OS-R4 cells. Despite using two different RSK antibodies, RSK2 was only detectable in the lysate, appearing as a faint upper band (Figure 4.4.2b, upper panels). This indicates a lack of RSK2 co-immunoprecipitation with FGFR4. In this experiment, we did not confirm RSK2 binding to FGFR4. However, we again confirmed that the MAPK signaling pathway was active upon FGF1-stimulation and repressed with U0126 treatment (Figure 4.4.2b, pERK1/2 panel).

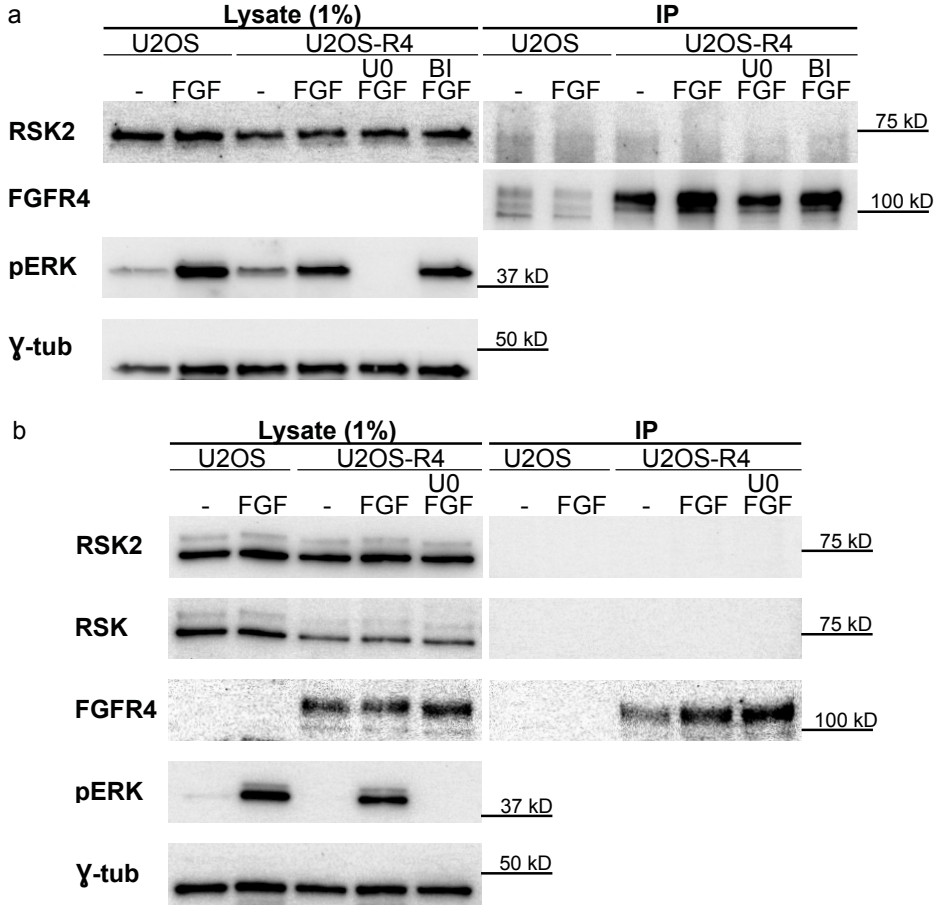

Figure 4.4.2: Co-immunoprecipitation of FGFR4 and RSK2 not detected. U2OS-R4 cells were serum-starved for 2 hours, with the addition of the MEK1/2 inhibitor (U0126, final conc. 20 μM) **(b)** and RSK2 inhibitor (BI-D1870, final conc. 10 μM) during the last 30 minutes, followed by stimulation with FGF1 (final conc. 100 ng/ml) and heparin (final conc. 50 U /mL) for 10 minutes. U2OS cells with and without FGF1-stimulation were included as controls. Subsequently, the cells were lysed and the lysates were incubated with **a)** sepharose beads coupled to FGFR4 antibody or **b)** magnetic beads coupled to FGFR4 antibody. The lysates (3% of IP) and immunoprecipitates were subjected to Western blotting. γ-tubulin (γ-tub) is the loading control. The "p" preceding the antibody names indicates the phosphorylated form. Images were contrast-adjusted in Fiji ImageJ and visualized in Adobe InDesign.

4.5 Increased migration or proliferation upon FGF1-stimulation

RTKs, including FGFRs, regulate cell functions such as growth, survival, and migration. Based on previous data, truncating the receptor tail to prevent RSK2 binding, phosphorylation, and subsequent negative feedback activation will hinder receptor internalization. This could lead to prolonged signaling and increased migration/proliferation. We indirectly tested this by inhibiting RSK2 in U2OS cells expressing FGFR1-4.

We performed one experiment with three technical replicates for each condition to test this. The treatments included control (no addition), FGF1 ligand, RSK2 inhibitor, and a combination of ligand and inhibitor. We expect migration/proliferation to increase with FGF1-stimulation and even more so when RSK2 is inhibited, assuming RSK2 receptor phosphorylation of the FGFRs (leading to reduced endocytosis and possibly increased signaling). Imaging started immediately after stimulation using an Incucyte S3 microscope, capturing images every 10 minutes for 19 hours for the migration assay and every third hour for 69 hours for the proliferation assay.

4.5.1 FGFR1-3 exhibited increased migration upon FGF1-stimulation over time

After imaging, we used CellTraxx software to automatically track cell migration by identifying individual cells and their movement over time [87]. The average cell velocity from one image to the next is plotted for the 19 hours the cells were recorded. In the control (-) group, where no FGF1 was added, there was no increase in average motility over time, as expected (Figure 4.5.1). For U2OS-R1, U2OS-R2, and U2OS-R3, there was a noticeable increase in motility following ligand stimulation, confirming the known role of FGFRs in regulating cell migration. However, in U2OS-R4, there was no observable difference in motility between the ligand-stimulated and control groups.

The addition of the RSK2 inhibitor did not yield the expected results. No significant increase in migration was observed compared to other treatments following ligand stimulation, except a slight increase over time in motility for FGFR3 with FGF1-stimulation in the presence of the RSK2 inhibitor. This was surprising since, from our endocytosis experiments, FGFR3 was the least dependent on RSK2 among the receptors. However, the increase is not as great as observed in the ligand-stimulated group without inhibitor treatment (Figure 4.5.1), indicating that signaling is not enhanced beyond normal ligand stimulation. The observed consistency, reflected in the similar graph patterns across technical replicates, provides reliability for this experiment. However, further biologically independent experiments are necessary to confirm the findings. To gain further insights into these observations, we examined proliferation over time.

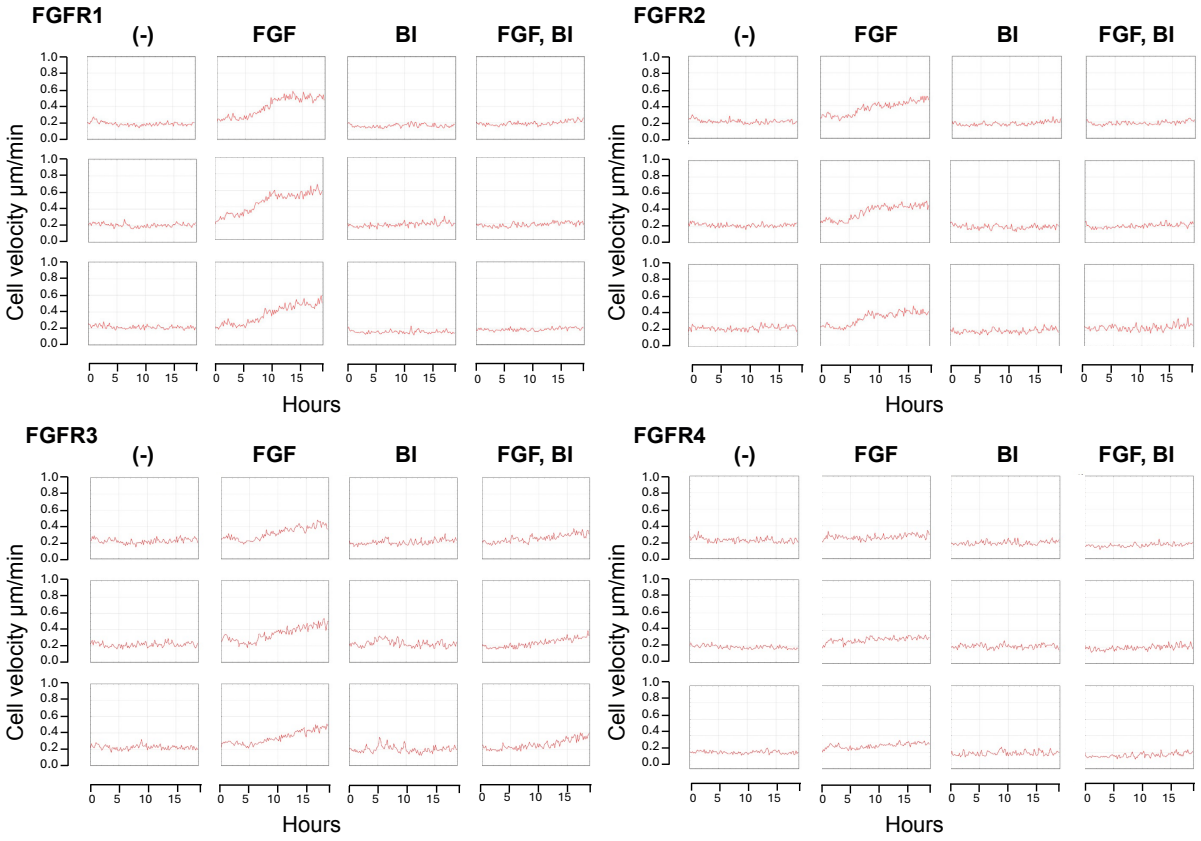

Figure 4.5.1: FGF1-stimulation increases FGFR1-3 migration, but not FGFR4. U2OS cells expressing individual FGFRs were seeded on a 96-well plate and maintained in 1% serum media with heparin (10 U/mL). Treatments included control (-), FGF1 ligand (final conc. 100 ng/mL), RSK2 inhibitor (BI-D1870, U0) (final conc. 10 μM), and both ligand and inhibitor. Since the inhibitors were dissolved in DMSO, DMSO was added to the other samples to achieve same amount of DMSO in all samples. Imaging using Incucyte S3 began immediately after stimulation, capturing images every 10 minutes for 19 hours. CellTraxx software tracked cell migration, visualized as average cell velocity over time for three technical replicates per treatment. The replicates are shown below each other, with graphs automatically generated by CellTraxx and visualized in Adobe InDesign.

4.5.2 FGFR4 exhibited increased proliferation upon FGF1-stimulation over time

The cells from the migration experiment were continuously imaged every third hour for 69 hours to measure proliferation. CellTraxx software was used to identify and automatically count cells over time [87]. The average cell count from three technical replicas was plotted to assess differences in cell proliferation across the four treatments (described above) of cells expressing the four FGFRs (Figure 4.5.2). A consistent starting point for all treatments within each cell line confirmed accurate seeding, ensuring reliable comparison of treatments. Equal initial cell density is crucial as it can influence proliferation rates. In the FGF1-stimulated treatments for FGFR1-3, proliferation patterns matched those of the control, indicating no significant increase compared to the control (compare red and grey lines in Figure 4.5.2). For FGFR4, FGF1-stimulation led to a substantially higher proliferation rate. These results suggest that FGFR4 has a higher proliferation rate compared to other FGFRs when expressed in U2OS cells and stimulated with FGF1. Nonetheless, these findings need to be repeated in biologically independent experiments for validation.

Regarding the hypothesis that active RSK2 is required for receptor internalization as a negative feedback response to ligand stimulation, we expected increased signaling and potentially increased proliferation with RSK2 inhibitor and FGF1-stimulation. However, RSK2-inhibited cells did not increase cell number over time for any FGFRs, indicating poor growth and potential cell death (Figure 4.5.2). This aligns with previous findings that cell velocity was not increased upon RSK2 inhibitor treatment. It is possible that the inhibitor is toxic at the concentration used, causing the cells to die or RSK2 is so essential to cells that they stop proliferating if RSK2 is not functional over time. RSK2 inhibition in the presence of FGF1-stimulation showed slightly higher proliferation than RSK2 inhibited cells alone, suggesting that FGF1 might aid survival.

To evaluate the cells' condition and the cell segmentation quality by CellTraxx, we examined the images from the Incucyte S3. Example images are shown in Figure 4.5.2a,c,e,g. Cells outlined in green are those identified as individual cells by the CellTraxx software, indicating that the segmentation was effective. Although the images might give the impression of uneven seeding due to random image selection, quantification in Figure 4.5.2b,d,f,h confirms that cell density was consistent at the start of the experiment. Over time, the cells underwent morphological changes, and those treated with the RSK2 inhibitor appeared to be dying. This observation likely explains their reduced ability to proliferate or migrate.

The increase in the number of cells from the start to the endpoint in the FGF1-stimulated U2OS-R4 was confirmed upon examination of the images from the Incucyte microscope (Figure 4.5.2). Notably, there was a change in morphology, particularly for FGFR1. This change occurs after ligand stimulation, where cells transition from a rounder form to an elongated form, likely enhancing motility. When examining the RSK2-inhibited cells, there is a higher frequency of dead cells, further supporting the conclusion that treatment with the RSK2 inhibitor over time probably was toxic to the cells, and hence, no increase in migration or proliferation was observed.

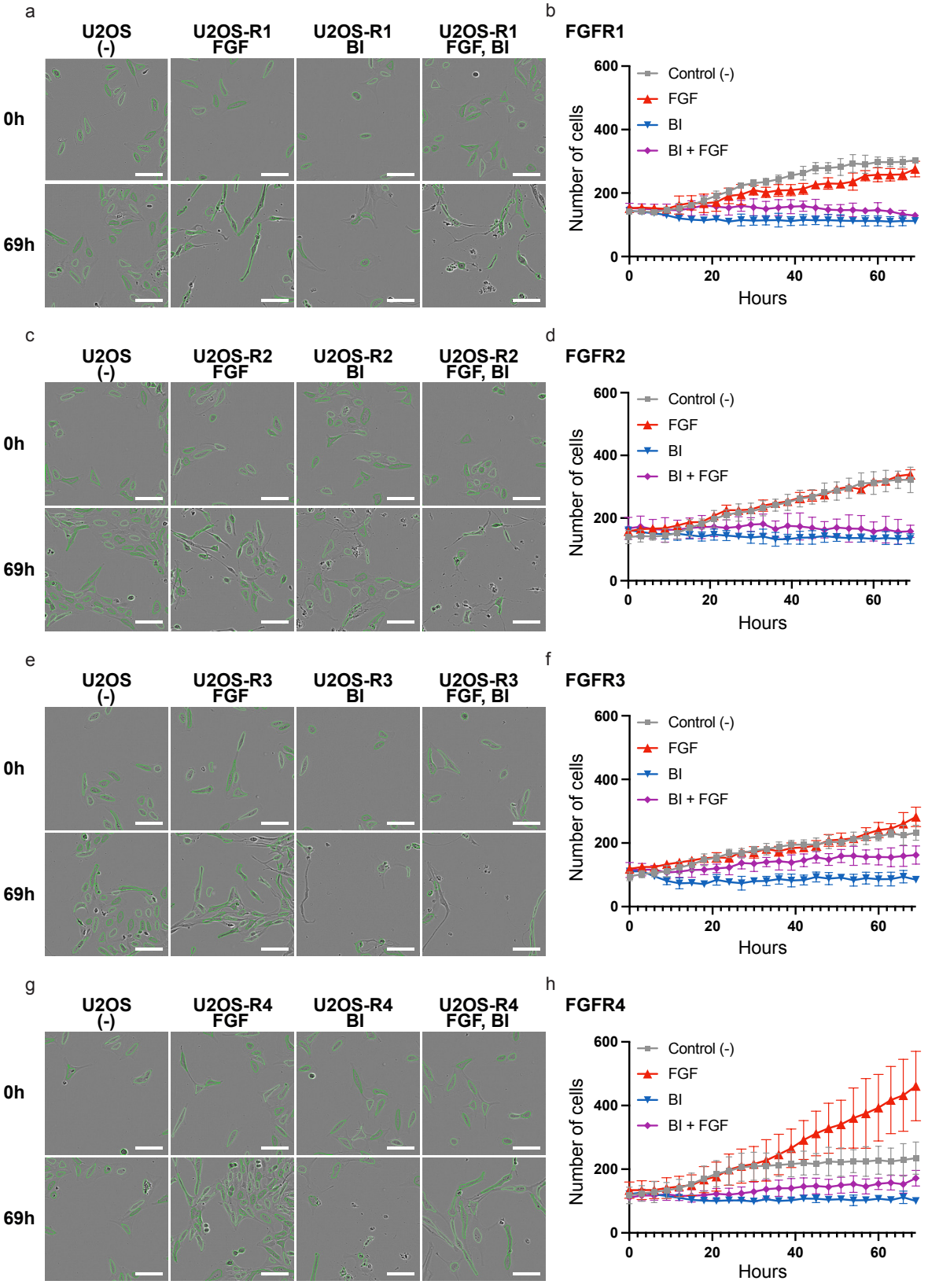

Figure 4.5.2: FGF1-stimulation increases FGFR4 proliferation. Imaging by Incucyte began immediately after stimulation, capturing images every third hour for 69 hours. CellTraxx software was used to track cell proliferation. **a,c,e,g)** Representative images from the beginning of the experiment (0 hours) and endpoint (69 hours) are shown; segmented/counted cells are outlined in green. One image from each time point was randomly selected from one technical replica, with a section captured from the same location in each image. Scale bar, 100 μm. **b,d,f,h)** The data were visualized in GraphPad Prism. The graphs display the average number of cells over time, combining all three technical replicates for each treatment. The figure is visualized in Adobe InDesign.

Based on the migration and proliferation assays, FGFR1-3 showed increased migration following FGF1-stimulation but no significant increase in proliferation. Conversely, FGFR4 exhibited no increase in migration but a notably higher proliferation rate. To confirm these findings, additional biologically independent experiments are needed. Furthermore, the potential effect of RSK2 inactivation on FGFR-mediated processes could not be assessed using the RSK2 inhibitor, likely due to toxicity issues. Alternative methods must be explored to investigate this further.

4.6 Little evidence for functional mutations in C-terminal tail of FGFRs in cancer

Our analysis indicates that active RSK2 plays a role in a negative feedback mechanism for endocytosis in FGFR1, FGFR2, and FGFR4. Mutations at phosphorylation sites S789 (FGFR1), S791 (FGFR2), and S776 (FGFR4) may impair endocytosis, potentially contributing to cancer progression through enhanced signaling. Recent studies by Zingg et al. (2022) identified truncation in the C-terminal tail of FGFR2 as a potent driver mutation, with loss of feedback mechanisms in the FGFR2 tail enhancing oncogenic potential [48]. We aimed to evaluate publicly available clinical data for alterations in the C-terminal tail of all four FGFRs. FGFR3 was included despite showing no effect on endocytosis with RSK2 inhibition, while FGFR2 served as a positive control.

4.6.1 Most of the naturally occurring splice variants of FGFRs retain potential RSK2 phosphorylation sites when possessing the catalytic domain

To fully understand FGFR mutations in tumor samples, exploring splice variants that differ from canonical sequences is important. Inspired by the FGFR2 study highlighting the prevalence of FGFR2 splice variants lacking the C-terminal tail in cancer, we investigated if natural splice variants of FGFRs lacked the C-terminal tail. We evaluated the conservation of phosphorylation sites across these structural variants and their frequency through isomer alignment. Our focus was on splice variants with intact kinase domains, as the kinase domain is needed for oncogenic potential.

Isomer definitions for FGFR1-4 were obtained from the UniProt database. Sequences were extracted and aligned using Jalview with default settings and visualized in Adobe InDesign (Figure 4.6.1). Isoforms lacking significant portions of the catalytic domain were excluded. The potential ERK1/2 and RSK2 phosphorylation sites were conserved across catalytically active FGFR1-4 isoforms, except for certain truncated FGFR2 isoforms lacking most of the C-terminal tail. Specifically, several isoforms (2, 7, 11, 16) of FGFR2 lack the C-terminal tail, including the last few amino acids of the catalytic site, remaining catalytically active but losing the potential negative feedback loop mediated by ERK1/2 and RSK2. This variant is often referred to as C3. Similarly, isoform 4 lacks the potential RSK2 and ERK1/2 phosphorylation sites while the kinase domain remains. The isoform 6 (referred to as C2) of FGFR2 lacks part of the C-terminal tail, including the potential RSK2 phosphorylation site but not the ERK1/2

site, while isoform 15 (C4) lacks only the very end of the C-terminal tail, with both potential phosphorylation sites intact.

This analysis shows that all catalytically active, naturally occurring isoforms of FGFR1, 3, and 4 retain intact C-terminal tails, including the potential ERK1/2 and RSK2 phosphorylation sites. While truncated splice variants of FGFR2 are frequently found in cancer, investigating the frequency of catalytically active isoforms of the other receptors in cancer is less relevant for studying C-terminal tail loss. Additionally, truncations of the C-terminal tail in FGFR1, FGFR3, and FGFR4 with intact kinase domains found in tumors are mutations rather than naturally occurring splice variants. We will analyze published DNA sequences from human tumor samples to quantify mutations affecting the potential negative feedback sites in FGFRs. This analysis aims to identify patterns where FGFRs retain their catalytic domain but lose the RSK2 phosphorylation site, potentially disrupting the feedback mechanism and potentially contributing to cancer progression.

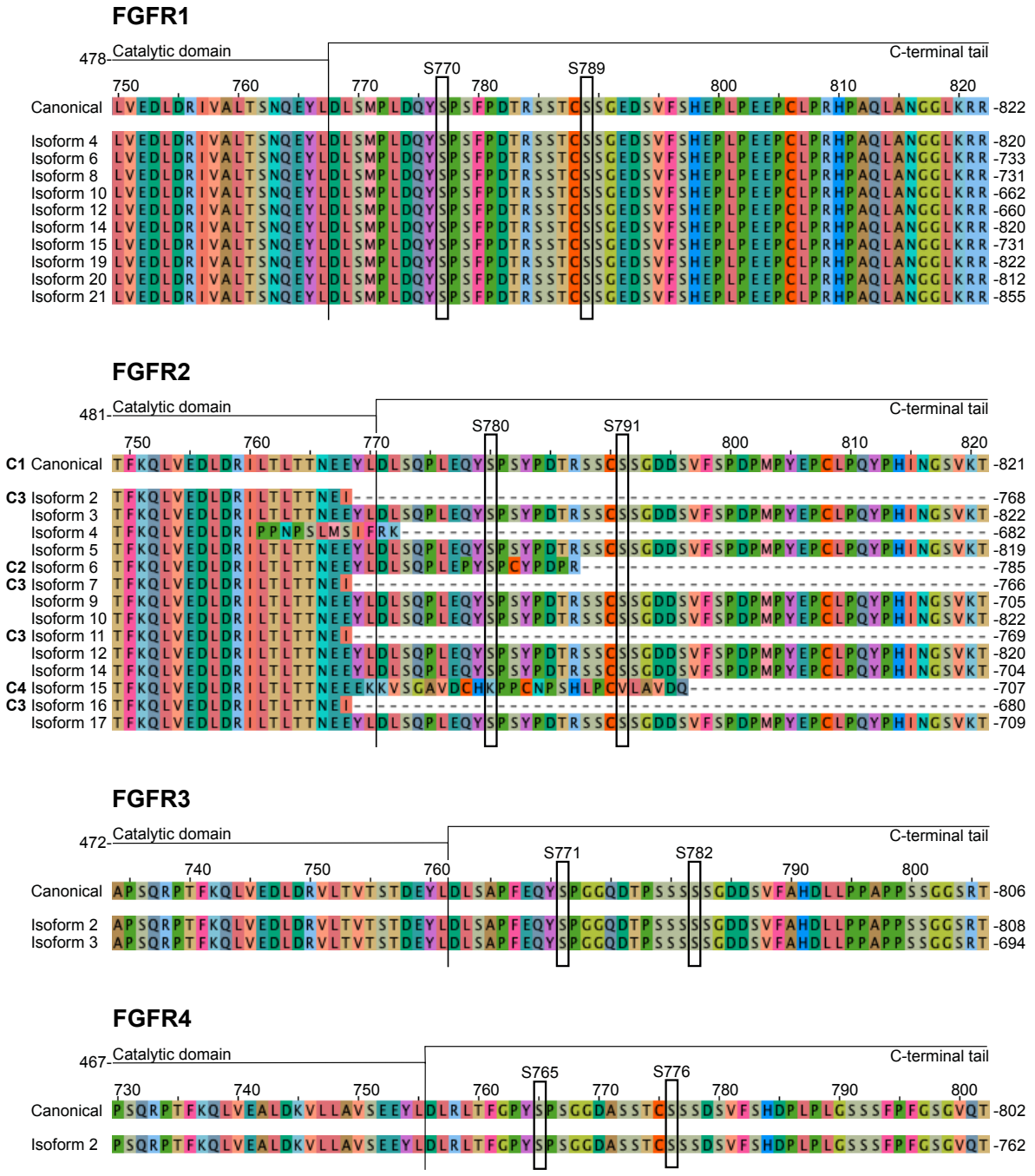

Figure 4.6.1: Serine residues of interest are conserved across all FGFR isoforms, except in some FGFR2 isoforms. Alignment of catalytically active FGFR1-4 isoforms was performed using Jalview software with the Clustal multiple alignment function with default settings. FGFR1-4 isoform sequences were obtained from UniProt. The catalytic domain and the C-terminal regions were defined by Katoh et al. [11], and only the end of the catalytic domain and the C-terminal tail are shown. Isoforms lacking significant portions of the catalytic domain are not included. Serines potentially phosphorylated by ERK1/2 (S770, S780, S771, and S765 for FGFR1-4, respectively) and RSK2 (S789, S791, S782, and S776 for FGFR1-4, respectively) were identified from canonical sequence alignment, refer to Figure 4.1.1. The common FGFR2 isoforms C1, C2, C3, and C4 are indicated [48]. The figure is visualized in Adobe InDesign.

4.6.1.1 Little evidence of mutation patterns retaining the intact catalytic domain while losing the RSK2 phosphorylation site

To get an overview of mutation patterns in FGFRs, we utilized the Catalogue of Somatic Mutations in Cancer (COSMIC) database, which collects somatic mutation data of human cancers [91]. For each FGFR, we extracted the somatic mutation data.

The respective CSV files containing the raw data of mutations for FGFR1-4 were downloaded, and a Python script was made using VS Code to analyze these raw data. The code, available via the GitHub link in Appendix B, was made to identify mutations influencing the C-terminal tail of the receptors. First, mutations marked as “Silent” or “Unknown” were discarded for further processing. "Unknown" denotes a mutation with an undetermined effect at the protein level, meaning the specific amino acid change is not identified. By this, 832, 1583, 5253, and 871 mutations leading to amino acid changes in FGFR1-4 were identified (Figure 4.6.2). The number of tested samples for FGFR1-4 were 86911, 90616, 102780, and 72724, respectively. The variation in sample sizes may have influenced the number of mutations identified. Next, mutations were categorized into in-frame insertions and deletions, frameshifts, premature stop codons, and missense mutations. Subsequently, the mutations were assessed to determine whether they affected the potential ERK1/2 and RSK2 phosphorylation sites in individual FGFR1-4 (Figure 4.6.2). Mutations leading to loss of potential phosphorylation sites were defined as truncating or frameshift mutations occurring at the same position or before the potential phosphorylation sites, or missense mutations affecting the specific serines of interest.

The Python script analyzed samples with mutations affecting the serines of interest within the C-terminal tail to assess the integrity of their catalytic domain. The goal was to identify mutations that retain catalytic activity while losing the negative feedback mechanism. Such gain-of-function mutations could enhance signaling and contribute to oncogenic events. The script used the kinase domain definition provided by Katoh et al. [11]. The script flagged the kinase domain as disrupted when it detected in-frame insertions/deletions, premature stop codons, or frameshifts before or within the kinase domain sequence. Few samples exhibited mutations that disrupted the phosphorylation sites of ERK1/2 and RSK2 while maintaining an intact kinase domain (Figure 4.6.2 provides an overview, with detailed data listed in Table C.1). Since there were few reported fusions for the four FGFRs in the COSMIC database (11 and 12 for FGFR1 and FGFR3, respectively, and none for the other FGFRs), these were manually checked to determine if the fusions resulted in the loss of potential negative feedback loops (Figure 4.6.2 and Appendix Figure C.1).

For FGFR1, 2 out of 823 mutations led to the loss of potential phosphorylation sites while retaining a fully intact catalytic domain. One mutation was a missense mutation affecting S789, the RSK2 phosphorylation site, and the other was a fusion protein. For FGFR2, 4 missense mutations affected S791, and 1 affected S780, corresponding to the ERK1/2 and RSK2 phos-

phorylation sites, respectively. In total, 8 out of 1583 mutations in FGFR2 retained the catalytic domain while affecting the phosphorylation sites (Figure 4.6.2 and Appendix Figure C.1).

FGFR3, which has the most mutations (5253) of the four receptors in the COSMIC database, showed 15 mutations, leading to a lack of the potential phosphorylation sites for ERK1/2 and RSK2 while retaining the kinase domain. This is only 7 more mutations than found for FGFR2, despite FGFR2 having fewer total mutations (1583). No missense mutations of the serines of interest were found in FGFR3. Among the mutations preserving an intact kinase domain, 4 frameshift mutations and 11 fusion proteins were identified. Specifically, 12 fusion events involving FGFR3 were observed in the COSMIC database. Of these, 11 were fused with another protein after exon 17, thereby losing exon 18, the final exon in the kinase domain of FGFRs, where the serines of interest are located [98]. This contrasts with FGFR1, where out of the 11 detected fusions, only 1 retained the kinase domain. In the case of FGFR4, all truncating mutations resulted in the loss of portions of the catalytic domain. Consequently, only missense mutations directly affecting the serines maintained an intact catalytic domain. There are 5 such mutations, with 4 occurring at the possible ERK1/2 phosphorylation site and 1 at the possible RSK2 phosphorylation site (Figure 4.6.2 and Appendix Figure C.1).

We hypothesized that mutations targeting RSK2 phosphorylated serines might be more prevalent in FGFR1, FGFR2, and FGFR4. However, FGFR3 showed a lower percentage of such mutations relative to its total mutations (0.29%) compared to FGFR2 (0.51%) and FGFR4 (0.57%) (Figure 4.6.2). However, the numbers are relatively low, and it is not known if the difference is relevant. Moreover, FGFR1 had the fewest mutations, potentially disrupting negative feedback mechanisms. When analyzing mutations leading to gain-of-function effects, with an intact kinase driving MAPK pathway activity and reduced feedback, only 0.24-0.57% of mutations in FGFR1-4 fit this criterion (Figure 4.6.2).

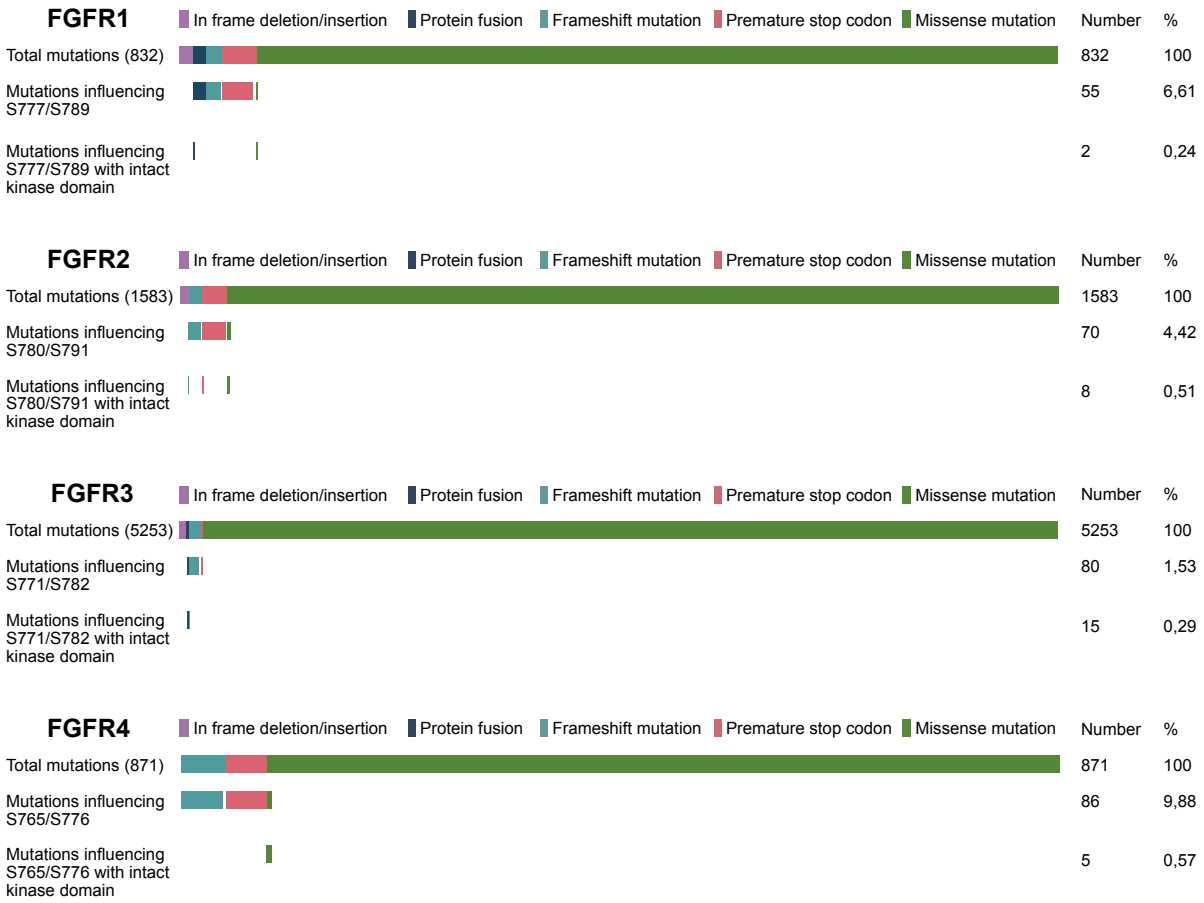

Figure 4.6.2: Overview of mutations affecting FGFR1-4 in sequenced tumor samples from database. Mutations were extracted from CSV files from the COSMIC database containing DNA sequencing data from human tumor samples. These mutations were categorized into different types and counted using a Python script in VS Code (Appendix B). Additionally, each mutation was assessed to determine its impact on potential phosphorylation sites of ERK1/2 and RSK2 in the FGFR tails and whether the mutations retained an active catalytic domain, indicating potential cancer-driving capabilities. The number of mutations and percentages are presented to the right. The raw data/coding output is represented in C.1. The results were subsequently visualized using Adobe Illustrator.

Truncating mutations, defined as those resulting in a premature stop codon, and frameshift mutations, leading to altered amino acid sequence, were found to impact potential ERK1/2 and RSK2 phosphorylation sites more frequently than other mutation types. To understand where these truncating events occur, we specifically extracted frameshift and premature stop codon mutations in FGFR1-4 from the CSV files sourced from the COSMIC database. This extraction aimed to visualize the possibility of some receptors remaining active despite the loss of parts of the catalytic domain. In Figure 4.6.2, only mutations retaining the entire catalytic domain were categorized as influencing the potential phosphorylation sites. However, it is possible that the catalytic domain remains active even if it is not entirely intact. The mutations were visualized alongside the receptor domains (Figure 4.6.3).

Truncating events between the end of the catalytic domain and the beginning of the C-terminal tail, preceding the serines of interest, may allow receptors to retain catalytic activity while losing the potential negative feedback mechanism. We observed no overall increase in mutations in

these regions for FGFR1 and FGFR4. However, data for FGFR2 show a slight clustering of mutations in this section. Some mutations cluster slightly further out in the C-terminal tail of FGFR3 not affecting the potential phosphorylation sites (Figure 4.6.3, note the different scale on the Y-axis in the figure).

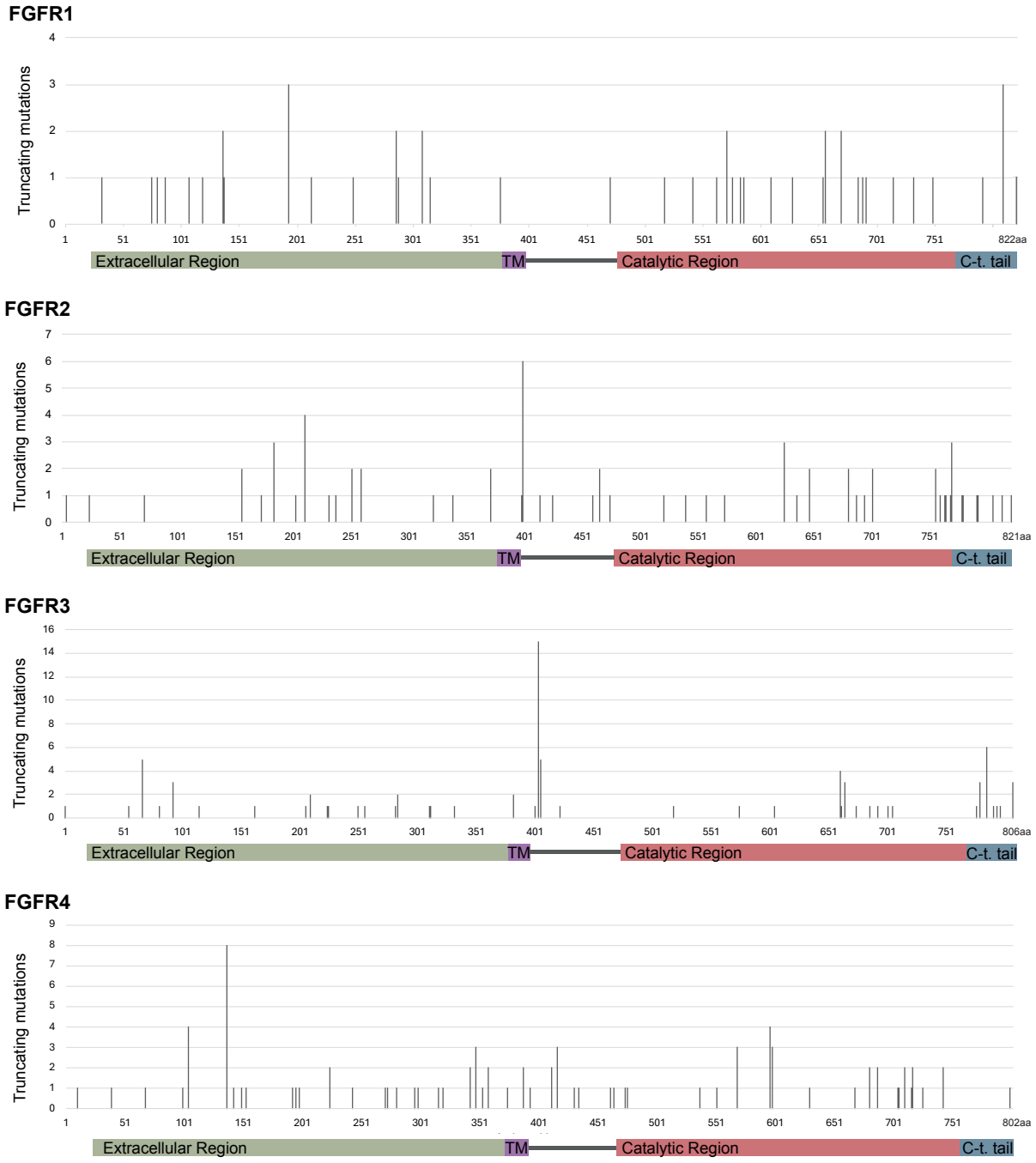

Figure 4.6.3: Truncating mutations in FGFR1-4 in sequenced tumor samples Mutations were sourced from CSV files in the COSMIC database, containing DNA sequencing data from human tumor samples. Truncating mutations, identified by stop codon or frameshift events, were extracted for FGFR1-4 (see CSV files in the GitHub repository link in Appendix B). The graph was created in Excel. The extracellular and transmembrane (TM) domains were defined according to UniProt's canonical FGFR1-4 domain definitions, while the catalytic domain and C-terminal tail were defined as in Katoh et al. [11]. The receptor domains and the graph from Excel were visualized together using Adobe Illustrator.

Examining mutation types and frequencies impacting phosphorylation sites (Figure 4.6.2) and

the distribution of truncating events (Figure 4.6.3) revealed low mutation rates affecting potential ERK1/2 and RSK2 phosphorylation sites in FGFRs in human cancer. ERK1/2 feedback occurs for FGFR1-2 [46, 45] (not investigated for FGFR3 and 4), while RSK2 activity is required for endocytosis of FGFR1 [49], FGFR2, and FGFR4 (Section 4.3.3). Notably, no clear increase in mutation rates for FGFR1, FGFR2, and FGFR4 versus FGFR3 impairing serine phosphorylation events while maintaining intact domains was observed (Figure 4.6.2). Truncating mutations were evenly distributed across the receptors, with some notable peaks observed around the transmembrane region, rendering them non-functional (Figure 4.6.3). Some mutations were clustered in FGFR2 and FGFR3 near the end of the catalytic domain and the start of the C-terminal tail. Overall, published cancer samples from the COSMIC database do not show a particularly high rate of gain-of-function mutations that disrupt ERK1/2 and RSK2 related negative feedback mechanisms in FGFRs.

CHAPTER

FIVE

DISCUSSION

In this thesis, we investigated whether an RSK2-mediated negative feedback loop regulates FGFR2-4, similar to FGFR1. We hypothesized that RSK2 binds to the C-terminal tails of FGFR2-4. This binding results in the phosphorylation of a specific serine residue, necessary for receptor internalization as a negative feedback mechanism. The hypothesis is based on previous findings that demonstrated RSK2 binding to the C-terminal tail of FGFR1 and phosphorylation at S789, resulting in reduced endocytosis of the receptor upon RSK2 inhibition [49]. Similarly, ERK1/2 is known to phosphorylate a serine residue nearby on the C-terminal tail of FGFR1 and FGFR2, serving as an additional negative feedback mechanism through an unknown pathway [45, 46]. Our main objective was to determine if inhibiting RSK2, which potentially phosphorylates serine residues on the C-terminal tails of FGFR2-4, would similarly reduce receptor endocytosis. Subsequently, we evaluated the potential relevance of RSK2 and ERK1/2 negative feedback mechanisms in cancer.

5.1 Inhibition of RSK2 significantly reduces receptor internalization in FGFR2 and FGFR4 similar to FGFR1

Through three independent biological experiments, we found that inhibiting RSK2 led to a statistically significant reduction in the internalization of DL-FGF1 in both FGFR2 and FGFR4 expressing cells (Figure 4.3.3). A similar experiment conducted for FGFR1 also showed reduced receptor internalization upon RSK2 inhibition (Figure 4.3.2). These results align with a previous study, which reported a decrease in FGFR1 internalization following RSK2 inhibition [49].

Our experimental protocol closely mirrored the one used in the previous study. In the prior research, U2OS-R1 cells were starved and then stimulated with DyLight 549-labeled FGF1 for 20 minutes, followed by washing with HSLP buffer to remove surface-bound ligands. The intensity of DL-FGF1 was imaged and quantified to indicate internalized FGF1 bound to FGFR1. The observed decrease in internalization upon RSK2 inhibition suggested that RSK2 phosphoryla-

tion at S789 on FGFR1 plays a crucial role in endocytosis as a negative feedback mechanism [49]. We used DyLight 550-labeled FGF1 in our experiments and implemented an automated image quantification pipeline (Appendix Figure A.1), unlike the previous study's cell-based DL-FGF1 uptake quantification [49]. Despite these minor methodological differences, our results for FGFR1 were consistent with the previous findings, confirming the reliability and functionality of our protocol.

We conducted specific staining for the receptors and confirmed no uptake in U2OS wild-type cells, in contrast to FGFR-expressing U2OS cells, indicating that the DL-FGF1 observed was specifically taken up by the overexpressed receptor (Figure 4.3.2a,c,e,). The HSLP specificity test verified that only internalized DL-FGF1 was quantified (Figure 4.3.1). We could have stained the cells for intracellular structures to further strengthen our confidence in the results, specifically targeting early endosomes with early endosome antigen 1 (EEA1) staining [106]. Observing that DL-FGF1 largely colocalized within these structures would provide additional evidence of internalization.

These findings suggest that FGFR2 and FGFR4 likely exhibit similar internalization behavior as FGFR1 under RSK2 inhibition.

5.1.1 Co-localization changes of FGFR2 and FGFR4 with different treatments

Interestingly, the U2OS-R2 control cells stimulated with FGF1 displayed brighter green/yellow dots than those treated with inhibitors (Figure 4.3.3a, upper panel). This might suggest a higher presence of FGFR2 per cell. However, since the inhibitor treatment is relatively short, it is not likely that the receptor will be massively degraded or lost within this time frame. The bright dots are likely due to FGF1 in endosomes, causing receptor clustering within these structures. The receptor clusters appear as intense yellow-green dots (a combination of green FGFR2 signals and red signals from bound DL-FGF1). In contrast, inhibitor-treated cells showed a more even green color, indicating that receptors are more spread out on the cell surface rather than clustered into endosomes. A concentrated fluorescent signal in endosomes appears stronger than a dispersed signal on the surface. This observation indicates that DL-FGF1 binding to FGFR2 leads to FGF-1 containing endosome formation, which is reduced when MEK1/2 or RSK2 is inhibited.

The receptor staining and DL-FGF1 uptake in U2OS-R4 cells appeared specific, as minimal staining and no uptake were detected in U2OS cells. However, the formation of endosome-like structures in FGFR2 cells, indicated by bright yellow-green dots (Figure 4.3.3a), was not as apparent in the U2OS-R4 cells (Figure 4.3.3e). Instead, FGFR4 showed a more uniform distribution on the cell surface across all treatments in U2OS-R4 cells. An interesting observation, particularly visible in the image of U2OS-R4 treated with only DL-FGF1, is the accumulation of FGFR4 in a pattern resembling the endocytic recycling compartment. This suggests that FGFR4 undergoes endocytic recycling, where internalized receptors are returned to the cell

surface, a known characteristic of FGFR4 [57].

The reduction in DL-FGF1 uptake was less pronounced in U2OS-R4 cells compared to U2OS-R2 cells. This may be attributed to the recycling property of FGFR4, which allows for the rapid return of internalized receptors to the cell surface. Additionally, FGFR2 appeared to have generally higher expression levels than FGFR4, potentially contributing to the observed differences. Western blot analysis indicated lower levels of phosphorylated FGFR (pFGFR) for FGFR4 compared to FGFR2, though it is important to note that the contrast adjustments for these blots were different (Figure 4.2.2).

To determine if low expression levels affect the observed structural differences, we need to consider the impact of receptor expression on the fluorescent signal. Weaker receptor expression can lead to the necessity of amplifying the fluorescent signal by increasing laser power or other settings during imaging. This could result in increased detection of background staining. However, since background (DL-FGF1 and antibody staining) was not visible in U2OS wildtype cells for FGFR4 and only slightly for FGFR3 (that also appeared to have a weaker receptor expression), increased detection of background is probably not the case here (Figure 4.3.3). Ensuring similar expression levels among the receptors could allow a more accurate comparison. This could be achieved using Clustered Regularly Interspaced Short Palindromic Repeats (CRISPR) technology to insert the FGFR genes under the same promoter, manipulating their gene expression and ensuring equal receptor expression levels.

5.1.2 Exploring the endocytic pathway of FGFR1 and its potential similarity to FGFR2 and FGFR4

RSK2 phosphorylation on the C-terminal tail of FGFR1 is required for FGFR1 clathrin-mediated endocytosis (CME) through an unknown mechanism [49, 55, 25]. FGFR1, FGFR2, and FGFR4 are known to be internalized via CME [55, 25]. Given that FGFR2 and FGFR4 exhibit the same reduced receptor internalization as FGFR1 when RSK2 is inhibited (Figure 4.3.2 and 4.3.3), it is plausible that RSK2-mediated phosphorylation on the C-terminal tail of FGFR2 and FGFR4 also contribute to CME through the same unknown mechanism. Further research into how RSK2 and C-terminal phosphorylation recruits specific proteins and which proteins are involved would be highly valuable.

5.2 Differential internalization of FGFR3 compared to FGFR1/2/4 under RSK2 inhibition

The amount of internalized FGFR3 was not significantly affected by treatment with RSK2 or MEK1/2 inhibitors (Figure 4.3.3c-d). However, comparing DL-FGF1-stimulated U2OS cells with U2OS-R3 cells suggests some endocytic pathway involvement, despite the lack of effect from RSK2 inhibition.

This indicates potential downstream signaling pathways or receptor dynamics differences between FGFR1/2/4 and FGFR3. Previous research suggests that FGFR3 utilizes an alternative endocytic pathway that is clathrin- and dynamin-independent (CIE), as FGFR3 internalization is only partly dependent on clathrin [55]. In contrast, FGFR1, FGFR2, and FGFR4 are primarily internalized through CME [55, 25]. Our findings further support that FGFR3 exhibits different endocytic properties than FGFR1, FGFR2, and FGFR4, which is evident in the differences in RSK2-dependent downregulation.

5.2.1 Potential impact of sequence and interaction differences on FGFR3 endocytic behavior

The distinct endocytic behavior of FGFR3 could be attributed to sequence differences. Sequence alignment revealed that the serine phosphorylation site targeted by RSK2 in FGFR1, and by ERK1/2 in FGFR1 and FGFR2, is conserved across all FGFRs. However, FGFR3 has a unique amino acid substitution adjacent to the serine potentially phosphorylated by RSK2 in the receptors. In FGFR1, FGFR2, and FGFR4, the amino acid adjacent to this serine is a cysteine, whereas in FGFR3, it is a serine (Figure 4.1.1). This substitution may influence the phosphorylation efficiency and, consequently, the endocytic behavior of FGFR3.

Although the consensus sequence recognized by RSK2 for phosphorylating serine or threonine residues on substrates typically follows the pattern R-X-R-X-X-pS/T or R-R-X-pS/T [49, 60], FGFR1 features a similar motif at position 784RSSTCS789. S789 is phosphorylated even though it does not fit the motif perfectly [49], indicating potential flexibility in RSK2 binding and phosphorylation. Given this, we examined the serine and adjacent amino acids in the C-terminal regions of FGFRs to understand their phosphorylation and endocytic behavior. Further experiments, such as mutating the serine in FGFR3 to a cysteine, could help determine if RSK2 can bind and phosphorylate FGFR3 under these modified conditions. This would provide insights into the unique endocytic pathway of FGFR3.

Examining previous data on interactions between RSK2 and FGFRs and phosphorylation events on the specific serines revealed several insights. Both low- and high-throughput studies have confirmed the binding between FGFR1 and RSK2. Additionally, high-throughput studies have identified interactions between RSK2 and FGFR2, as well as RSK2 and FGFR4. Notably, no relevant low- or high-throughput studies report interactions between FGFR3 C-terminal tail and RSK2 (Table 4.1.1). This absence suggests that FGFR3 may not interact with RSK2 in contrast to FGFR1, FGFR2, and FGFR4. However, the lack of studies indicating the binding of RSK2 to FGFR3 could also be a coincidence if, for example, less research is done for FGFR3.

The interaction with a kinase often leads to phosphorylation at specific sites of interest. One study confirmed that FGFR1 is phosphorylated at S789 by RSK2 [49], with additional high-throughput studies supporting this finding (Figure 4.1.2). Similarly, S791 in FGFR2 has been

identified as a phosphorylation site in two high-throughput studies. Although there are no specific reports on FGFR4, the absence of data for FGFR3 might underscore the potential differences in its interaction patterns with RSK2 compared to FGFR1, FGFR2, and FGFR4.

Taken together, it appears that FGFR3 exhibits different endocytic properties than the other FGFRs. Although FGFR3 seems to have lower expression levels than FGFR1, and FGFR2, and possibly FGFR4 (pFGFR levels, Figure 4.2.2), we believe this is not the sole reason for the observed differences in endocytic behavior. This hypothesis should be further investigated, potentially using CRISPR technology to equalize expression levels and determine if the distinct endocytic properties of FGFR3 persist.

5.3 Evidence for RSK2-binding and phosphorylation of FGFR2 and FGFR4 remains unconfirmed

Our findings indicate that RSK2 inhibition affects the endocytosis of FGFR2 and FGFR4. However, we did not provide direct evidence of RSK2 binding and phosphorylation on the C-terminal tail of these receptors. To address this, we attempted to demonstrate the binding through co-immunoprecipitation (co-IP) experiments. A previous have confirmed the interaction between RSK2 and FGFR1 via co-IP, with a significant increase in binding upon FGF1-stimulation [49]. Our efforts aimed to replicate these findings for FGFR1 and extend them to FGFR2, (FGFR3), and FGFR4, although we only attempted FGFR1 and FGFR4 in this study.

We observed a weak band for FGF1-stimulated U2OS-R1 in the IP assay, confirming that RSK2 binds to the receptor tail of FGFR1 (Figure 4.4.1). Based on this, we attempted to demonstrate the binding of RSK2 to FGFR4 using two different IP protocols. Despite these efforts, we could not detect the binding (Figure 4.4.2). The RSK antibodies performed well with the lysates, and FGFR4 was successfully immunoprecipitated. This suggests that the washing protocol might have been too harsh, potentially disrupting the RSK2-FGFR4 interaction. Alternatively, it could indicate that RSK2 does not bind to FGFR4.

Given that similar internalization results are observed for FGFR2 and FGFR4 upon RSK2 inhibition (Figure 4.3.3), it is plausible that a similar mechanism is at play. To confirm this, we need to investigate whether RSK2 binds and phosphorylates FGFR2 and FGFR4 similar to FGFR1. Furthermore, it is essential to test our hypothesis that RSK2 does not bind to or does not phosphorylate FGFR3, which could explain the differences in internalization of FGFR3 upon RSK2 inhibition. Developing antibodies targeting specific phosphorylated serine residues in FGFR2 and FGFR4, such as anti-pS789 for FGFR1, would allow direct detection of phosphorylation on other FGFRs.

Applying similar assays used for FGFR1 in the previous study to check for RSK2 binding and phosphorylation to the C-terminal tail of FGFR2-4 will help confirm these interactions and

mechanisms. This includes *in vitro* phosphorylation and binding studies with recombinant proteins. In the previous study, RSK2 phosphorylation on the C-terminal tail increased auto-transphosphorylation of FGFR1 tyrosine residues when RSK2 was inhibited or knocked out by siRNA [49]. This could also be applied to FGFR2-4.

If no binding is found between RSK2 and FGFR2 or FGFR4 after optimizing the experimental protocol, the reduced internalization of these receptors when RSK2 is inhibited might not be due to RSK2 binding and phosphorylation of the receptor tail, as observed with FGFR1. Instead, this could suggest that a downstream substrate of RSK2 might be important for receptor endocytosis, explaining the reduced internalization upon RSK2 inhibition.

If similar mechanisms can be confirmed for FGFR2 and FGFR4, it would provide a comprehensive understanding of RSK2's role in FGF1-receptor endocytosis. If disruption of this feedback loop is found to have pro-cancerous effects, this knowledge could be of importance and should be taken into consideration when targeting the MAPK pathway in cancer.

5.4 RSK2 does not need to be active but phosphorylated to bind to the C-terminal tail

Interestingly, the previous study demonstrated no binding in co-IP experiments between RSK2 and FGFR1 in U2OS-R1 cells when treated with a MEK1/2 inhibitor (U0126). However, binding was present with the RSK2 inhibitor (BI-D1870) [49]. The RSK2 inhibitor inactivates RSK2 but does not prevent its phosphorylation by ERK1/2, whereas the MEK1/2 inhibitor stops ERK1/2 phosphorylation, thus preventing RSK2 phosphorylation. This indicates that RSK2 does not need to be active but must be phosphorylated to bind to the C-terminal tail of FGFR1. However, when inactive, it cannot phosphorylate the receptor tail [49]. In contrast, our co-IP with U2OS-R1 cells showed binding even in the presence of the MEK1/2 inhibitor (Figure 4.4.1). To resolve this discrepancy, further studies are needed, such as repeating the co-IP experiments or employing additional assays.

5.5 Potential ERK1/2 negative feedback mechanism in FGFR3 and FGFR4 similar to FGFR1 and FGFR2

Previous studies have shown that ERK1/2 phosphorylation acts as a negative feedback mechanism for FGFR1 and FGFR2 [46, 45]. Mutating serine 777 to alanine (S777A) in FGFR1 prevents phosphorylation and prolongs tyrosine phosphorylation, increasing mitogenic response and migration properties [46]. Similarly, mutating serine 780 to alanine (S780A) in FGFR2 increases receptor activity, suggesting a similar feedback mechanism [45].

Our alignment analysis shows that the serine phosphorylated by ERK1/2 and its adjacent amino acids are conserved across FGFR1, FGFR2, FGFR3, and FGFR4 (Figure 4.1.1). The known

ERK1/2 phosphorylation site, where a serine is followed by a proline (forming a pS/T-P motif) [47], fits all receptors. Some differences exist in the amino acids two positions from the serine of interest in FGFR3 and FGFR4. However, it is plausible that the negative feedback by ERK1/2 is also present in FGFR3 and FGFR4. This hypothesis could be investigated by conducting similar experiments as those performed for FGFR1 and FGFR2.

5.5.1 ERK1/2 does not impact endocytosis in FGFRs

Previous research has shown that ERK1/2 phosphorylation does not significantly impact FGFR1 endocytosis. The study used a FGFR1 version with mutant S777 and was based on kinetic assays and confocal microscopy to investigate if ERK1/2 phosphorylation at S777 affected endocytosis. Findings showed that ERK1/2 phosphorylation didn't significantly influence endocytosis, but inhibiting RSK2 decreased internalization [49]. Our experiments further support this by demonstrating no significant change in internalization when the cells were treated with the RSK2 inhibitor (BI) compared to the MEK1/2 inhibitor (U0) that inhibits both ERK1/2 and RSK2 (Figure 4.3.3). This aligns with the understanding that RSK2-mediated phosphorylation at the receptor tails is a key regulatory step for proper endocytosis.

5.6 Exploring RSK2 inhibition effects on migration and proliferation

The main goal of the proliferation and migration experiments was to demonstrate that inhibiting RSK2 over time would lead to increased proliferation and migration activities (for FGFR1, 2, and 4) due to the loss of the negative feedback mechanism. This hypothesis is based on the idea that fewer receptors would be taken into the cell, letting them stay longer at the cell surface and continue signaling. However, the use of the RSK2 inhibitor revealed possible toxic effects over time (Figure 4.5.1 and 4.5.2). These effects were attributed not to DMSO (as all samples received the same concentration of DMSO) but to the toxicity of the RSK2 inhibitor itself. Lowering the concentration of the RSK2 inhibitor might improve experimental outcomes, but finding the right balance between functionality and cell viability is challenging.

Our Western blot analysis showed that a concentration of 10 μM effectively reduced RSK2 activity to background levels, as evidenced by decreased phosphorylation of LKB1, a downstream substrate of RSK2 (Figure 4.2.2). This finding aligns with the literature, which states that 10 μM of BI-D1870 inhibits LKB1 [99]. To determine if a lower concentration could be effective, we refer to Ellen Margrethe Haugsten's experiment, which indicated that concentrations of 2 μM or less were insufficient, as pLKB1 remained phosphorylated, indicating active RSK2 (Appendix Figure D.2). Previous research using kinase assays suggests that BI-D1870 could be effective at much lower concentrations, as indicated by IC50 values of 20 nM for RSK2 with 100 μM ATP [107]. To refine our understanding, dose-response experiments could assess if concentrations lower than 10 μM (but higher than 2 μM) effectively inhibit RSK2 while minimizing toxicity risks. This approach could potentially identify an optimal RSK2 inhibitor concentration to test for increased migration and proliferation without toxic effects. Alternative methods, include

using other RSK inhibitors such as SL0101 [108] or siRNA to knock down RSK2 could also be used. However, it is possible that RSK2 is essential to cells and that inhibiting or removing RSK2 over time would eventually kill the cells. If this is the case, an alternative approach could be to generate new cell lines expressing truncated FGFRs lacking the RSK2 phosphorylation site (which will be described later) or FGFRs where the potential phosphorylation sites are mutated. These methods would eliminate the need for inhibitors and potentially prevent cell death. However, generating such mutants and stable cell lines is time-consuming, and the time constraints of this thesis did not allow for their implementation.

It is also worth keeping in mind that even if RSK2 inhibition might increase FGFR signaling, it is not given that this would lead to increased migration and proliferation. RSK2 has many downstream targets, and it is possible that these are important for migration and/or proliferation and that their inhibition would counteract the positive effect of increased FGFR signaling on proliferation/endocytosis.

The proliferation and migration assays revealed distinct differences between the FGFRs. Stimulation of FGFR1-3 with FGF1 appeared to induce more migration, while FGFR4 seemed to promote proliferation when stimulated with FGF1 ligand in U2OS cells (Figure 4.5.1 and 4.5.2). More biologically independent experiments are necessary to confirm these observations, as the current results are based on a single experiment.

Previous research has shown that different FGFRs respond uniquely to various FGF ligands. Therefore, the differences observed between the FGFRs in this study might change when stimulated with other FGF ligands. Conducting experiments with different ligands could test this hypothesis. For instance, FGFR2 stimulated with FGF10 is recycled, leading to prolonged signaling and increased migration [109]. Conversely, when FGFR2 is stimulated with FGF7, the receptor is more degraded, resulting in short-lived signaling and increased proliferation. It is also believed that short pulses of ERK1/2 activation can lead to proliferation, while stable long ERK1/2 activation leads to migration [110]. It is unclear how these data fit our results, as FGFR4 primarily recycles but showed increased proliferation and limited migration upon FGF1-stimulation. Further investigations are needed to confirm and understand the potential differences between the receptors.

5.6.1 Spiky cell morphology when stimulated with FGF1 ligand for FGFR1-3

A notable change in cell morphology was observed during the migration and proliferation experiments. Upon stimulation with the FGF1 ligand, cells expressing FGFR1-3 exhibited a more elongated, thin, and spiky appearance compared to their rounder shape when unstimulated (Figure 4.5.2a,c,e). This morphological transformation likely indicates their migratory potential, as migrating cells are known for their flexibility, changing shapes, and extending parts of their membrane (protrusions) to move [111]. Conversely, in U2OS-R4 cells, which showed increased

proliferation with FGF1 treatment, the cells appeared somewhat elongated but not as pronounced and did not include threadlike shapes (Figure 4.5.2g).

5.7 Exploring future experiments to investigate the role of RSK2 in regulation of FGFRs

Given more time to validate our findings regarding the role of RSK2 in FGFR signaling, we could have explored alternative experimental approaches using diverse tools and cell models. One potential strategy involves developing cell lines expressing truncated FGFRs while preserving the kinase domains. This focused approach would allow us to investigate the loss of C-terminal tail phosphorylation on endocytosis, signaling, and biological output. Utilizing these cell lines, we could first perform experiments (for example, Western blot analyses) to verify the functionality of the kinase domains and the activation of the MAPK pathway following FGF ligand stimulation in the absence of the C-terminal tail. Once confirmed, we could compare endocytosis levels between full-length and truncated FGFR-expressing cell lines, mirroring the methodology of our confocal microscopy experiments measuring internalization upon RSK2 inhibition. Next, RSK2 binding experiments as well as migration and proliferation experiments could be performed. This analysis would help address the importance of the C-terminal tail and the possible negative feedback associated with the C-terminal tail without concerns regarding the functionality or potential toxicity of RSK inhibitors. By employing this strategy, we would ensure that any observed effects are specifically attributable to events on the C-terminal tails of the receptors.

To specifically identify and examine which sites undergo phosphorylation, we could have performed mutagenesis to generate FGFR variants with the potential phosphorylation sites mutated. A previous study has shown that mutating specific serine residues to alanine in FGFR1 (e.g., S777A) resulted in prolonged tyrosine phosphorylation and increased mitogenic response and migration [46]. Building upon this, we could have employed the same technique to mutate corresponding serine residues in FGFR2 (S791A), FGFR3 (S782A), and FGFR4 (S776A) as identified through sequence alignment in Figure 4.1.1. Our objective would have been to generate U2OS cell lines expressing these mutated receptors. We would then have evaluated whether these mutations impact endocytosis compared to the wild-type counterpart using a similar setup to that used in this thesis. This would have helped confirm whether phosphorylation of these receptors indeed is required for endocytosis, likely mediated by interaction and phosphorylation by RSK2. If the mutated receptors, except in the case of FGFR3, exhibited reduced internalization compared to wild-type expressing cells, it would have supported the findings in this thesis. RSK2 binding experiments (Co-IP), phosphorylation experiments and measurements of biological response to FGF1 in cells expressing the mutated receptors compared to wild-type would then reveal if the negative feedback loop is important for all FGFRs or not. Further exploration involving mutations in nearby serines or threonines could have provided additional insights into potential phosphorylation sites, following established patterns such as R-X-R-X-X-pS/T

or R-R-X-pS/T [49, 60]. Moreover, as previously discussed, replacing S781 with a cysteine in FGFR3 (S781C) to align with the CSS sequence observed in other receptors (Figure 4.1.1) would provide an opportunity to investigate whether this modification triggers phosphorylation and binding by RSK2 to the receptor tail of FGFR3, potentially regulating endocytosis.

To strengthen the reliability of our findings, we could utilize multiple clones of U2OS cell lines (R1, R2, R3, R4) and conduct identical experiments for comparison. Our currently used cell lines are derived from a single clone. By employing this approach, we could determine whether any observed differences in RSK2 effects on the receptors result from the specific expression of receptors in U2OS cell lines or anomalies within a particular clone. Additionally, investigating other cell lines that naturally express FGFRs or utilizing transfected cell lines from non-osteosarcoma origins would help clarify whether the observed effects are exclusive to U2OS or applicable across diverse systems. Moreover, establishing CRISPR-engineered cell lines would provide a more controlled setting for investigating RSK2 effects on FGFR endocytosis and phosphorylation. This advanced technology allows for precise gene editing, ensuring consistent expression levels of FGFR1-4. Confirming equal FGFR levels across all cell lines would potentially validate if the lack of RSK inhibition on FGFR3 endocytosis is due to functional differences or expression level differences.

We could further validate our findings by conducting additional experiments inspired by a previous study on FGFR1 and RSK2 [49]. These experiments could help demonstrate that RSK2 binding and phosphorylation regulate endocytosis in FGFR2/4 but not FGFR3. For example, we could conduct Western blotting, to monitor signaling dynamics over time and determine if there is an increase in signaling when RSK2 is inhibited or when the receptor is mutated/truncated compared to the control. *In vitro* phosphorylation assays could help to determine if the receptors are directly phosphorylated by RSK2. Applying similar assays as those used for FGFR1 in the previous study would help us to assess the effects of RSK2-mediated phosphorylation on FGFR2-4 and their impact on endocytosis, signaling and biological output (migration/proliferation) providing valuable insights. Through these experiments, we could robustly demonstrate whether or not the RSK2-mediated negative feedback loop plays a role in FGFR regulation.

5.8 *In vitro* vs. *in vivo*

The studies on FGFR endocytosis and signaling in this thesis were conducted in cell lines, thus limiting the understanding of these mechanisms *in vivo*. *In vitro* systems offer several research benefits. They are cost-effective compared to *in vivo* studies and allow high control over experimental conditions, enabling precise manipulation of variables. This control is essential for accurate hypothesis testing. However, *in vitro* systems do not replicate the complex interactions present in living organisms. Therefore, while *in vitro* experiments are valuable for initial hypothesis testing and data collection, their findings must be confirmed through *in vivo*

studies to ensure real-world applicability [112, 113, 114]. An intermediate step that can enhance the relevance of *in vitro* findings is using 3D cell culture models and organ-on-a-chip systems, which better mimic the *in vivo* environment by providing a more physiologically relevant context for cell interactions and microenvironment [113, 115]. When our *in vitro* findings are further validated, we can move on to *in vivo* studies to confirm their relevance in a more complex biological context. Scientists typically start with *in vitro* experiments to test hypotheses and gather preliminary data, followed by *in vivo* studies to confirm the relevance and translate the findings into practical applications [112, 113].

5.9 Interpretation and implications of FGFR mutation patterns on oncogenic potential

In our study, we utilized the COSMIC database to examine mutation patterns in FGFR1-4 in sequenced human tumor samples, specifically focusing on mutations influencing the receptor's C-terminal tail that retains an intact catalytic domain. Verifying the integrity of the catalytic domain was crucial, as it ensures that the receptors can still activate the signaling pathways, potentially driving migration, proliferation, and contributing to oncogenic progression. Using Python scripts, we identified mutations, mainly truncating mutations, that delete the C-terminal tail of the receptor, disrupting the ERK1/2 and RSK2 phosphorylation sites in FGFR1-4 (Appendix B). Our analysis revealed that only a few mutations led to the loss of these phosphorylation sites while preserving an active kinase domain, suggesting that such mutations are relatively uncommon in FGFRs in tumor samples (Figure 4.6.2 and 4.6.3).

Our findings revealed that mutations affecting the C-terminal tail and the serine phosphorylation sites were rare in FGFRs, with only a small percentage of mutations leading to the loss of these sites while preserving the catalytic domain's integrity. For FGFR1, only 2 out of 832 mutations led to the loss of phosphorylation sites while retaining an intact catalytic domain. FGFR2 had 8 such mutations out of 1583, FGFR3 had 15 out of 5253, and FGFR4 had 5 out of 871 (Figure 4.6.2 and Appendix Figure C.1). These mutations included missense mutations and fusion proteins, with frameshift mutations particularly impactful. It's important to note that our criteria for considering a mutation as catalytically active were strict, requiring the catalytic domain to be fully intact. This was due to the uncertainty regarding how much of the catalytic domain must remain for the receptor to retain its activity.

Examining the figure depicting truncating mutations in FGFRs (Figure 4.6.3), it is evident that not many truncating mutations leave the catalytic domain fully intact or with significant parts intact, potentially remaining catalytically active. We noticed a small clustering of such mutations in the C-terminal tail of FGFR2 and FGFR3 (Figure 4.6.3). If these observations supported our findings on the effects of RSK2 inhibition on FGFR endocytosis, we would expect similar clustering of mutations in FGFR1, FGFR2, and FGFR4 towards the end of the catalytic domain, and not in FGFR3. FGFR3 endocytosis was not dependent on possibly implying that

it does not have the negative feedback mechanism, and thus, mutations in this region would not likely induce any oncogenic advantages. However, other feedback loops (such as, for example, the ERK1/2-mediated) or regulatory events may exist in the C-terminal tail of FGFR3. However, there is uncertainty about how frequently mutations in these areas of interest are expected to occur to indicate oncogenic advantages in cancer. Comparing these frequencies to known hotspot mutations or other significant mutational patterns in oncogenes might provide a clearer context.

Our study analyzed the prevalence and impact of truncating mutations in FGFRs, specifically examining the potential loss of the negative feedback mechanisms mediated by ERK1/2 and RSK2 phosphorylation sites in the C-terminal tail. We found that truncating mutations, which retained an intact or partially intact catalytic domain, were relatively uncommon in FGFRs across the tumor samples collected in the COSMIC database. This finding contrasts with the study by Zingg et al. (2022), which identified FGFR2 truncations, particularly those involving loss of the last exon (E18), as significant driver mutations frequently found in various cancers [48]. The E18 of FGFR2, includes the regions for ERK1/2 and potential RSK2 phosphorylation, and the frequent loss of this region in cancer highlights the disruption of these feedback mechanisms, leading to enhanced signaling as a potential oncogenic event in cancer.

It is worth mentioning that in the study by Zingg et al., the overall frequency of FGFR2 mutations identified that led to the loss of the C-terminal tail of FGFR2 was not very high. For example, among the 249570 samples in the Foundation Medicine FMI database, analysed by Zingg et al., only 1367 samples (0.55% incidence) were identified to potentially lead to loss of the C-terminal tail of FGFR2. For comparisons, missense hotspot mutations were found in 978 samples (incidence 0.39%). Given that FGFR hotspots are known to drive cancer progression, this suggests that FGFR2 C-terminal truncation might also contribute to cancer development. However, Zingg et al., demonstrated that a large proportion of the FGFR2 alterations identified, led to loss of the C-terminal tail (more than 1/3), indicating the importance of the C-terminal tail [48].

We utilized the COSMIC database, which compiles somatic mutations from various large-scale projects, including The Cancer Genome Atlas (TCGA) and the International Cancer Genome Consortium/The Cancer Genome Atlas Pan-Cancer Analysis of Whole Genomes project (ICGC/TCGA PCAWG) [92, 91]. In contrast, Zingg et al. employed several databases, including the Foundation Medicine Inc. (FMI) database, Hartwig Medical Foundation (HMF), and TCGA. Consequently, some overlap in data is expected due to the shared TCGA data. Most of the mutations affecting the C-terminal tail of FGFR2 in the FMI database involved gene rearrangement leading to fusion proteins [92, 91]. However, in the COSMIC database analyzed in this thesis, only a few fusion proteins were reported.

While the FGFR2 study by Zingg et al. posited that truncation was highly significant, our

findings suggest a more nuanced view. Our results suggests that the lack of significant truncating mutations in our data might imply that negative feedback mechanisms, such as those mediated by ERK1/2 and RSK2, may not be as critical in cancer progression as suggested by Zingg et al. Zingg et al. did not specifically address these negative feedback mechanisms but focused on the direct oncogenic potential of truncated FGFR2 variants and found that these were highly oncogenic *in vitro* and *in vivo* experiments. They speculated that this could be due to the loss of the negative feedback loop. More studies are needed to investigate this.

5.9.1 Further research to understand the relevance of FGFR negative feedback loops in cancer

To build on our findings and those of Zingg et al., further research can be considered to deepen our understanding of mutations in the FGFR terminal tail and their role in cancer. Firstly, additional databases beyond COSMIC, could be utilized and combined to identify and analyze FGFR mutations. This may reveal different mutation patterns and provide a broader context for our findings. In this thesis, we did not use the FMI database due to its subscription-based access compared to the free availability of the data in the COSMIC database. Moreover, the analysis could be done by stratifying samples into different cancer types. It is possible that FGFR signaling and its regulation are more important in some cancer types than in others.

Further *in vivo* studies using mouse models should be conducted to evaluate the tumorigenic potential of truncating and point mutations in FGFRs interfering with the potential feedback loops. These studies should focus on assessing tumor size, metastasis, and progression to determine the biological relevance of loss of the potential feedback loops. Inducing mutations in FGFRs at the specific ERK1/2 and RSK2 phosphorylation sites in these models could help establish whether they lead to increased metastasis and/or tumor growth, thereby confirming their role in cancer development.

In conclusion, while Zingg et al. emphasized the importance of FGFR2 truncations, our findings were unclear. Future research should aim to clarify the roles of these mechanisms in cancer.

5.10 How relevant are these negative feedback mechanisms in cancer?

FGFR signaling is crucial in many cancers, contributing to tumor growth and metastasis through genetic alterations leading to increased signaling. These alterations include point mutations, gene rearrangements, and genomic amplifications, identified in many human cancers [9, 28]. The role of FGFRs in promoting angiogenesis further underscores their importance in cancer progression [29]. It is therefore clear that knowledge of how these receptors are regulated is of importance to prevent oncogenic signaling.

A more specific example of why looking at negative feedback mechanisms in growth factor receptors is important for cancer research can be seen in the treatment of melanoma and colon

cancer. In melanoma patients with a specific mutation in B-RafV600E (B-Raf), a constitutively active Raf kinase leads to constitutive MAPK signaling. Specific B-Raf inhibitors target this abnormal kinase activity and are successfully used in the clinic for melanoma patients [116]. In contrast, the high expression of epidermal growth factor receptor (EGFR), a receptor tyrosine kinase, in colon cancer cells complicates this treatment approach in patients with colon cancer. When Raf is inhibited, a negative feedback loop from ERK1/2 to EGFR is disrupted, leading to compensatory signaling through EGFR that undermines the treatment's effectiveness. Combining Raf and EGFR inhibitors has improved responses in these cases [116]. This combination treatment is now implemented in the clinic for metastatic colon cancer patients [117].

This distinction underscores the importance of understanding the regulatory mechanisms in different signaling contexts. While EGFR and FGFR are distinct receptors, their roles as growth receptors suggest that insights from EGFR feedback mechanisms could inform strategies for FGFR-related cancers [44]. Hence, understanding negative feedback mechanisms is crucial for optimizing cancer treatments, improving therapeutic responses, and overcoming drug resistance [116, 44, 117].

CHAPTER

SIX

CONCLUSION AND FUTURE PERSPECTIVES

In this thesis, our findings demonstrate that RSK2 plays a crucial role in the endocytosis of FGFR2 and FGFR4, similar to FGFR1, with decreased receptor internalization observed upon MEK1/2 and RSK2 inhibition, while FGFR3 remained unaffected.

RSK2 was found to bind to the FGFR1 receptor tail upon ligand stimulation but we were not able to detect binding between RSK2 and FGFR4. More research is needed to elucidate if RSK2 binds to FGFRs. Increased migration was observed in FGFR1-3 expressing cells upon FGF1 stimulation, while FGFR4 showed increased proliferation. However, migration or proliferation were not increased with RSK2 inhibition, possibly due to toxicity.

Furthermore, we analyzed the prevalence of truncating mutations in FGFRs, focusing on the loss of the potential negative feedback mechanisms mediated by ERK1/2 and RSK2 phosphorylation sites in the C-terminal tail. Few such alterations were observed. Further analysis is necessary to understand their potential relevance in FGFR-driven tumorigenicity.

This study highlights a crucial role of RSK2-mediated feedback for regulation of FGFR internalization with possible differences among the FGFRs in their dependency of RSK2. Although some alterations leading to loss of the potential feedback loops were identified in cancer, the frequency was not very high. Future research should explore alternative approaches, additional databases, and in vivo models to confirm and expand these findings.

REFERENCES

[1] Khawaja Ashfaque Ahmed and Jim Xiang. "Mechanisms of cellular communication through intercellular protein transfer". In: *Journal of Cellular and Molecular Medicine* 15.7 (July 2011), pp. 1458–1473. ISSN: 1582-1838. DOI: 10.1111/j.1582-4934.2010.01008.x.

[2] Qi Liu et al. "Dysregulated ligand–receptor interactions from single-cell transcriptomics". In: *Bioinformatics* 38.12 (June 13, 2022), pp. 3216–3221. ISSN: 1367-4803. DOI: 10.1093/bioinformatics/btac294.

[3] Athina-Myrto Chioni and Richard P. Grose. "Biological Significance and Targeting of the FGFR Axis in Cancer". In: *Cancers* 13.22 (Nov. 13, 2021), p. 5681. ISSN: 2072-6694. DOI: 10.3390/cancers13225681.

[4] G. Steven Martin. "Cell signaling and cancer". In: *Cancer Cell* 4.3 (Sept. 2003), pp. 167–174. ISSN: 1535-6108. DOI: 10.1016/s1535-6108(03)00216-2.

[5] Matin Chehelgerdi et al. "Exploring the promising potential of induced pluripotent stem cells in cancer research and therapy". In: *Molecular Cancer* 22 (Nov. 28, 2023), p. 189. ISSN: 1476-4598. DOI: 10.1186/s12943-023-01873-0.

[6] Mark A. Lemmon and Joseph Schlessinger. "Cell signaling by receptor tyrosine kinases". In: *Cell* 141.7 (June 25, 2010), pp. 1117–1134. ISSN: 1097-4172. DOI: 10.1016/j.cell.2010.06.011.

[7] Punit Saraon et al. "Receptor tyrosine kinases and cancer: oncogenic mechanisms and therapeutic approaches". In: *Oncogene* 40.24 (June 2021), pp. 4079–4093. ISSN: 1476-5594. DOI: 10.1038/s41388-021-01841-2.

[8] Zhenfang Du and Christine M. Lovly. "Mechanisms of receptor tyrosine kinase activation in cancer". In: *Molecular Cancer* 17 (Feb. 19, 2018), p. 58. ISSN: 1476-4598. DOI: 10.1186/s12943-018-0782-4.

[9] Teresa Helsten, Maria Schwaederle, and Razelle Kurzrock. "Fibroblast growth factor receptor signaling in hereditary and neoplastic disease: biologic and clinical implications". In: *Cancer Metastasis Reviews* 34 (2015), pp. 479–496. ISSN: 0167-7659. DOI: 10.1007/s10555-015-9579-8.

[10] Nobuyuki Itoh and David M. Ornitz. “Fibroblast growth factors: from molecular evolution to roles in development, metabolism and disease”. In: *The Journal of Biochemistry* 149.2 (Feb. 1, 2011), pp. 121–130. ISSN: 0021-924X. DOI: 10.1093/jb/mvq121.

[11] Masuko Katoh et al. “FGFR-targeted therapeutics: clinical activity, mechanisms of resistance and new directions”. In: *Nature Reviews Clinical Oncology* 21.4 (Apr. 2024), pp. 312–329. ISSN: 1759-4782. DOI: 10.1038/s41571-024-00869-z.

[12] Shuyan Dai et al. “Fibroblast Growth Factor Receptors (FGFRs): Structures and Small Molecule Inhibitors”. In: *Cells* 8.6 (June 18, 2019), p. 614. ISSN: 2073-4409. DOI: 10.3390/cells8060614.

[13] M. Wiedemann and B. Trueb. “Characterization of a novel protein (FGFRL1) from human cartilage related to FGF receptors”. In: *Genomics* 69.2 (Oct. 15, 2000), pp. 275–279. ISSN: 0888-7543. DOI: 10.1006/geno.2000.6332.

[14] Dandan Guan et al. “Regulation of fibroblast growth factor 15/19 and 21 on metabolism: in the fed or fasted state”. In: *Journal of Translational Medicine* 14 (Mar. 1, 2016), p. 63. ISSN: 1479-5876. DOI: 10.1186/s12967-016-0821-0.

[15] Vigdis Sørensen et al. “Different abilities of the four FGFRs to mediate FGF-1 translocation are linked to differences in the receptor C-terminal tail”. In: *Journal of Cell Science* 119.20 (Oct. 15, 2006), pp. 4332–4341. ISSN: 0021-9533. DOI: 10.1242/jcs.03209.

[16] David M. Ornitz and Nobuyuki Itoh. “New developments in the biology of fibroblast growth factors”. In: *WIREs mechanisms of disease* 14.4 (July 2022), e1549. ISSN: 2692-9368. DOI: 10.1002/wsbm.1549.

[17] Nobuyuki Itoh and David M. Ornitz. “Evolution of the *Fgf* and *Fgfr* gene families”. In: *Trends in Genetics* 20.11 (Nov. 1, 2004), pp. 563–569. ISSN: 0168-9525. DOI: 10.1016/j.tig.2004.08.007.

[18] Brendan Farrell and Alexander L. Breeze. “Structure, activation and dysregulation of fibroblast growth factor receptor kinases: perspectives for clinical targeting”. In: *Biochemical Society Transactions* 46.6 (Dec. 17, 2018), pp. 1753–1770. ISSN: 0300-5127. DOI: 10.1042/BST20180004.

[19] Klaus Holzmann et al. “Alternative Splicing of Fibroblast Growth Factor Receptor IgIII Loops in Cancer”. In: *Journal of Nucleic Acids* 2012 (2012), p. 950508. ISSN: 2090-0201. DOI: 10.1155/2012/950508.

[20] Lingfeng Chen et al. “Structural basis for FGF hormone signalling”. In: *Nature* 618.7966 (June 2023), pp. 862–870. ISSN: 1476-4687. DOI: 10.1038/s41586-023-06155-9.

[21] Johan Kreuger et al. “Fibroblast growth factors share binding sites in heparan sulphate”. In: *Biochemical Journal* 389 (Pt 1 July 1, 2005), pp. 145–150. ISSN: 0264-6021. DOI: 10.1042/BJ20042129.

[22] Omar A. Ibrahimi et al. “Kinetic Model for FGF, FGFR, and Proteoglycan Signal Transduction Complex Assembly”. In: *Biochemistry* 43.16 (Apr. 1, 2004), pp. 4724–4730. ISSN: 0006-2960. DOI: 10.1021/bi0352320.

[23] Hiroshi Kurosu et al. “Tissue-specific Expression of Klotho and Fibroblast Growth Factor (FGF) Receptor Isoforms Determines Metabolic Activity of FGF19 and FGF21*”. In: *Journal of Biological Chemistry* 282.37 (Sept. 14, 2007), pp. 26687–26695. ISSN: 0021-9258. DOI: 10.1074/jbc.M704165200.

[24] Yasushi Ogawa et al. “Klotho is required for metabolic activity of fibroblast growth factor 21”. In: *Proceedings of the National Academy of Sciences* 104.18 (May 2007), pp. 7432–7437. DOI: 10.1073/pnas.0701600104.

[25] Patrycja Szybowska et al. “Negative Regulation of FGFR (Fibroblast Growth Factor Receptor) Signaling”. In: *Cells* 10.6 (May 28, 2021), p. 1342. ISSN: 2073-4409. DOI: 10.3390/cells10061342.

[26] Mariya Farooq et al. “The Role of Fibroblast Growth Factor (FGF) Signaling in Tissue Repair and Regeneration”. In: *Cells* 10.11 (Nov. 19, 2021), p. 3242. ISSN: 2073-4409. DOI: 10.3390/cells10113242.

[27] Marie Cargnello and Philippe P. Roux. “Activation and Function of the MAPKs and Their Substrates, the MAPK-Activated Protein Kinases”. In: *Microbiology and Molecular Biology Reviews : MMBR* 75.1 (Mar. 2011), pp. 50–83. ISSN: 1092-2172. DOI: 10.1128/MMBR.00031-10.

[28] Melanie A. Krook et al. “Fibroblast growth factor receptors in cancer: genetic alterations, diagnostics, therapeutic targets and mechanisms of resistance”. In: *British Journal of Cancer* 124.5 (Mar. 2021), pp. 880–892. ISSN: 1532-1827. DOI: 10.1038/s41416-020-01157-0.

[29] Roberto Ronca et al. “The potential of fibroblast growth factor/fibroblast growth factor receptor signaling as a therapeutic target in tumor angiogenesis”. In: *Expert Opinion on Therapeutic Targets* 19.10 (2015), pp. 1361–1377. ISSN: 1744-7631. DOI: 10.1517/14728222.2015.1062475.

[30] Irina S. Babina and Nicholas C. Turner. “Advances and challenges in targeting FGFR signalling in cancer”. In: *Nature Reviews. Cancer* 17.5 (May 2017), pp. 318–332. ISSN: 1474-1768. DOI: 10.1038/nrc.2017.8.

[31] Sophie Engelhardt et al. “Frequent FGFR1 hotspot alterations in driver-unknown low-grade glioma and mixed neuronal-glial tumors”. In: *Journal of Cancer Research and Clinical Oncology* 148.4 (Apr. 1, 2022), pp. 857–866. ISSN: 1432-1335. DOI: 10.1007/s00432-021-03906-x.

[32] Andrea Napolitano et al. “Fibroblast Growth Factor Receptor (FGFR) Signaling in GIST and Soft Tissue Sarcomas”. In: *Cells* 10.6 (June 2021), p. 1533. ISSN: 2073-4409. DOI: 10.3390/cells10061533.

[33] Janice N. Cormier and Raphael E. Pollock. “Soft Tissue Sarcomas”. In: *CA: A Cancer Journal for Clinicians* 54.2 (2004), pp. 94–109. ISSN: 1542-4863. DOI: 10.3322/canjclin.54.2.94.

[34] Wen-Ya Zhou et al. “Characterization of FGFR signaling pathway as therapeutic targets for sarcoma patients”. In: *Cancer Biology & Medicine* 13.2 (June 2016), pp. 260–268. ISSN: 2095-3941. DOI: 10.20892/j.issn.2095-3941.2015.0102.

[35] Carina A. Dehner et al. “Genetic Characterization, Current Model Systems and Prognostic Stratification in PAX Fusion-Negative vs. PAX Fusion-Positive Rhabdomyosarcoma”. In: *Genes* 12.10 (Sept. 25, 2021), p. 1500. ISSN: 2073-4425. DOI: 10.3390/genes12101500.

[36] Jack F. Shern et al. “Comprehensive Genomic Analysis of Rhabdomyosarcoma Reveals a Landscape of Alterations Affecting a Common Genetic Axis in Fusion-Positive and Fusion-Negative Tumors”. In: *Cancer Discovery* 4.2 (Feb. 4, 2014), pp. 216–231. ISSN: 2159-8274. DOI: 10.1158/2159-8290.CD-13-0639.

[37] Anthony Markham. “Erdafitinib: First Global Approval”. In: *Drugs* 79.9 (June 2019), pp. 1017–1021. ISSN: 0012-6667, 1179-1950. DOI: 10.1007/s40265-019-01142-9.

[38] Sheridan M. Hoy. “Pemigatinib: First Approval”. In: *Drugs (New York, N.Y.)* 80.9 (2020), pp. 923–929. ISSN: 0012-6667. DOI: 10.1007/s40265-020-01330-y.

[39] Goyal Lipika et al. “Futibatinib for FGFR2-Rearranged Intrahepatic Cholangiocarcinoma”. In: *New England Journal of Medicine* 388.3 (Jan. 18, 2023), pp. 228–239. DOI: 10.1056/NEJMoa2206834.

[40] Elizabeth Catherine Smyth et al. “Trial in progress: Phase 3 study of bemarituzumab + mFOLFOX6 versus placebo + mFOLFOX6 in previously untreated advanced gastric or gastroesophageal junction (GEJ) cancer with FGFR2b overexpression (FORTITUDE-101).” In: *Journal of Clinical Oncology* 40.16 (June 2022), TPS4164–TPS4164. ISSN: 0732-183X. DOI: 10.1200/JCO.2022.40.16_suppl.TPS4164.

[41] Michal Kostas et al. “Protein Tyrosine Phosphatase Receptor Type G (PTPRG) Controls Fibroblast Growth Factor Receptor (FGFR) 1 Activity and Influences Sensitivity to FGFR Kinase Inhibitors *”. In: *Molecular & Cellular Proteomics* 17.5 (May 1, 2018), pp. 850–870. ISSN: 1535-9476, 1535-9484. DOI: 10.1074/mcp.RA117.000538.

[42] Permeen Yusoff et al. “Sprouty2 Inhibits the Ras/MAP Kinase Pathway by Inhibiting the Activation of Raf *”. In: *Journal of Biological Chemistry* 277.5 (Feb. 1, 2002), pp. 3195–3201. ISSN: 0021-9258, 1083-351X. DOI: 10.1074/jbc.M108368200.

[43] Jacqueline M. Mason et al. “Tyrosine Phosphorylation of Sprouty Proteins Regulates Their Ability to Inhibit Growth Factor Signaling: A Dual Feedback Loop”. In: *Molecular Biology of the Cell* 15.5 (May 2004), pp. 2176–2188. ISSN: 1059-1524. DOI: 10.1091/mbc.e03-07-0503.

[44] David Lake, Sonia A. L. Corrêa, and Jürgen Müller. "Negative feedback regulation of the ERK1/2 MAPK pathway". In: *Cellular and Molecular Life Sciences* 73.23 (Dec. 1, 2016), pp. 4397–4413. ISSN: 1420-9071. DOI: 10.1007/s00018-016-2297-8.

[45] Patrycja Szybowska et al. "Cancer Mutations in FGFR2 Prevent a Negative Feedback Loop Mediated by the ERK1/2 Pathway". In: *Cells* 8.6 (June 2019), p. 518. ISSN: 2073-4409. DOI: 10.3390/cells8060518.

[46] Malgorzata Zakrzewska et al. "ERK-Mediated Phosphorylation of Fibroblast Growth Factor Receptor 1 on Ser777 Inhibits Signaling". In: *Science Signaling* 6.262 (Feb. 12, 2013), ra11–ra11. DOI: 10.1126/scisignal.2003087.

[47] Evrim B. Ünal, Florian Uhlitz, and Nils Blüthgen. "A compendium of ERK targets". In: *FEBS Letters* 591.17 (2017), pp. 2607–2615. ISSN: 1873-3468. DOI: 10.1002/1873-3468.12740.

[48] Daniel Zingg et al. "Truncated FGFR2 is a clinically actionable oncogene in multiple cancers". In: *Nature* 608.7923 (Aug. 2022), pp. 609–617. ISSN: 1476-4687. DOI: 10.1038/s41586-022-05066-5.

[49] B. Nadratowska-Wesolowska et al. "RSK2 regulates endocytosis of FGF receptor 1 by phosphorylation on serine 789". In: *Oncogene* 33.40 (Oct. 2014), pp. 4823–4836. ISSN: 1476-5594. DOI: 10.1038/onc.2013.425.

[50] Jonathan L. Jeger. "Endosomes, lysosomes, and the role of endosomal and lysosomal biogenesis in cancer development". In: *Molecular Biology Reports* 47.12 (Dec. 1, 2020), pp. 9801–9810. ISSN: 1573-4978. DOI: 10.1007/s11033-020-05993-4.

[51] Sarah R. Elkin, Ashley M. Lakoduk, and Sandra L. Schmid. "Endocytic Pathways and Endosomal Trafficking: A Primer". In: *Wiener medizinische Wochenschrift (1946)* 166.7 (May 2016), pp. 196–204. ISSN: 0043-5341. DOI: 10.1007/s10354-016-0432-7.

[52] Peter J. Cullen and Florian Steinberg. "To degrade or not to degrade: mechanisms and significance of endocytic recycling". In: *Nature Reviews Molecular Cell Biology* 19.11 (Nov. 2018), pp. 679–696. ISSN: 1471-0080. DOI: 10.1038/s41580-018-0053-7.

[53] Marcel Mettlen et al. "Regulation of Clathrin-Mediated Endocytosis". In: *Annual review of biochemistry* 87 (June 20, 2018), pp. 871–896. ISSN: 0066-4154. DOI: 10.1146/annurev-biochem-062917-012644.

[54] Ellen Margrethe Haugsten et al. "Proximity Labeling Reveals Molecular Determinants of FGFR4 Endosomal Transport". In: *Journal of Proteome Research* 15.10 (Oct. 7, 2016), pp. 3841–3855. ISSN: 1535-3893. DOI: 10.1021/acs.jproteome.6b00652.

[55] Ellen Margrethe Haugsten et al. "Clathrin- and dynamin-independent endocytosis of FGFR3–implications for signalling". In: *PloS One* 6.7 (2011), e21708. ISSN: 1932-6203. DOI: 10.1371/journal.pone.0021708.

[56] Ellen Margrethe Haugsten et al. “Ubiquitination of Fibroblast Growth Factor Receptor 1 Is Required for Its Intracellular Sorting but Not for Its Endocytosis”. In: *Molecular Biology of the Cell* 19.8 (Aug. 2008), pp. 3390–3403. ISSN: 1059-1524. DOI: 10.1091/mbc.e07-12-1219.

[57] Ellen Margrethe Haugsten et al. “Different intracellular trafficking of FGF1 endocytosed by the four homologous FGF receptors”. In: *Journal of Cell Science* 118.17 (Sept. 1, 2005), pp. 3869–3881. ISSN: 0021-9533. DOI: 10.1242/jcs.02509.

[58] Romain Lara, Michael J. Seckl, and Olivier E. Pardo. “The p90 RSK family members: common functions and isoform specificity”. In: *Cancer Research* 73.17 (Sept. 1, 2013), pp. 5301–5308. ISSN: 1538-7445. DOI: 10.1158/0008-5472.CAN-12-4448.

[59] Yves Romeo, Xiaocui Zhang, and Philippe P. Roux. “Regulation and function of the RSK family of protein kinases”. In: *Biochemical Journal* 441.2 (Dec. 21, 2011), pp. 553–569. ISSN: 0264-6021. DOI: 10.1042/BJ20110289.

[60] Ian A. Leighton et al. “Comparison of the specificities of p70 S6 kinase and MAPKAP kinase-1 identifies a relatively specific substrate for p70 S6 kinase: the N-terminal kinase domain of MAPKAP kinase-1 is essential for peptide phosphorylation”. In: *FEBS Letters* 375.3 (1995), pp. 289–293. ISSN: 1873-3468. DOI: 10.1016/0014-5793(95)01170-J.

[61] Tae Hoon Jang et al. “Cryopreservation and its clinical applications”. In: *Integrative Medicine Research* 6.1 (Mar. 1, 2017), pp. 12–18. ISSN: 2213-4220. DOI: 10.1016/j.imr.2016.12.001.

[62] David Whaley et al. “Cryopreservation: An Overview of Principles and Cell-Specific Considerations”. In: *Cell Transplantation* 30 (2021), p. 963689721999617. ISSN: 1555-3892. DOI: 10.1177/0963689721999617.

[63] Anthony O. Olarerin-George and John B. Hogenesch. “Assessing the prevalence of mycoplasma contamination in cell culture via a survey of NCBI’s RNA-seq archive”. In: *Nucleic Acids Research* 43.5 (Mar. 11, 2015), pp. 2535–2542. ISSN: 0305-1048. DOI: 10.1093/nar/gkv136.

[64] Andrew B. Nowakowski, William J. Wobig, and David H. Petering. “Native SDS-PAGE: high resolution electrophoretic separation of proteins with retention of native properties including bound metal ions”. In: *Metallomics* 6.5 (2014), pp. 168–178. ISSN: 1756-5901. DOI: 10.1039/c4mt00033a.

[65] J. D. Fritz, D. R. Swartz, and M. L. Greaser. “Factors affecting polyacrylamide gel electrophoresis and electroblotting of high-molecular-weight myofibrillar proteins”. In: *Analytical Biochemistry* 180.2 (Aug. 1, 1989), pp. 205–210. ISSN: 0003-2697. DOI: 10.1016/0003-2697(89)90116-4.

[66] Mark C. Alliegro. “Effects of Dithiothreitol on Protein Activity Unrelated to Thiol–Disulfide Exchange: For Consideration in the Analysis of Protein Function with Cleland’s Reagent”. In: *Analytical biochemistry* 282.1 (2000), pp. 102–106. ISSN: 0003-2697. DOI: 10.1006/abio.2000.4557.

[67] Biji T. Kurien and R. Hal Scofield. “Western Blotting: An Introduction”. In: *Methods in molecular biology (Clifton, N.J.)* 1312 (2015), pp. 17–30. ISSN: 1064-3745. DOI: 10.1007/978-1-4939-2694-7_5.

[68] *Western Blot Transfer Buffer | Bio-Rad*. URL: https://www.bio-rad.com/en-no/feature/western-blot-transfer-buffer.html (visited on 05/10/2024).

[69] Junseon Min et al. “A Recombinant Secondary Antibody Mimic as a Target-specific Signal Amplifier and an Antibody Immobilizer in Immunoassays”. In: *Scientific Reports* 6 (Apr. 11, 2016), p. 24159. ISSN: 2045-2322. DOI: 10.1038/srep24159.

[70] *HRP Linked Secondary Antibodies - NO*. URL: https://www.thermofisher.com/uk/en/home/life-science/antibodies/secondary-antibodies/hrp-secondary-antibodies.html (visited on 05/16/2024).

[71] Pietro P. M. Iannetta et al. “Ethylene and carbon dioxide production by developing strawberries show a correlative pattern that is indicative of ripening climacteric fruit”. In: *Physiologia Plantarum* 127.2 (2006), pp. 247–259. ISSN: 1399-3054. DOI: 10.1111/j.1399-3054.2006.00656.x.

[72] Yuhong Xiao and Stuart N. Isaacs. “Enzyme-Linked Immunosorbent Assay (ELISA) and Blocking with Bovine Serum Albumin (BSA) - Not all BSAs are alike”. In: *Journal of immunological methods* 384.1 (Oct. 31, 2012), pp. 148–151. ISSN: 0022-1759. DOI: 10.1016/j.jim.2012.06.009.

[73] Lakshmi Pillai-Kastoori, Amy R. Schutz-Geschwender, and Jeff A. Harford. “A systematic approach to quantitative Western blot analysis”. In: *Analytical Biochemistry* 593 (Mar. 15, 2020), p. 113608. ISSN: 0003-2697. DOI: 10.1016/j.ab.2020.113608.

[74] Krishna Kumar Singh et al. “Emerging techniques of western blotting for purification and analysis of protein”. In: *Future Journal of Pharmaceutical Sciences* 7.1 (Dec. 14, 2021), p. 239. ISSN: 2314-7253. DOI: 10.1186/s43094-021-00386-1.

[75] Andrea Degasperi et al. “Evaluating Strategies to Normalise Biological Replicates of Western Blot Data”. In: *PLOS ONE* 9.1 (Jan. 27, 2014), e87293. ISSN: 1932-6203. DOI: 10.1371/journal.pone.0087293.

[76] Julian R. Avila, Jin Suk Lee, and Keiko U. Torii. “Co-Immunoprecipitation of Membrane-Bound Receptors”. In: *The Arabidopsis Book / American Society of Plant Biologists* 13 (June 3, 2015), e0180. ISSN: 1543-8120. DOI: 10.1199/tab.0180.

[77] Amicia D. Elliott. “Confocal Microscopy: Principles and Modern Practices”. In: *Current protocols in cytometry* 92.1 (Mar. 2020), e68. ISSN: 1934-9297. DOI: 10.1002/cpcy.68.

[78] Vigdis Sørensen et al. “Phosphorylation of Fibroblast Growth Factor (FGF) Receptor 1 at Ser777 by p38 Mitogen-Activated Protein Kinase Regulates Translocation of Exogenous FGF1 to the Cytosol and Nucleus”. In: *Molecular and Cellular Biology* 28.12 (June 2008), pp. 4129–4141. ISSN: 0270-7306. DOI: 10.1128/MCB.02117-07.

[79] Rooban Thavarajah et al. “Chemical and physical basics of routine formaldehyde fixation”. In: *Journal of Oral and Maxillofacial Pathology : JOMFP* 16.3 (2012), pp. 400–405. ISSN: 0973-029X. DOI: 10.4103/0973-029X.102496.

[80] Shuanghui Luo et al. “Effect of HEPES buffer on the uptake and transport of P-glycoprotein substrates and large neutral amino acids”. In: *Molecular pharmaceutics* 7.2 (Apr. 5, 2010), pp. 412–420. ISSN: 1543-8384. DOI: 10.1021/mp900193e.

[81] *DAPI and Hoechst Nucleic Acid Stains*. URL: https://www.thermofisher.com/order/catalog/product/H3570 (visited on 05/19/2024).

[82] Joseph R. Lakowicz, ed. *Principles of Fluorescence Spectroscopy*. Boston, MA: Springer US, 2006. ISBN: 978-0-387-31278-1 978-0-387-46312-4. DOI: 10.1007/978-0-387-46312-4.

[83] Michael J. Sanderson et al. “Fluorescence Microscopy”. In: *Cold Spring Harbor protocols* 2014.10 (Oct. 1, 2014), pdb.top071795. ISSN: 1940-3402. DOI: 10.1101/pdb.top071795.

[84] Mahbubul H. Shihan et al. “A simple method for quantitating confocal fluorescent images”. In: *Biochemistry and Biophysics Reports* 25 (Feb. 1, 2021), p. 100916. ISSN: 2405-5808. DOI: 10.1016/j.bbrep.2021.100916.

[85] Siân Culley et al. “Made to measure: An introduction to quantifying microscopy data in the life sciences”. In: *Journal of Microscopy* n/a (n/a). ISSN: 1365-2818. DOI: 10.1111/jmi.13208.

[86] Melanie M. Frigault et al. “Live-cell microscopy – tips and tools”. In: *Journal of Cell Science* 122.6 (Mar. 15, 2009), pp. 753–767. ISSN: 0021-9533. DOI: 10.1242/jcs.033837.

[87] Børge Holme et al. “Automated tracking of cell migration in phase contrast images with CellTraxx”. In: *Scientific Reports* 13.1 (Dec. 27, 2023), p. 22982. ISSN: 2045-2322. DOI: 10.1038/s41598-023-50227-9.

[88] “The Universal Protein Resource (UniProt)”. In: *Nucleic Acids Research* 36 (Database issue Jan. 2008), pp. D190–D195. ISSN: 0305-1048. DOI: 10.1093/nar/gkm895.

[89] Rose Oughtred et al. “The BioGRID database: A comprehensive biomedical resource of curated protein, genetic, and chemical interactions”. In: *Protein Science : A Publication of the Protein Society* 30.1 (Jan. 2021), pp. 187–200. ISSN: 0961-8368. DOI: 10.1002/pro.3978.

[90] Peter V. Hornbeck et al. “PhosphoSitePlus, 2014: mutations, PTMs and recalibrations”. In: *Nucleic Acids Research* 43 (D1 Jan. 28, 2015), pp. D512–D520. ISSN: 0305-1048. DOI: 10.1093/nar/gku1267.

[91] S. Bamford et al. “The COSMIC (Catalogue of Somatic Mutations in Cancer) database and website”. In: *British Journal of Cancer* 91.2 (July 2004), pp. 355–358. ISSN: 1532-1827. DOI: 10.1038/sj.bjc.6601894.

[92] Zbyslaw Sondka et al. “COSMIC: a curated database of somatic variants and clinical data for cancer”. In: *Nucleic Acids Research* 52 (D1 Jan. 5, 2024), pp. D1210–D1217. ISSN: 0305-1048. DOI: 10.1093/nar/gkad986.

[93] Xiang Wan et al. “Estimating the sample mean and standard deviation from the sample size, median, range and/or interquartile range”. In: *BMC Medical Research Methodology* 14.1 (Dec. 19, 2014), p. 135. ISSN: 1471-2288. DOI: 10.1186/1471-2288-14-135.

[94] Graeme D. Ruxton and Guy Beauchamp. “Time for some a priori thinking about post hoc testing”. In: *Behavioral Ecology* 19.3 (May 1, 2008), pp. 690–693. ISSN: 1045-2249. DOI: 10.1093/beheco/arn020.

[95] Stephen Midway et al. “Comparing multiple comparisons: practical guidance for choosing the best multiple comparisons test”. In: *PeerJ* 8 (Dec. 4, 2020), e10387. ISSN: 2167-8359. DOI: 10.7717/peerj.10387.

[96] Esther Herberich, Johannes Sikorski, and Torsten Hothorn. “A Robust Procedure for Comparing Multiple Means under Heteroscedasticity in Unbalanced Designs”. In: *PLoS ONE* 5.3 (Mar. 29, 2010), e9788. ISSN: 1932-6203. DOI: 10.1371/journal.pone.0009788.

[97] Neychelle Fernandes and Nancy .L. Allbritton. “Effect of the DEF motif on phosphorylation of peptide substrates by ERK”. In: *Biochemical and biophysical research communications* 387.2 (Sept. 18, 2009), pp. 414–418. ISSN: 0006-291X. DOI: 10.1016/j.bbrc.2009.07.049.

[98] Joanna Moes-Sosnowska and Joanna Chorostowska-Wynimko. “Fibroblast Growth Factor Receptor 1-4 Genetic Aberrations as Clinically Relevant Biomarkers in Squamous Cell Lung Cancer”. In: *Frontiers in oncology* 12 (2022), pp. 780650–780650. ISSN: 2234-943X. DOI: 10.3389/fonc.2022.780650.

[99] Kari Salokas et al. “Physical and functional interactome atlas of human receptor tyrosine kinases”. In: *EMBO reports* 23.6 (June 7, 2022), e54041. ISSN: 1469-221X. DOI: 10.15252/embr.202154041.

[100] Star M. Dunham-Ems et al. “Fibroblast Growth Factor Receptor-1 (FGFR1) Nuclear Dynamics Reveal a Novel Mechanism in Transcription Control”. In: *Molecular Biology of the Cell* 20.9 (May 2009), pp. 2401–2412. ISSN: 1059-1524. DOI: 10.1091/mbc.e08-06-0600.

[101] Yafang Hu et al. “90-kDa ribosomal S6 kinase is a direct target for the nuclear fibroblast growth factor receptor 1 (FGFR1): role in FGFR1 signaling”. In: *The Journal of Biological Chemistry* 279.28 (July 9, 2004), pp. 29325–29335. ISSN: 0021-9258. DOI: 10.1074/jbc.M311144200.

[102] Zhifeng Huang et al. “Two FGFR kinase molecules act in concert to recruit and transphosphorylate PLC”. In: *Molecular cell* 61.1 (Jan. 7, 2016), pp. 98–110. ISSN: 1097-2765. DOI: 10.1016/j.molcel.2015.11.010.

[103] M. H. Cobb. "MAP kinase pathways". In: *Progress in Biophysics and Molecular Biology* 71.3 (1999), pp. 479–500. ISSN: 0079-6107. DOI: 10.1016/s0079-6107(98)00056-x.

[104] Hassan Dana et al. "Molecular Mechanisms and Biological Functions of siRNA". In: *International Journal of Biomedical Science : IJBS* 13.2 (June 2017), pp. 48–57. ISSN: 1550-9702.

[105] C. J. Jensen et al. "90-kDa ribosomal S6 kinase is phosphorylated and activated by 3-phosphoinositide-dependent protein kinase-1". In: *The Journal of Biological Chemistry* 274.38 (Sept. 17, 1999), pp. 27168–27176. ISSN: 0021-9258. DOI: 10.1074/jbc.274.38.27168.

[106] Ellen M. Haugsten et al. "Photoactivation Approaches Reveal a Role for Rab11 in FGFR4 Recycling and Signalling". In: *Traffic* 15.6 (2014), pp. 665–683. ISSN: 1600-0854. DOI: 10.1111/tra.12168.

[107] Gopal P. Sapkota et al. "BI-D1870 is a specific inhibitor of the p90 RSK (ribosomal S6 kinase) isoforms in vitro and in vivo". In: *Biochemical Journal* 401.1 (Dec. 11, 2006), pp. 29–38. ISSN: 0264-6021. DOI: 10.1042/BJ20061088.

[108] Sun-Mi Yoo, Sung Jun Cho, and Yong-Yeon Cho. "Molecular Targeting of ERKs/RSK2 Signaling Axis in Cancer Prevention". In: *Journal of Cancer Prevention* 20.3 (Sept. 30, 2015), pp. 165–171. DOI: 10.15430/JCP.2015.20.3.165.

[109] Chiara Francavilla et al. "Functional proteomics defines the molecular switch underlying FGF receptor trafficking and cellular outputs". In: *Molecular Cell* 51.6 (Sept. 26, 2013), pp. 707–722. ISSN: 1097-4164. DOI: 10.1016/j.molcel.2013.08.002.

[110] Shiela C. Samson, Akib M. Khan, and Michelle C. Mendoza. "ERK signaling for cell migration and invasion". In: *Frontiers in Molecular Biosciences* 9 (Oct. 3, 2022). ISSN: 2296-889X. DOI: 10.3389/fmolb.2022.998475.

[111] Dani L. Bodor et al. "Of Cell Shapes and Motion: The Physical Basis of Animal Cell Migration". In: *Developmental Cell* 52.5 (Mar. 9, 2020), pp. 550–562. ISSN: 1534-5807. DOI: 10.1016/j.devcel.2020.02.013.

[112] James R Vinyard and Antonio P Faciola. "Unraveling the pros and cons of various in vitro methodologies for ruminant nutrition: a review". In: *Translational Animal Science* 6.4 (Oct. 1, 2022), txac130. ISSN: 2573-2102. DOI: 10.1093/tas/txac130.

[113] Oliver Graudejus et al. "Bridging the gap between in vivo and in vitro research: Reproducing in vitro the mechanical and electrical environment of cells in vivo". In: *Frontiers in cellular neuroscience* 12 (2018). ISSN: 1662-5102. DOI: 10.3389/conf.fncel.2018.38.00069.

[114] Jialong Zhu et al. "Organoids and organs-on-chips: insights into predicting the efficacy of systemic treatment in colorectal cancer". In: *Cell Death Discovery* 9 (Feb. 22, 2023), p. 72. ISSN: 2058-7716. DOI: 10.1038/s41420-023-01354-9.

[115] Camille Jubelin et al. “Three-dimensional in vitro culture models in oncology research”. In: *Cell & Bioscience* 12.1 (Sept. 11, 2022), p. 155. ISSN: 2045-3701. DOI: 10.1186/s13578-022-00887-3.

[116] Lan K. Nguyen and Boris N. Kholodenko. “Feedback regulation in cell signalling: Lessons for cancer therapeutics”. In: *Seminars in Cell & Developmental Biology*. Gap Junctions 50 (Feb. 1, 2016), pp. 85–94. ISSN: 1084-9521. DOI: 10.1016/j.semcdb.2015.09.024.

[117] Center for Drug Evaluation and Research. “FDA approves encorafenib in combination with cetuximab for metastatic colorectal cancer with a BRAF V600E mutation”. In: *FDA* (Apr. 9, 2020).

APPENDICES

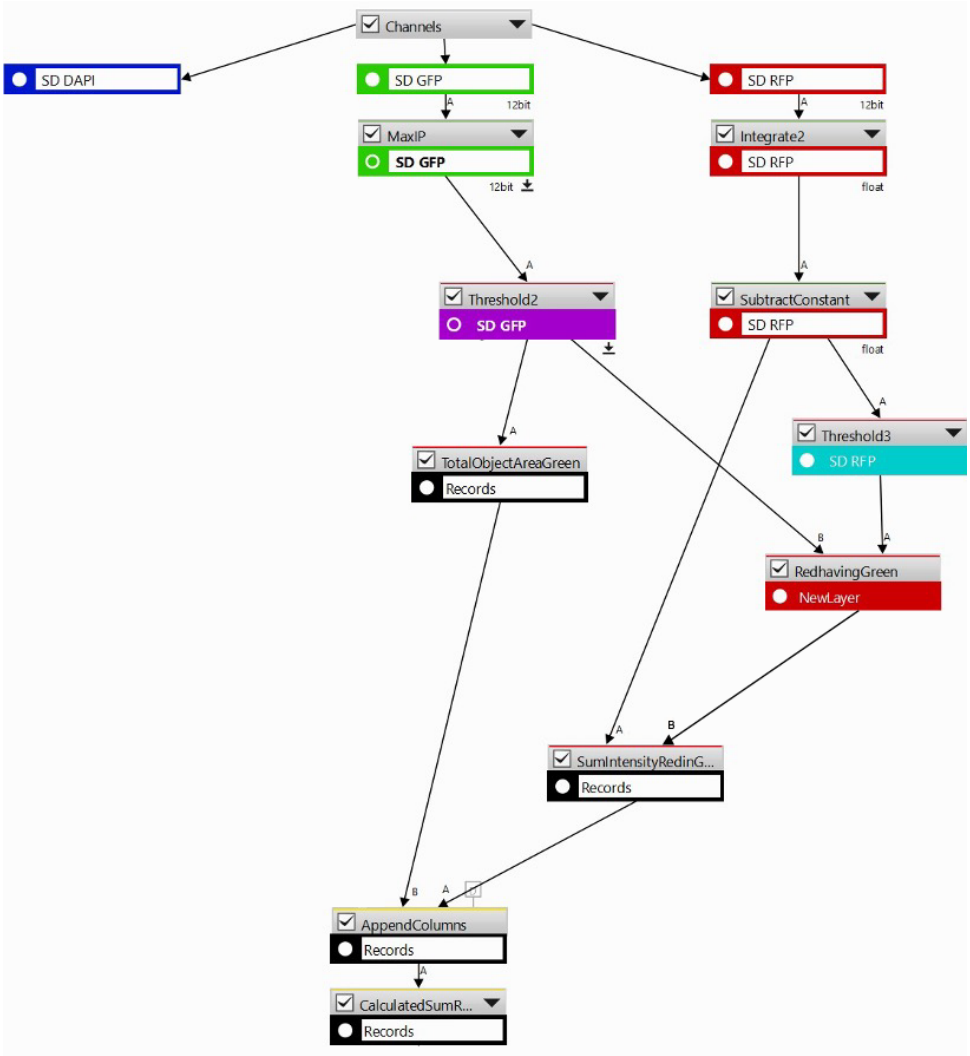

Figure A.1: Quantification pipeline for DL-FGF uptake in confocal microscopy. A customized quantification pipeline in NIS Elements software to analyze DL-FGF uptake per cell area in confocal microscopy images. SD-GFP (Alexa488 antibody stained FGFR) and SD-RFP (Dylight 550-FGF1) channels were used. Maximum Projection of the 20 stacks per image for SD-GFP-defined receptor cell areas, while IntegrateProjection for SD-RFP quantified DL-FGF1 internalized receptors. Thresholding on SD-GFP (Threshold2, range: 118 to 140) and SD-RFP (Threshold3, range: 118 to 2000, typically 300-800) defined relevant areas, with SD-RFP background subtraction set at 2000 (SubtractConstant). A verification step (RedHavingGreen) ensured only SD-RFP signals within SD-GFP areas were analyzed. Data were collected and stored, with DL-FGF1 internalization quantified per image by dividing red pixel intensity within green areas by total green area (CalculatedSumRedinGreen).

Table A.1: Overview of Celltraxx experimental settings. The Celltraxx software was utilized in migration (migr.) and proliferation (prol.) assays. Detailed settings descriptions are available at: `https://github.com/borge-holme/celltraxx_download`.

Parameter	Value (migr./prol.)
Wound healing mode	no
Perform flat field correction	no
Perform image shift correction	yes/no
Perform interactive tuning	no
Version	4.6
Track smoothing iterations	0
Pixel size [um]	1.24
Gaussian filter radius [um]	18
Smallest cell diameter [um]	19
Largest cell diameter [um]	56
Cutting cell diameter [um]	19
Top crop margin [pixels]	15
Bottom crop margin [pixels]	21
Left crop margin [pixels]	16
Right crop margin [pixels]	14
Time between images [min]	10/180
Highest cell velocity [um/min]	3
Shortest cell track [images]	20
First image number	0
Last image number	114/23
Image number increment	1
Make identified cell videos	yes
Make matched cell videos	no
Make valid track videos	yes/no
Tracking dot diameter [um]	9
Valid track image contrast	2
Scale bar color	white
Draw cell outline	no/yes
Draw cell track line	yes
Write mirror margin images	no
Write shifted images	no
Write gaussian smoothed images	no
Write segmented cell images	no
Write cut cell images	no
Write identified cell images	no
Write matched cell images	no
Write valid track images	no
Keep cells from previous image	yes/no
Segmentation limit [SDs]	1.5
# bins in histogram	100
Tuning image code	0

B - GITHUB REPOSITORY

The code used to analyze raw mutation data for FGFR1-4 from COSMIC database and the respective CSV files are included in the GitHub repository linked below. Explanatory comments and results have been added for clarity. To test the code, it may be necessary to update the file paths to match the location where the CSV files are stored.

Github repository link

- `https://github.com/Karenir/FGFR_mutations.git`

C - SUPPLEMENTARY

FGFR1_ENST00000447712	Counted by Python, data from Cosmic (csv file)				Fusions, counted on Cosmic	**Total**
	In frame del/ins	Frameshift mutation	Premature stop codon	Missense mutation		
All mutations	13	15	33	760	11	**832**
Mutations influencing S777/S789	0	14	29	1 (on S789)	11	**55**
Mutations influencing S777/S789 with intact kinase domain (->767 aa)	0	0	0	1	1	**2**

FGFR2_ENST00000358487	Counted by Python, data from Cosmic (csv file)				Fusions, counted on Cosmic	**Total**
	In frame del/ins	Frameshift mutation	Premature stop codon	Missense mutation		
All mutations	16	25	44	1498	0	**1583**
Mutations influencing S780/S791	0	23	42	1 (on S780), 4 (on S791)	0	**70**
Mutations influencing S780/S791 with intact kinase domain (->770 aa)	0	1	2	5	0	**8**

FGFR3_ENST00000440486	Counted by Python, data from Cosmic (csv file)				Fusions, counted on Cosmic	**Total**
	In frame del/ins	Frameshift mutation	Premature stop codon	Missense mutation		
All mutations	43	71	10	5117	12	**5253**
Mutations influencing S771/S782	0	59	10	0	11	**80**
Mutations influencing S771/S782 with intact kinase domain (->761 aa)	0	4	0	0	11	**15**

FGFR4	Counted by Python, data from Cosmic (csv file)				Fusions, counted on Cosmic	**Total**
	In frame del/ins	Frameshift mutation	Premature stop codon	Missense mutation		
All mutations	0	44	40	787	0	**871**
Mutations influencing S765/S776	0	41	40	4 (on S765), 1 (on S776)	0	**86**
Mutations influencing S765/S776 with intact kinase domain (->755 aa)	0	0	0	5	0	**5**

Figure C.1: Mutation data affecting FGFR1-4 in sequenced tumor samples were obtained from the COSMIC database. Mutations of FGFR1-4 were extracted from CSV files obtained from the COSMIC database (see COSMIC ID names). These mutations were categorized (as indicated) and counted using a Python script in VS Code (Appendix B). Additionally, each mutation was assessed for its impact on potential phosphorylation sites of ERK1/2 and RSK2 in the FGFR tails and whether the mutations retained an active catalytic domain, indicating potential cancer-driving capabilities. Phosphorylation sites of FGFR1 were defined from relevant literature [46, 49], and corresponding sites in FGFR2-4 were determined by sequence alignment (Figure 4.1.1b). The sequence of the catalytic domain used was defined by Katoh et al. [11]. The number of tested samples for FGFR1-4 were 86911, 90616, 102780, and 72724, respectively. Deletions (del). Insertions (ins). Made in Excel.

D - ADDITIONAL EXPERIMENTS

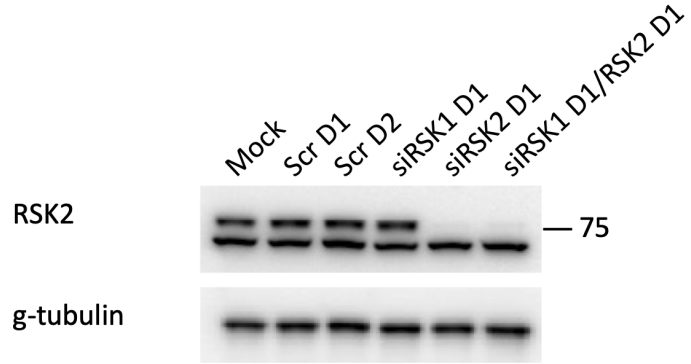

Figure D.1: Upper band of the RSK2-antibody corresponds to RSK2. U2OS-R1 cells were treated with 20 nM siRNAs targeting RSK1 or RSK2 or in combination and non-targeting siRNAs (Scr 1 and 2) for 72 hours. Mock cells are treated as other cells but without siRNAs. The cells were lysed, and the lysate was subjected to western blotting with the indicated antibodies. The result demonstrates that the upper band is lost when targeting RSK2 with siRNA, indicating that the upper band represents the RSK2 band, while the bottom band is background noise. γ-tubulin (g-tubulin) was used as a loading control. The experiment was conducted by Ellen Margrethe Haugsten from the Department of Tumor Biology, Institute of Cancer Research. Contact her for more details if needed.

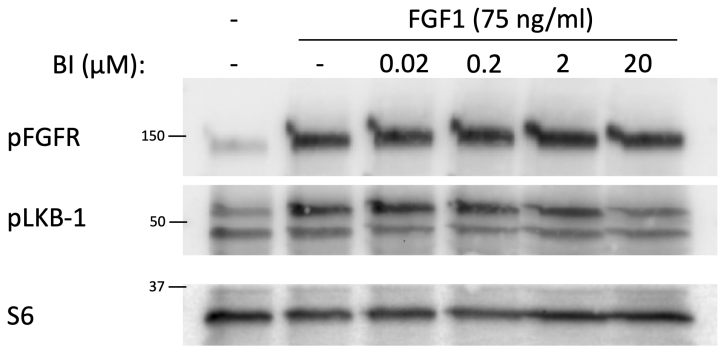

Figure D.2: BI-D1870 reduces FGF1-stimulated LKB1 phosphorylation to background levels at 20 μM. U2OS-R1 cells were serum-starved for 1 hour. Increasing concentrations of BI-D1870 (BI) (as indicated) were added after 30 minutes. Then, cells were incubated with FGF1 (75 ng/mL) and heparin (10U/μL) for 10 minutes. The cells were then lysed, and the lysate was subjected to western blotting with the indicated antibodies. The result demonstrates that FGF1-stimulated phosphorylation of LKB1 is reduced to background levels with 20 μM BI. S6 was used as a loading control. The experiment was conducted by Ellen Margrethe Haugsten from the Department of Tumor Biology, Institute of Cancer Research. Contact her for more details if needed.

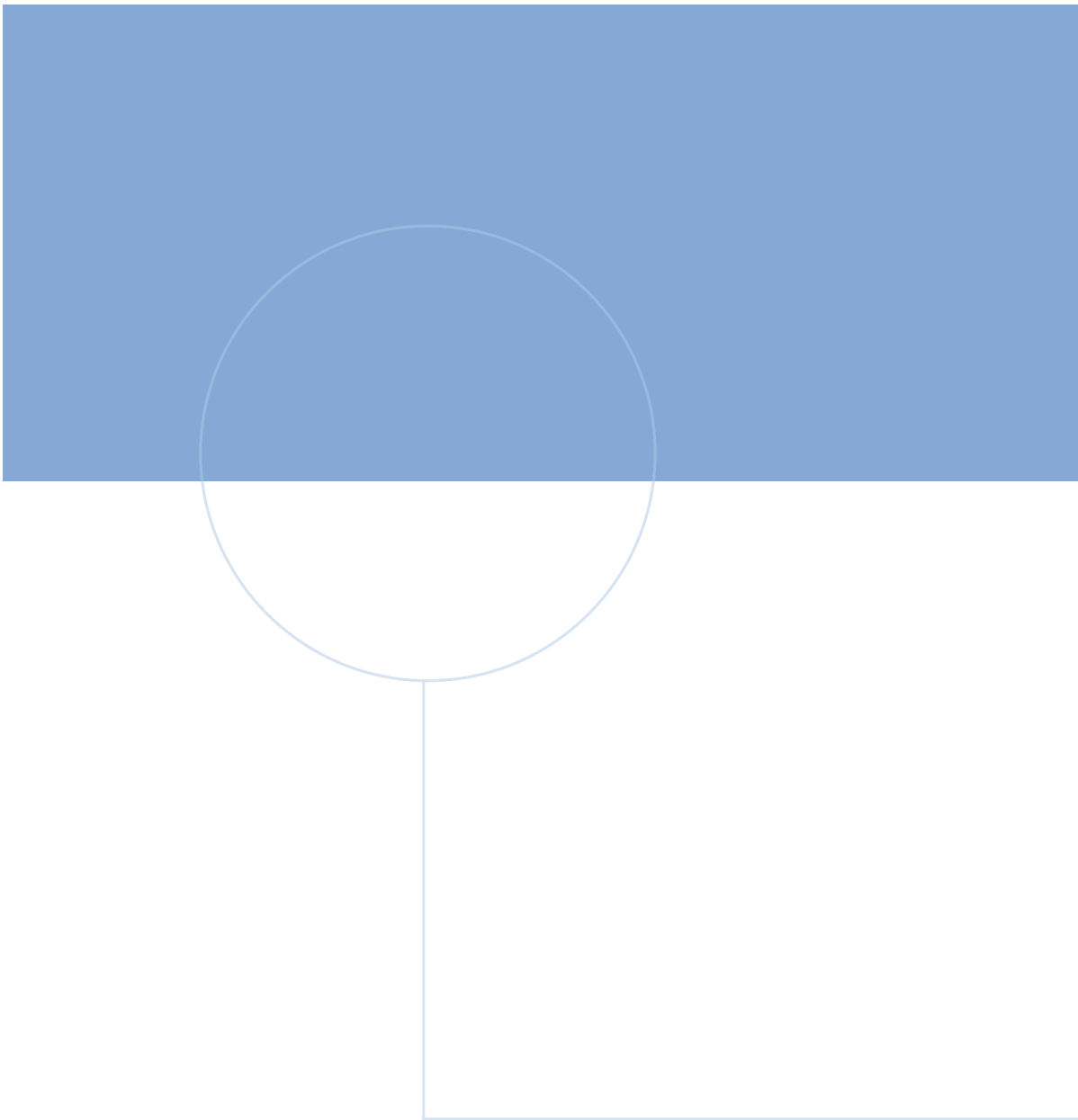

NTNU
Norwegian University of
Science and Technology

Oslo
University Hospital
Norwegian Radium Hospital